

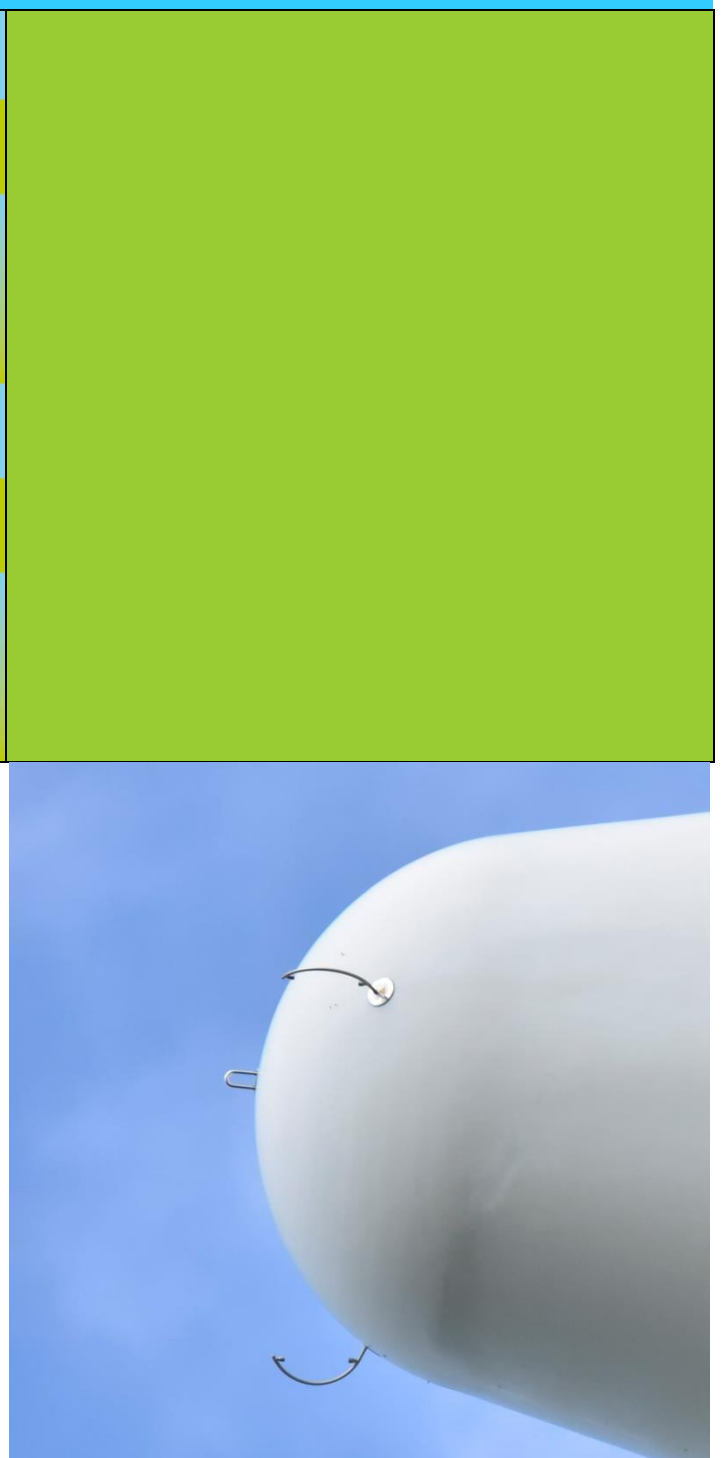
Spinner Anemometry – Uncertainty Analysis

DTU Vindenergi
Report 2018

Troels F Pedersen, Paula Gómez Arranz

DTU Wind Energy E-0166

April 2018



Authors: Troels F Pedersen, Paula Gómez Arranz

Title: Spinner Anemometry – Uncertainty Analysis

Institute: Wind Energy Division

Abstract (max 2000 char.):

The spinner anemometer is an integrated instrument on a wind turbine that can measure traceable calibrated and free wind speed according to the standard IEC61400-12-2. The uncertainty analysis of spinner anemometer wind speed measurements is due to the integrated six sensors and unlinear conversion algorithm rather complex. An uncertainty analysis method has been proposed which considers all potential influential parameters and derives uncertainty components that are relevant for the analysis. Due to the large variability of sonic sensor wind speed measurements and the accelerometer measurements during rotation and operation the regular GUM method for determination of sensitivity factors was not found feasible. Instead a simulation model was developed. It simulates the normal measurements of the spinner anemometer during operation of the wind turbine. A procedure for evaluation and expression of the uncertainty components on horizontal wind speed uncertainty was made. Combination of uncertainties was then performed with sensitivity factors equal to one and correlation coefficients assumed fully correlated or non-correlated. An example of uncertainty of measurements with a spinner anemometer was included. The results showed an overall standard uncertainty of 1.4% for horizontal wind speed measurements with the spinner anemometer.

DTU Wind Energy E-0166

April 2018

Contract no.:

Sponsorship:

ROMO Wind A/S & EUDP PTP

Front page:

Spinner anemometer on wind turbine at Nørrekær Enge

Pages: 83

Tables: 16

References: 14

Technical University of Denmark
DTU Wind Energy
Frederiksborgvej 399
Building 125
4000 Roskilde
trpe@dtu.dk
www.vindenergi.dtu.dk

Preface

This report covers an uncertainty analysis of absolute traceable wind speed measurements made by spinner anemometers for wind speed and power curve measurements. The great extent of the work was made for ROMO Wind A/S on a research contract dated 10th August 2015. The original results were reviewed under the EUDP “Performance Transparency Project” (PTP).

This report is the published version of DTU Wind Energy I-0384, ver. 2 (December 2017).

DTU, Risø Campus, April 2018

Content

Abstract	5
1. Introduction	6
2. Basic characteristics	6
2.1 Measurement principles	6
2.2 Conversion algorithm	8
3. Spinner anemometer uncertainty components	10
3.1 Calibration uncertainties	10
3.2 Mounting deviations	15
3.3 Operational influences	20
3.4 Other uncertainty components	34
3.5 Summary on uncertainty components	36
4. Modelling the measurand – combination of uncertainties	38
4.1 Combination of uncertainties according to GUM	38
4.2 Modeling of the measurand according to GUM	38
4.3 Overall simulation approach	40
5. Nacelle transfer function	46
6. Free and absolute wind speed measurements with the spinner anemometer	46
6.1 Uncertainty of the free wind speed measurements	46
7. Example of measurement uncertainty of a spinner anemometer	47
7.1 Spinner anemometer uncertainty	50
55	
8. Examples of AEP uncertainty from spinner anemometer and mast power curves	65
9. Conclusions.....	69
References	71
Acknowledgements	72
Annex A – calibration certificates	73
Annex A – Calibration certificates	

Abstract

The spinner anemometer is an integrated instrument on a wind turbine that can measure traceable calibrated and free wind speed according to the standard IEC61400-12-2. The uncertainty analysis of spinner anemometer wind speed measurements is due to the integrated six sensors and unlinear conversion algorithm rather complex. An uncertainty analysis method has been proposed which considers all potential influential parameters and derives uncertainty components that are relevant for the analysis. Due to the large variability of sonic sensor wind speed measurements and the accelerometer measurements during rotation and operation the regular GUM method for determination of sensitivity factors was not found feasible. Instead a simulation model was developed. It simulates the normal measurements of the spinner anemometer during operation of the wind turbine. A procedure for evaluation and expression of the uncertainty components on horizontal wind speed uncertainty was made. Combination of uncertainties was then performed with sensitivity factors equal to one and correlation coefficients assumed fully correlated or non-correlated. An example of uncertainty of measurements with a spinner anemometer was included. The results showed an overall standard uncertainty of 1.4% for free horizontal wind speed measurements with the spinner anemometer.

1. Introduction

The measurement uncertainty of wind measurements made with a spinner anemometer requires a thorough analysis due to the complex sensing and conversion principle. The spinner anemometer is a sensor which in itself comprises six sensors. Each of these sensors may provide uncertainty from traceable calibration, from intrinsic bias characteristics and from installation deviations. As the spinner anemometer is based on the flow over the spinner the spinner geometry is an important part of the sensor. Also, the wind climate and operation of the wind turbine provides parameters that influence on the measurements of the spinner anemometer due to variation of local measurement conditions of each sub-sensor during rotation.

In order to understand the complexity of the uncertainty analysis the basic characteristics of the spinner anemometer are outlined. The potential uncertainty components are described and finally the propagation of the uncertainty components into the uncertainty of the measured wind components is derived.

The basis for the uncertainty analysis is measurement of the absolute free horizontal wind speed by application of a nacelle transfer function, NTF, according to the standard IEC61400-12-2.

2. Basic characteristics

The output of the spinner anemometer is horizontal wind speed, yaw misalignment and flow inclination angle. The basic measurements are based on three 1D sonic sensors and three accelerometers.

2.1 Measurement principles

The spinner anemometer uses the aerodynamics of the spinner of a wind turbine for measurement of wind conditions. Directional wind speeds are measured in three positions on the spinner, as illustrated in Figure 1. Each sonic sensor has an accelerometer mounted in the sensor foot, aligned so that the path of the sonic sensor in a horizontal position measures the gravity with max and min values. Flow speeds around a spinner are visualized in Figure 2 in colours for an upwards flow on the spinner (blue for low speed, red for high speed). From the stagnation point on the nose of the spinner the flow accelerates over the surface and reaches flow speeds above free wind speed. The sonic sensors are positioned on the spinner where flow speed is approximately the same as the free wind speed.

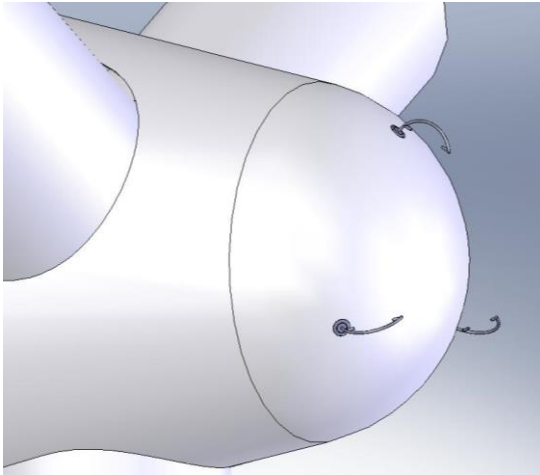


Figure 1 A spinner anemometer consisting of a spinner mounted with three sonic sensors with an accelerometer mounted into the foot of each sonic sensor

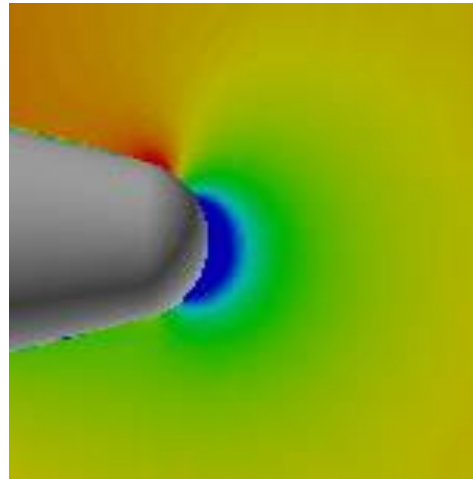


Figure 2 Flow speed contours around a spinner with wind from the right at a flow inclination angle of 10° , which means upwards flow

The spinner itself may have different shapes, being semi-spherical, pointed or flat. The flow over different spinners varies with the different shapes. The measured flow with the three sonic sensors has to be converted with a conversion algorithm to horizontal wind speed, yaw misalignment and flow inclination angle. One assumption for the spinner anemometer algorithm on the flow is that with an axially aligned wind the sonic sensor path flow speeds are proportional to the wind speed ahead of the rotor. At non-axial and constant wind speed the sonic sensor path flow speeds are assumed cosine shaped over one rotation. The average path flow speed over one rotation is reduced with the cosine to the inflow angle relative to the rotor axis and the amplitude of the cosine shaped variation over one revolution is increasing with the sinus to the same inflow angle. For different spinner shapes it is assumed that the conversion algorithm can be fitted to the air flow that the spinner shapes develop, especially for normal operating conditions where the spinner is mainly pointing into the wind. These assumptions were successfully verified for a conical spinner with a semi spherical nose in a wind tunnel experiment [1, 2].

The sonic sensors measure directional wind speed. This means that the lateral flow speeds on the sonic sensor paths due to the rotation of the spinner in principle are cancelled out when the lateral angular characteristics is cosine shaped. This also means that rotation of flow in front of the spinner due to induction by the rotor in principle also is cancelled out.

Furthermore, the conversion algorithm presumes spinners should have accurate rotor symmetric geometry and the sonic sensors should be mounted perfectly correct. These assumptions are ideal, but in reality not easy to meet. Spinners are not perfectly symmetric in geometry and they are not perfectly mounted, and the sonic sensors are not mounted perfectly on the spinners. Some imperfections can be compensated for. Compensation can be made to reduce 1P variations in the output signal due to imperfect geometry or imperfect mounting of sensors. The compensation with the “internal calibration” (described in chapter 3.1.3) is based on the assumption that the sonic sensors must measure the same average flow speed over a longer time to reduce the 1P variations, and that the average of the three shall persist to be the

same after the compensation. The compensation will then not influence on the overall average wind speed and direction measurements but improve the quality of instantaneous measurements.

2.2 Conversion algorithm

2.2.1 3D conversion algorithm for wind measurement

On a three bladed wind turbine the three sonic sensors are mounted on the spinner in front of the gaps between the blade roots. The conversion algorithm relates the sonic sensor path flow velocities to the horizontal wind speed and flow direction in front of the rotor. The measured horizontal wind speed is defined as the free wind speed when the rotor is at standstill. This means that the measured wind speed is not considering the influence of the rotor induction due to the operating rotor and neither the influence of the drag of the spinner, blade and nacelle arrangement. The generic relation between the sonic sensor path flow velocities V_1, V_2, V_3 , the wind speed U and the inflow angle to the shaft axis α at the azimuth position of the flow stagnation point on the spinner θ is:

$$V_1 = U(k_1 \cos \alpha - k_2 \sin \alpha \cos \theta) \quad (1)$$

$$V_2 = U(k_1 \cos \alpha - k_2 \sin \alpha \cos(\theta - \frac{2\pi}{3})) \quad (2)$$

$$V_3 = U(k_1 \cos \alpha - k_2 \sin \alpha \cos(\theta - \frac{4\pi}{3})) \quad (3)$$

The generic equations include the two spinner anemometer algorithm constants k_1 and k_2 . The ratio between the two constants $k_\alpha = k_2/k_1$ is a constant that must be calibrated to measure flow angles correctly. The constant k_1 must be calibrated afterwards to measure wind speeds correctly. And furthermore, a nacelle transfer function, NTF, must be made in order to measure free wind speeds correctly.

The transformation from sonic sensor measurements to spinner anemometer parameters follows four steps, described in detail in [3]. It converts the sonic sensor path flow velocities and the rotor azimuth position φ to horizontal wind speed, yaw misalignment and flow inclination angle with the direct transformation, shown in Figure 3.

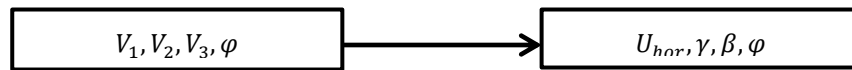


Figure 3 Direct transformation from sonic sensor flow velocities to spinner anemometer parameters

The first transformation step relates the sonic sensor flow velocities V_1, V_2, V_3 to the wind speed U , the inflow angle to the shaft axis α and the azimuth position of the flow stagnation point on the spinner θ in the rotating spinner anemometer coordinate system. These parameters are directly derived from the generic equations:

$$\alpha = \text{atan2}\left(\frac{k_1 \sqrt{3(V_1 - V_{ave})^2 + (V_2 - V_3)^2}}{\sqrt{3}k_2 V_{ave}}\right) \quad (4)$$

$$U = \frac{V_{ave}}{k_1 \cos \alpha} \quad (5)$$

$$V_{ave} = \frac{1}{3}(V_1 + V_2 + V_3) \quad (6)$$

The second transformation step converts the parameters to three wind speed components $U_{x,s}, U_{y,s}, U_{z,s}$ in the non-rotating shaft coordinate system taking the rotor azimuth position φ into account. The third transformation step converts the parameters to three wind speed components U_x, U_y, U_z in a fixed nacelle coordinate system taking the shaft tilt angle δ into account. The fourth transformation step converts the parameters into the horizontal wind speed U_{hor} , yaw misalignment angle γ , flow inclination angle β and rotor azimuth position angle φ .

The inverse transformation is made with the four transformation steps in opposite direction as shown in Figure 4.



Figure 4 Inverse transformation from spinner anemometer parameters to sonic sensor flow velocities

The details of the transformation steps with derivation of all equations are best described in [3].

2.2.2 Conversion algorithm for rotor azimuth position

The rotor azimuth position angle φ is measured by three accelerometers mounted in the feet of the sonic sensors. The azimuth position of the inflow stagnation point on the spinner is defined by the angle from vertical to the azimuth position of the accelerometer in sonic sensor 1. The accelerometers within the sonic wind sensors are oriented so that they measure acceleration tangentially to the rotation, and perpendicular to the rotor shaft. In this way the centrifugal forces on the accelerometers are zero at all rotational speeds. The coordinate system and definition of parameters is described in Figure 5.

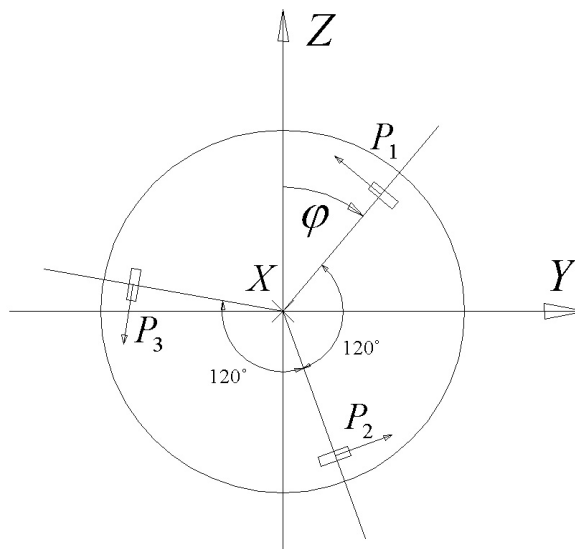


Figure 5 Sketch showing positioning of the three accelerometers as seen from the front of the spinner in the non-rotating shaft coordinate system. Gravity acceleration is downwards.

The three accelerometers will for constant rotational speed measure sinusoidal signals during rotation:

$$P_1 = -G \sin \varphi + A_t \quad (7)$$

$$P_2 = -G \sin(\varphi + 2\pi/3) + A_t \quad (8)$$

$$P_3 = -G \sin(\varphi + 4\pi/3) + A_t \quad (9)$$

Here G is the gravity acceleration, and φ is the rotor azimuth position, as determined from the position of sonic sensor 1 relative to the vertical Z-axis. A_t is the tangential acceleration, which, in deducing the rotor position, is eliminated by the mathematical algorithm when three sensors are available.

The influence of tangential acceleration during rotation due to sideway vibrations of the spinner is not avoided, and this will influence differently on the three accelerometers. The rotor position is determined from the three 1D acceleration measurements by:

$$\sin \varphi = (2P_1 - P_2 - P_3)/3G \quad (10)$$

$$\cos \varphi = (P_2 - P_3)/\sqrt{3}G \quad (11)$$

Taking care of the quadrant of the cos and sin function, the rotor position is determined as:

$$\varphi = \text{Atan2} \frac{\sin \varphi}{\cos \varphi} \quad (12)$$

3. Spinner anemometer uncertainty components

Power curve measurements with use of spinner anemometers can be made according to the IEC61400-12-2 standard [7]. The standard describes how wind speed measurements made on the nacelle or spinner can be related to free wind speed measurements. The uncertainty on traceable calibrated free wind speed measurements as well as the uncertainty of traceable calibrated wind speed measurements at the spinner with spinner anemometry according to this standard is analysed in the following chapters.

First we consider the calibration uncertainties. Then we consider uncertainties due to mounting and uncertainties due to operational influence parameters.

3.1 Calibration uncertainties

Calibration of the spinner anemometer for absolute free wind speed measurements is made according to [7] in several steps. Calibration values may be inserted into the spinner anemometer box after calibration ("calibrated path", see Figure 31), or default values of the constants may be inserted in the box, and averaged data may be converted by first making an inverse transformation with the default constants and then an inverse transformation with the calibrated constants. In case 10min average values are converted then a deviation is made compared to converting raw time trace data due to the unlinear conversion algorithm.

Calibrations are assumed made in the following order:

1. Sonic sensor zero wind calibration
2. Sonic sensor wind tunnel calibration
3. Spinner anemometer internal calibration
4. Yaw misalignment calibration (determination of k_α)

5. Wind speed calibration (determination of k_1 , which may be determined as part of the NTF)
6. Nacelle transfer function calibration, NTF

3.1.1 Sonic sensor zero wind calibration

The manufacturer of the spinner anemometer makes a zero wind calibration of individual sonic sensors in combination with the specific electronic box so that the measured wind speed at zero wind is output as zero, see the spinner anemometer manual [4] or ASTM document [5]. Values of the path lengths, air temperatures and zero wind calibration results are stored in the spinner anemometer box and used by the conversion algorithm. The procedure is a standard ab factory calibration procedure for any type of sonic anemometer. A new zero wind calibration is only made if a sonic sensor is damaged on the turbine and a substitute sensor is inserted.

No uncertainty is associated with a zero wind calibration in this connection as this calibration only ensures that zero wind speed is correct, and that the default type wind speed algorithm can be applied. No traceable calibration of non-zero wind speeds is made.

3.1.2 Sonic sensor wind tunnel calibration uncertainty

To achieve traceability sonic sensors must be calibrated in an accredited wind tunnel. Wind tunnel calibration of a spinner anemometer sonic sensor is very similar to calibration of a cup anemometer described in IEC61400-12-1, annex F [6]. A clarification sheet [8] under IECRE describes requirements for calibration and use of spinner anemometers for power performance verification according to IEC61400-12-2 [7]. The mounting setup for such calibrations in the wind tunnel is shown in Figure 6.

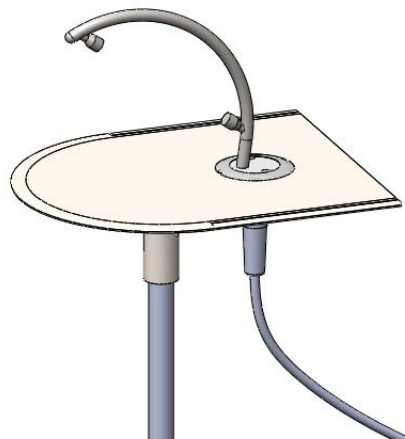


Figure 6 Calibration setup for wind tunnel calibration of a spinner anemometer sonic sensor [8]

The sonic sensor is mounted on a mounting plate that simulates the mounting on the spinner surface and keeps the flow distortion due to the sensor fitting below the plate as low as possible. This makes it possible to exchange a sonic sensor during a measurement campaign. The mounting plate should be completely parallel to the flow direction. Influence of a non-zero angle of attack may be significant but is avoided with a new wind tunnel calibration factor, k_c for the sonic path centre for setup of the mounting plate. The sonic sensor is mounted so that the flow has an angle to the sonic sensor path (default 35.0°). The path angle has a tolerance. The exact angle must be measured at the calibration setup with an accuracy of 0.1° . After the tunnel

calibration the calibration is converted to the sonic sensor path so that the calibration in fact relates to a calibration of the sonic sensor path at the actual measured path angle. The mounting plate is made so that the leading edge of the plate is having an arc with the centre below the sonic sensor path centre. This makes the calibration plate useful also for measurement of lateral angle response characteristics.

Additional to the wind tunnel calibration uncertainties for cup anemometers, annex F [6], some additional uncertainty components due to the tilted sonic sensor path apply to the spinner anemometer sonic sensor and the setup, as described in [8].

When converting the wind tunnel calibration result from the calibration certificate to the sonic sensor path calibration the actual measured sonic sensor path angle φ shall be used and be converted by the expression:

$$V_n = A_{cal} \cos \varphi \cdot V_{n,meas} + B_{cal} \cos \varphi \quad (13)$$

Where

V_n	is the calibrated wind speed along the sonic sensor path
$V_{n,meas}$	is the measured wind speed by the sonic sensor
A_{cal}	is the calibration line gain value from the calibration certificate
B_{cal}	is the calibration line offset value from the calibration certificate
φ	is the sonic sensor path angle measured when mounted on the mounting plate

The uncertainty of the calibrated wind speed along the sonic sensor path is influenced by the uncertainty of the wind tunnel wind speed and the measured sonic sensor path angle. The relation is:

$$V_n = V_t \cos \varphi \quad (14)$$

where V_t is the wind tunnel wind speed. The combined standard uncertainty is:

$$u_{N1,i}^2 = \left(\frac{\partial(V_t \cos \varphi)}{\partial V_t} \right)^2 u_t^2 + \left(\frac{\partial(V_t \cos \varphi)}{\partial \varphi} \right)^2 u_\varphi^2 = \cos^2 \varphi \cdot u_{t,i}^2 + V_{t,i}^2 \sin^2 \varphi \cdot u_\varphi^2 \quad (15)$$

Where

$u_{N1,i}$	is the standard uncertainty on the calibration, [7] annex G
u_t	is the standard uncertainty on the tunnel wind speed from the calibration certificate, [6] annex F
u_φ	is the standard uncertainty on the measured sonic sensor path angle, [8]

Application of the wind tunnel calibration on the spinner anemometer sonic sensor should be made for the default sonic sensor path angle 35°. When the calibrations are normalized to this default angle the NTF transfer from the calibration wind turbine to other wind turbines is consistent. The normalization can then be made by the equation:

$$V_i = \left(\frac{\cos 35^\circ}{\cos \varphi} A_{i,cal} \right) V_{i,meas} + \left(\frac{\cos 35^\circ}{\cos \varphi} B_{i,cal} \right)$$

The calibration constants to be inserted into the spinner anemometer box are then $A_{cal} \cos 35^\circ$ and $B_{cal} \cos 35^\circ$. When mounted on the spinner the sonic sensor path angles should be compared by photographic techniques (see chapter 7) to estimate the uncertainty on inflow angle due to local spinner surface angle variations.

3.1.3 Spinner anemometer internal calibration uncertainty

The general assumption for the spinner anemometer algorithm is that the spinner has a perfect rotational symmetric geometry, and that geometry of sonic sensors are perfect, and that they are mounted with perfectly the same orientation and position on the spinner. However, the geometry of spinners is not perfect, sensors are not perfect, and mounting of sensors are not perfect. The internal calibration of the spinner anemometer compensates such geometric influences such that 1P variations are minimized in the output signals as described in detail in [4].

The fundamental principle of the internal calibration is that the average value of each of the three sonic sensors is the same over time (hours). The internal calibration then makes a local correction of the k_1 and k_2 value for each sonic sensor. A requirement for the local corrections is that the average value of the three sonic sensor wind speeds over time is the same before and after correction. The internal calibration will therefore not influence on the measurement of average wind speeds, and no uncertainties should be applied due to the internal calibration. Additionally, output parameter variations over one revolution are minimized.

3.1.4 Angular measurement calibration uncertainty

The preferred method for calibration of a spinner anemometer for yaw misalignment measurements [3] is by yawing the stopped wind turbine in and out of the wind several times at moderate wind speeds while yaw direction and spinner anemometer output is recorded. The measurements are plotted against each other and a linear regression is made, where the gain determines k_α . When k_α is inserted into the spinner anemometer box as the correct ratio between k_2 and k_1 then absolute yaw misalignment measurements can be made, and wind speed measurements can be converted linearly. An internal calibration must be made before a yaw misalignment calibration in order to make the yaw misalignment measurement independent of the azimuth position of the stopped rotor.

The uncertainty from the yaw misalignment calibration is determined from the uncertainty on the yaw direction measurement combined with the standard deviation of the slope of the linear regression. Figure 7 shows an example of a yaw misalignment calibration.

3.1.5 Wind speed measurement calibration uncertainty

The calibration for wind speed measurements is a calibration for determination of the constant k_1 [9]. With k_α fixed k_1 can be calibrated against a reference wind speed measurement with a stopped rotor pointing towards the wind, using a calibrated reference such as a met mast with a top mounted cup anemometer, a nacelle based lidar or a ground based lidar. For default settings, CFD analysis can be used for determination of k_1 and k_2 [9].

Though the k_1 constant is defined for the relation to free wind for a stopped wind turbine the most feasible calibration of k_1 is made during operation of the wind turbine [3] and combining the calibration with measurement of the NTF, see next chapter. The k_1 constant may be

determined for very low and very high wind speeds, where the induction is reduced to very low values, see Figure 8. When applying the k_1 constant the NTF can be considered to be the same as the induction. The NTF, including determination of the uncertainty, will make a full relation to the free wind speed. As the uncertainty of the NTF is fully determined by the procedure in [7] no uncertainty should be applied to determination of the k_1 constant when considering free wind speed measurements. For measurements of wind speed at the spinner the k_1 constant should be applied the uncertainty from the high wind speeds in the NTF from which the k_1 constant was determined.

Calibration of k_1 /NTF during operation actually provides different operational conditions for the sonic sensors than calibration of k_1 for stopped conditions. In stopped conditions, the lateral inflow angle to the sonic sensors is close to zero, and the lateral angle response will not have an influence. If the lateral angle response has a tendency to increase the response at higher inflow angles then the k_1 constant will be determined higher in stopped condition than during operation.

3.1.6 Nacelle transfer function calibration uncertainty

The NTF can be considered equal to the induction due to the rotor blades in the rotor centre as the wind speed measured by the spinner anemometer is defined as the free wind speed for a stopped rotor and k_1 is defined according to this condition. The NTF can be made directly from measurements with the default $k_{1,d}$ value, but k_1 must be determined in order to convert measured data to the definition of the measured wind speed with the unlinear inverse and direct conversion algorithms.

A measured NTF is shown in Figure 8. The uncertainty of the NTF measurement is derived from the method description in [7], annex G, with the uncertainty components from table G.2 in the annex.

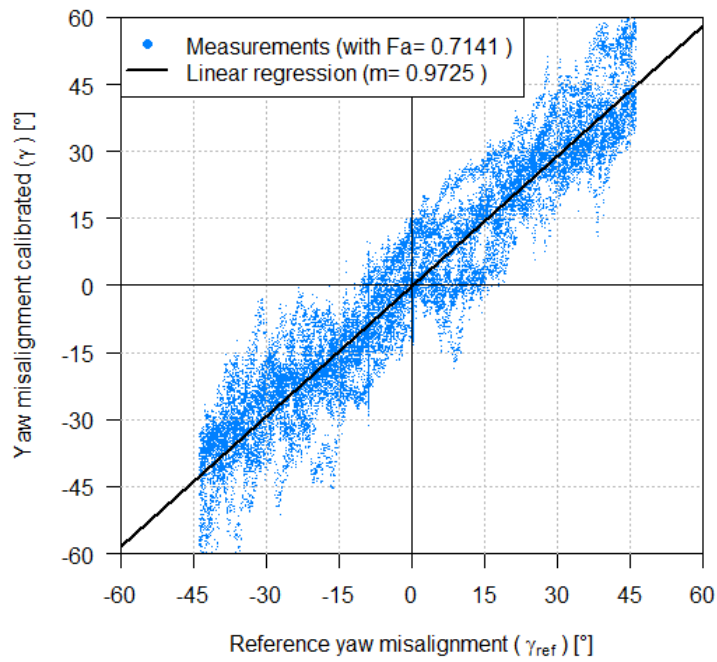


Figure 7 Linear regression of yaw misalignment measurements with spinner anemometer against yaw direction measurements [3]

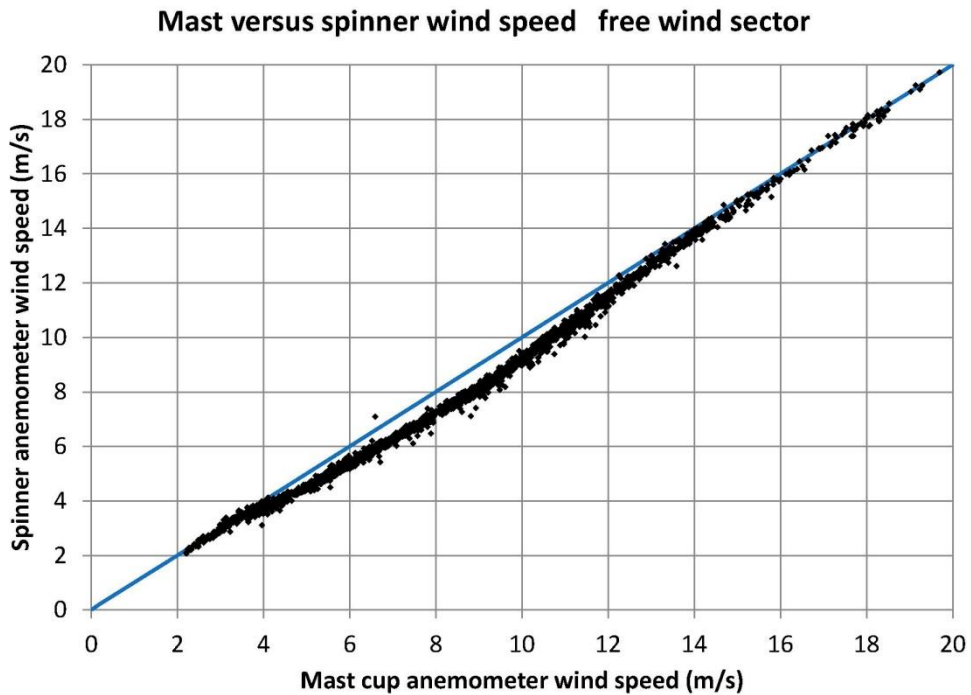


Figure 8 Spinner anemometer wind speed versus mast wind speed (10min averages) [9]

3.2 Mounting deviations

The positioning of the sonic sensors on the spinner is a key issue with respect to the wind speed measurement characteristics of the overall spinner anemometer. The positions of the

sonic sensors should be clearly defined on beforehand before mounting, and the positions should be used as reference position of sonic sensors on the wind turbine on which the NTF is measured. In comparison with installations on other wind turbines of the same type these reference positions may be used to evaluate the validity of the NTF with reference to IEC61400-12-2 [7] when transferring a measured NTF.

3.2.1 Sonic sensor longitudinal alignment uncertainty

The flow from the stagnation point in the nose of the spinner is accelerated over the surface in the longitudinal axial direction. Due to this accelerated flow the longitudinal positioning of the sensors on the spinner surface is very sensitive to the exact determination of the k_1 constant or for achievement of a reference k_1 constant that might have been achieved on another turbine.

The longitudinal positioning on the spinner surface is close to where the spinner surface has a slope angle to the shaft axis of 35° . The default sonic sensor path angle is tilted upwards with an angle of 35° relative to the mounting foot surface. This means that the sonic sensor path often is parallel with the shaft axis after installation on the spinner. However, there may be various reasons to deviate from this default position.

An estimate of the influence on the sonic sensor measured wind speed on the longitudinal positioning for the ideal reference mounting can be made with potential theory for a sphere.

The potential flow on a sphere for an incompressible, inviscid, irrotational fluid is determined as:

$$V_r = U \cos \varphi \left(1 - \left(\frac{r}{R}\right)^3\right) \quad (16)$$

$$V_t = U \sin \varphi \left(1 + 0.5 \left(\frac{r}{R}\right)^3\right) \quad (17)$$

Where

V_r	is the radial flow speed towards the centre of the sphere
V_t	is the tangential flow speed
U	is the free wind speed
φ	is the position angle on the sphere
r	is the radius to the sonic path centre
R	is the radius of the sphere

The sonic sensor path flow speed is then the projection of V_r and V_t on the sonic sensor path, as shown in Figure 9:

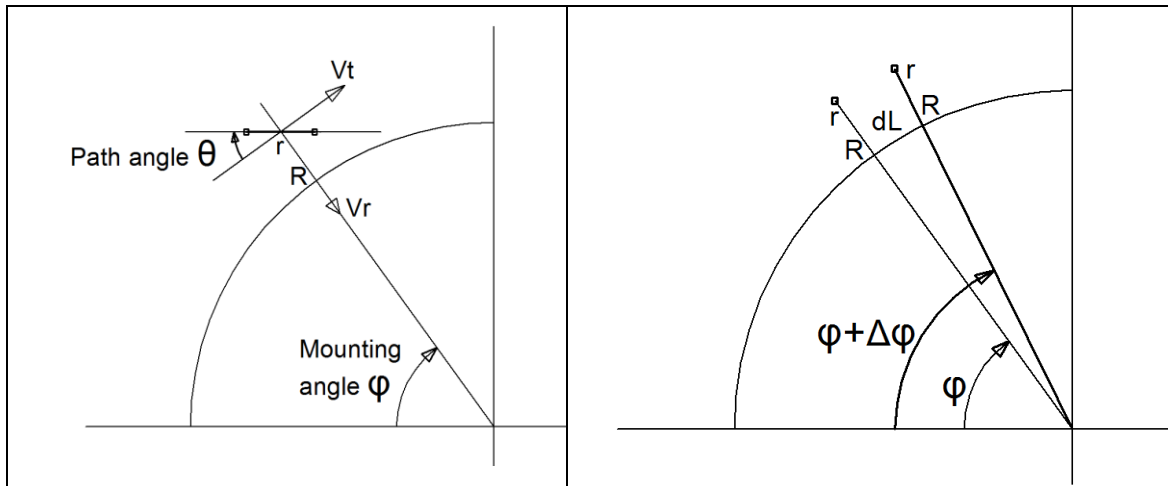


Figure 9 Mounting and path angles for determination of sonic path flow speed for potential flow over sphere (left) and deviation angle for longitudinal deviation (right)

$$V_1 = V_t \cos \theta + V_r \sin \theta \quad (18)$$

Where

θ is the sonic sensor path angle

The sensitivity of the longitudinal mounting deviation to the sonic sensor flow speed is made by converting the tangential deviation dL to the change in position angle ϕ , then deriving the radial and tangential flow speeds, and project these on the sensor path and then derive the deviation in wind speed. The sensitivity is shown in Figure 10, where radius is the distance perpendicular from the shaft axis to the mounting position of the sensor (to center of sonic path). For example, for a radius of 1m radially from the shaft we can estimate a 0.45% difference in sonic sensor output per cm sonic sensor mounting error. The deviation in longitudinal alignment is considered positive for deviations in direction of the nacelle.

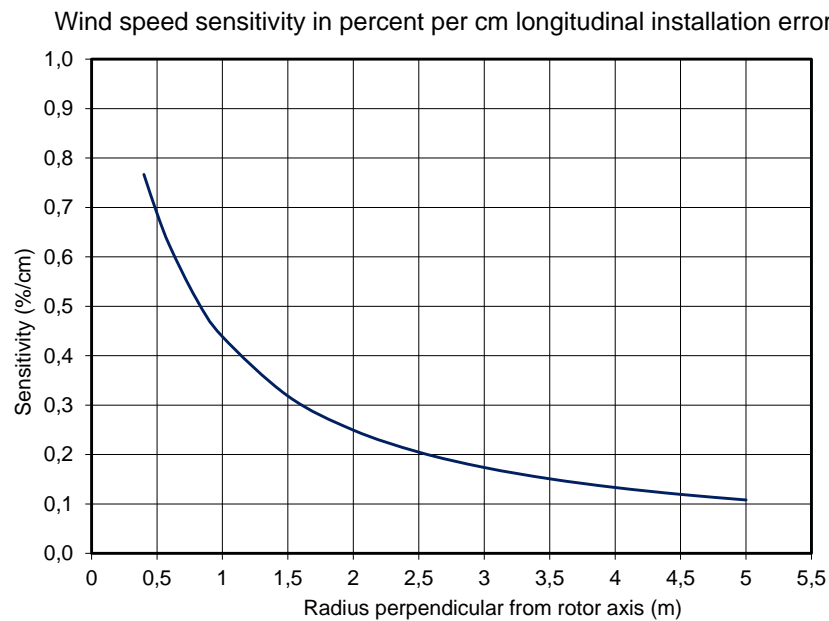


Figure 10 Sketch showing the calculation of sonic sensor path wind speed from potential flow over sphere

3.2.2 Sonic sensor direction alignment uncertainty

The direction alignment of the sonic sensors (angular alignment) is important since the actual inflow angle to the sonic sensor is influenced by lateral flow due to the rotational speed, and this influences on the signal output. The direction alignment sensitivity depends on the radius from the rotor axis to where the sonic sensor is positioned on the spinner. For larger radii the lateral wind speed component is increased and this increases the sensitivity to direction alignment. Figure 11 shows the sensitivity as a function of the lateral inflow angle. The estimated lateral inflow angles and percentage wind speed deviations of three types of wind turbines see Table 1, and two different wind speeds are shown on the curve as well. The percentage wind speed deviation is estimated by calculating the ratio of the cosine to the lateral inflow angle and the cosine to the lateral inflow angle plus one degree.

Table 1 Data of two wind turbine types for estimate of sideways inflow angles during operation

Turbine type	Spinner diameter	Rotor speed	Wind speeds
V90 – 3MW	3.6m	8.6 – 18.4 rpm	4 – 14 m/s
E-126 – 7MW	12m	5.0 – 11.7 rpm	4 – 16 m/s
S-2.3MW-93	0.65m at SA sonics	6 - 16 rpm	4 – 14 m/s

3.2.3 Sonic sensor path angle uncertainty

From the wind tunnel calibration the path wind speed is calibrated based on the actual measured sonic path tilt angle. This means that the path wind speed is traceable calibrated and measures the correct wind speed at the local position on the spinner. Deviations on the sonic sensor path angle (default 35.0°) may occur and has a significant influence on the measured flow speed because the vertical inflow angle to the sensor path always depends on the cosine

to the path angle, see Figure 12, which shows the inflow angle relative to the position on a sphere calculated with potential flow theory. The actual sonic sensor path angle should be measured during calibration as described in the wind tunnel calibration procedure [8]. A deviation from the default value has the same influence as the lateral angle deviation considered in the previous chapter. Thus Figure 11 can be used for the sonic sensor path angle sensitivity as well. At the path angle 35° the deviation sensitivity is seen to be 1.25% of the wind speed per degree deviation. The deviation is considered positive for upwards tilting of the path angle.

For practical reasons it is appropriate to normalize the wind tunnel calibrations to the default 35° path angle. When wind tunnel calibrations on all sonic sensors on several wind turbines are normalized to the default angle then the wind tunnel calibrations takes care of the variations of actual sonic sensor path angles, and no uncertainty needs to be applied to the sonic sensor path angle variations. However, an uncertainty must be applied due to spinner surface angle variations at the sonic sensor installation positions.

3.2.4 Sonic sensor lateral alignment uncertainty

If one sonic sensor is not positioned exactly in the middle between two blades then there will not be 120° between the sonic sensors. This will have an influence on the both the sonic path wind speed measurement and on the accelerometer measurement as there will be a phase shift on the output from these sensors. The wind speed measurement will be offset with an angle that corresponds to the lateral alignment deviation, and the deviation in wind speed will correspond to an offset in the sinusoidal variation over a full rotation of the rotor. The accelerometer measurement will be offset with a similar angle and the deviation in acceleration will correspond to an offset in the sinusoidal variation over a full rotation of the rotor. Deviations are considered positive in the rotation direction.

3.2.5 Sonic sensor accelerometer alignment uncertainty

The accelerometer in the foot of each sonic sensor must be correctly aligned in the lateral direction in order to measure the azimuth position correctly. If an accelerometer is not correctly aligned the determination of the azimuth position of the rotor will deviate from the correct position and there will be a phase shift in the signal. The influence of the sonic sensor accelerometer alignment in the sonic sensor foot will correspond to an offset in the sinusoidal variation over a full rotation of the rotor as for the sonic sensor lateral alignment.

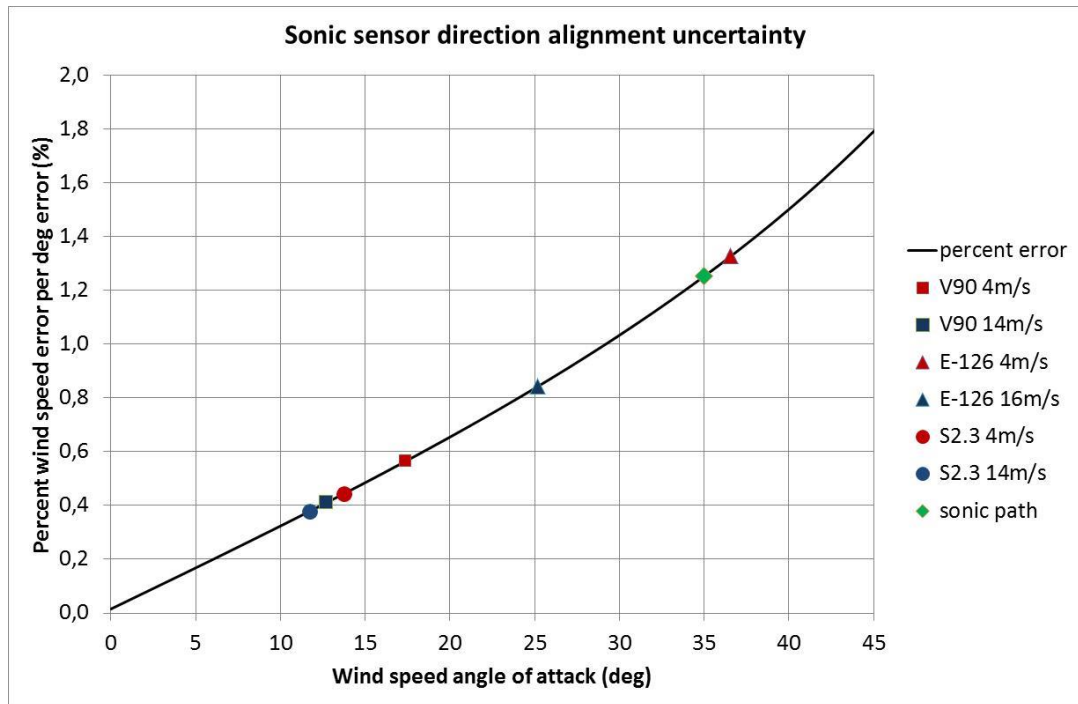


Figure 11 Sensitivity in percent of sonic sensor measured wind speed on the lateral mounting angle deviation of sonic sensors as function of lateral inflow angle to the sonic sensor path. Additionally, the sensitivity of the sonic sensor path uncertainty is shown

3.3 Operational influences

The spinner anemometer measurements are influenced by the climatic conditions and the turbine behaviour during operation of the wind turbine. The climatic conditions that should be considered are the same influential parameters as for cup and sonic anemometers in the IEC61400-12-1 standard [6]: wind speed, turbulence intensity, average flow inclination angle and temperature. Additional influential parameters depend on the operating wind turbine. The inflow angle to each sonic sensor depends on rotational speed, yaw misalignment, turbulence, and on shaft tilt bending due to thrust on the rotor.

3.3.1 Vertical inflow angle to sonic sensors

The vertical inflow angle variations to the rotor for class A in Table I.1 in the IEC61400-12-1 standard [6] vary from -3° to 3° and -15° to 15° for class B.

With a shaft axis tilt angle of, typically 5° , and only considering the class B conditions the variations correspond to rotor inflow angles from -20° to 10° relative to the rotor axis. These inflow angles give rise to inflow angle variations on the individual sonic sensor paths. This is investigated with potential flow on a sphere with a radius of 1.22m, corresponding to 1m radius at the 55° position on the sphere. The inflow angle on a sonic sensor pointing upwards on a sphere at the position 55° relative to the shaft is 34.3° , see Figure 12. For -20° inflow angle to the axis, corresponding to 75° position angle on the sphere (when inflow angles are considered to be analogue to change of sonic position on the sphere as the stagnation point move accordingly), the inflow angle to the sonic path is 34.7° , and for 10° inflow angle to the axis, corresponding to 45° position angle on the sphere, the inflow angle is 34.0° . For a sonic sensor

pointing downwards on the sphere, corresponding to 35° position angle on the sphere, the flow angle to the sonic path is 33.5° . The vertical inflow angle to the sonic sensor is thus varying only a few degrees from 35° , the angle at which the sonic sensors are calibrated in wind tunnel. The inflow angle on the sphere does therefore not seem to influence significantly on the vertical inflow angle on the sonic sensor path. For larger radii of sonic sensor positions the inflow angles to the sonic path will be much closer to 35° . The vertical inflow angle on the sonic sensor path is under these conditions so close to the inflow angle during wind tunnel calibration that the influence is small enough to be neglected for both class A and class B climate conditions.

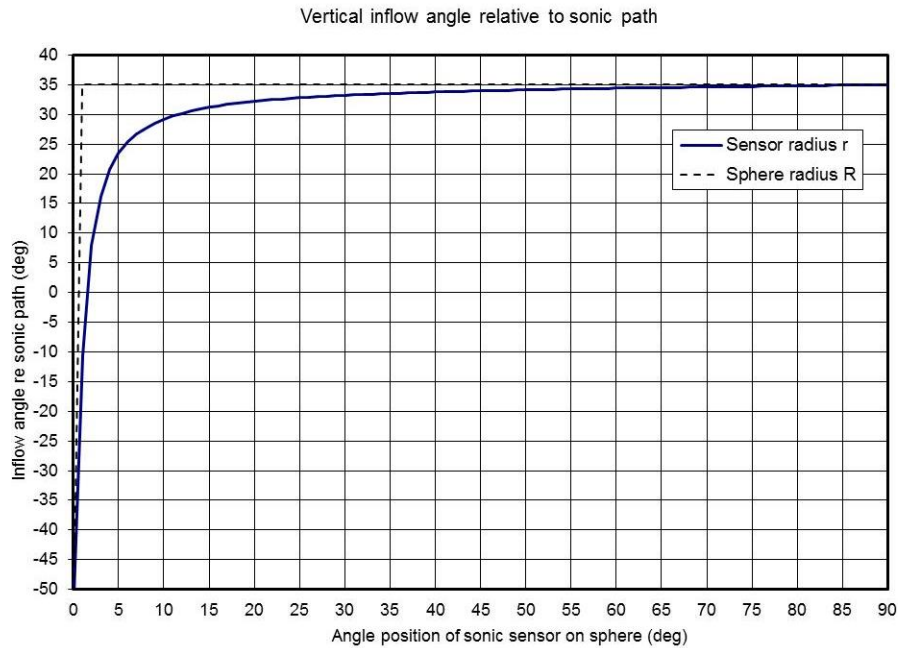


Figure 12 Vertical inflow angle relative to sonic sensor path calculated by potential flow over sphere. Angle position may also be used to consider inflow angle variations to the spinner anemometer

3.3.2 Lateral inflow angles to sonic sensors

The influence from the lateral inflow angle to the sonic sensor path is quite different as the angle varies significantly during operation. With the sonic sensor in a horizontal position the rotor flow inclination angle give rise to a vertical wind speed component that leads to a significant lateral inflow angle to the sonic sensor path. With an inflow angle to the spinner of -20° the vertical upwards component is 36% of the horizontal wind speed. This vertical component must be added to the existing lateral wind speed component due to rotor rotation.

For a V90 turbine at 4m/s the upwards component is 1.44m/s which results in lateral wind speeds of 2.35m/s and -0.54m/s, respectively on either side. This corresponds to lateral inflow angles of 30.4° and -7.7° , respectively. With an inflow angle of $+10^\circ$ to the spinner, the upwards wind speed component is -17.6%, corresponding to -0.70m/s, and lateral wind speeds to the sonic paths of 1.60m/s and 0.20m/s. This corresponds again to lateral inflow angles of 21.8° and 2.8° . Figure 13 to Figure 16 show the combined inflow angle and turbulence influence for 4m/s and 16m/s for Class A and Class B climate conditions for a V90 and an E-126 wind turbine.

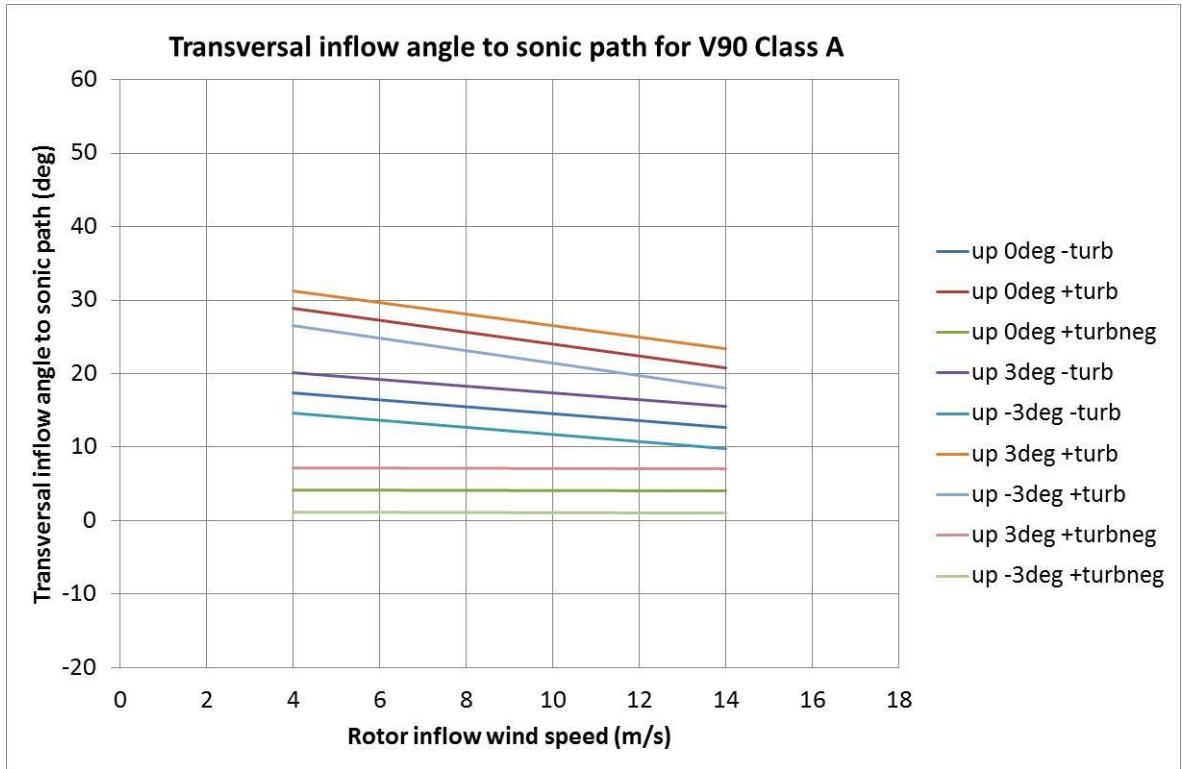


Figure 13 Lateral inflow angle variations on a sonic sensor on a V90 turbine for Class A variations

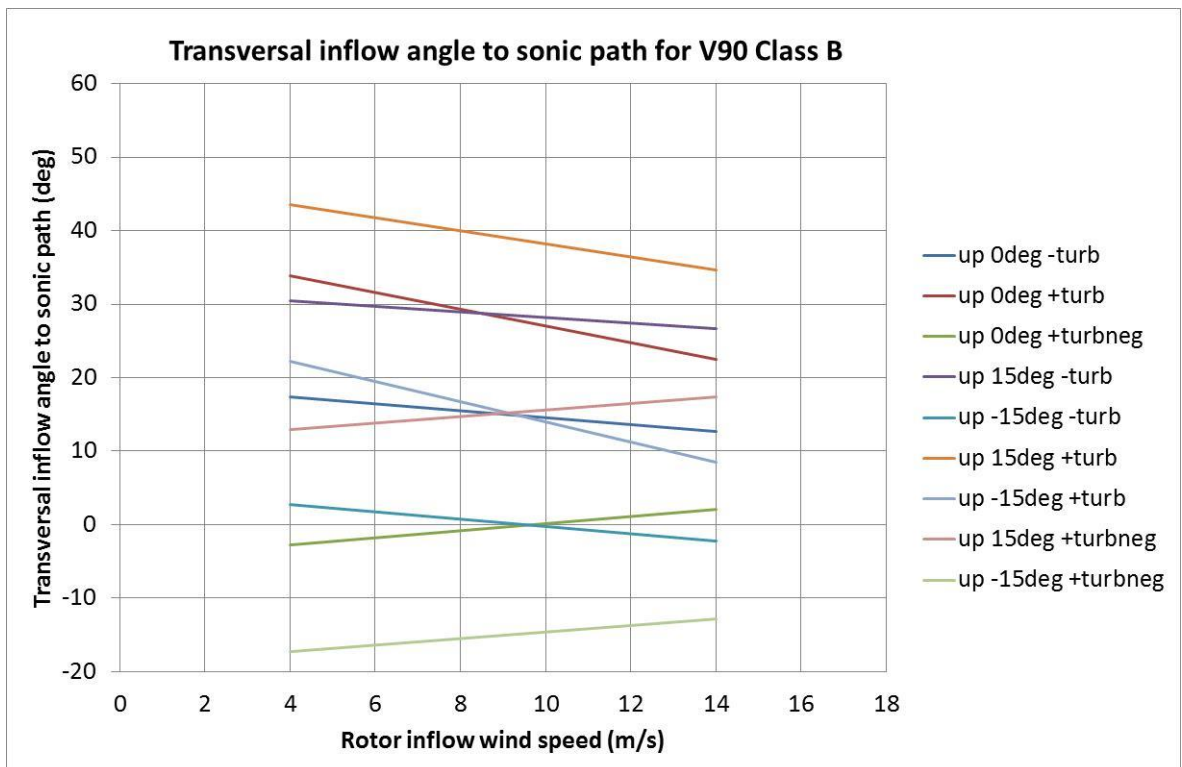


Figure 14 Lateral inflow angle variations on a sonic sensor on a V90 turbine for Class B variations

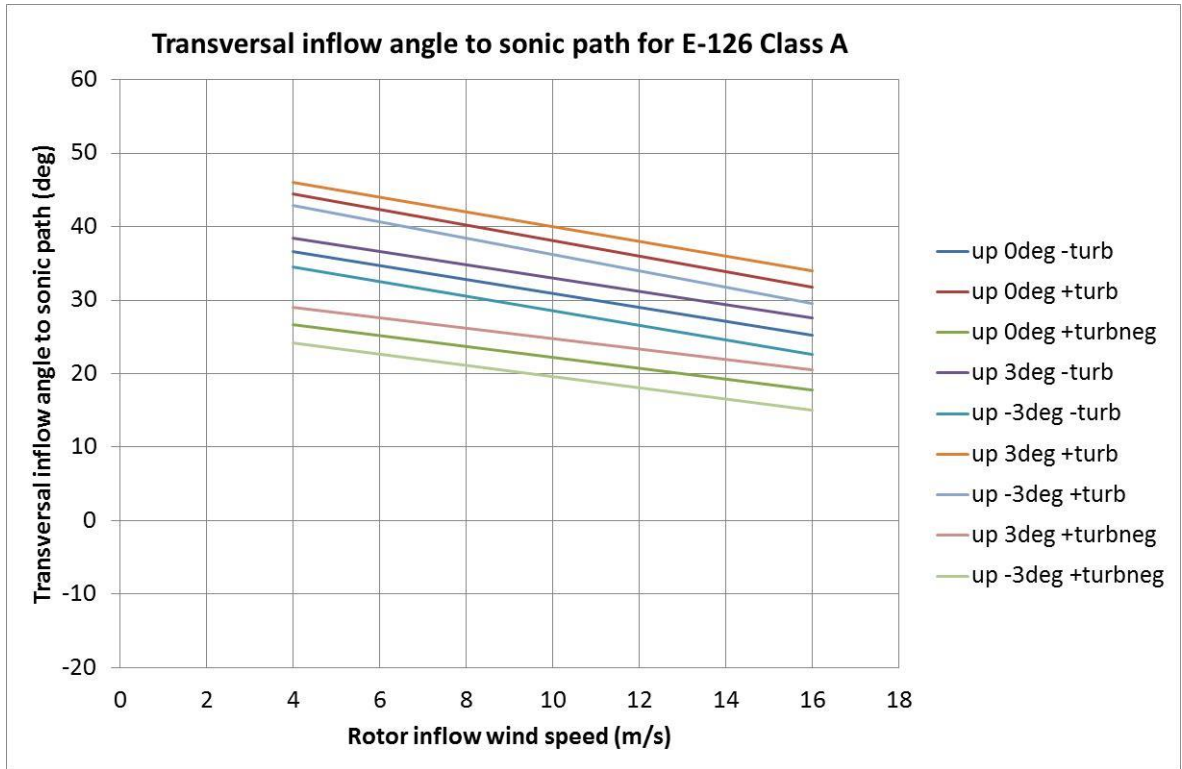


Figure 15 Lateral inflow angle variations on a sonic sensor on a E-126 turbine for Class A variations

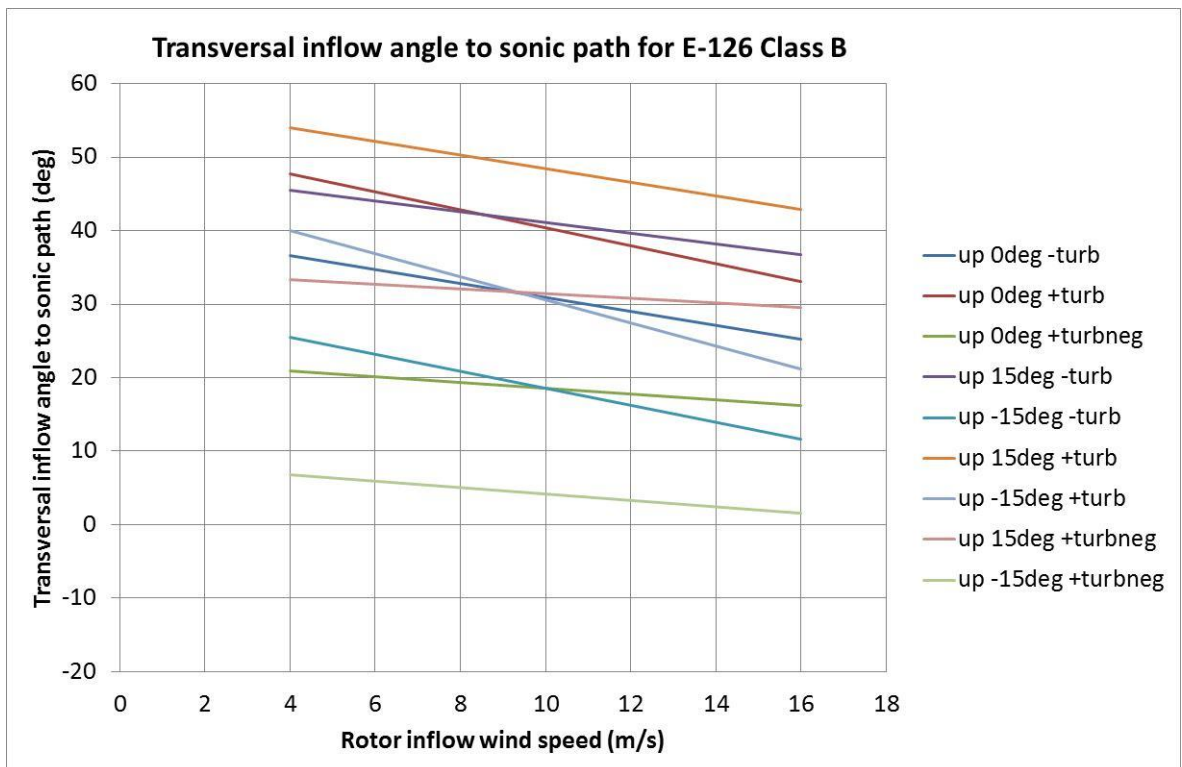


Figure 16 Lateral inflow angle variations on a sonic sensor on a E-126 turbine for Class B variations

With these significant lateral inflow angle variations during rotation the response of the sonic sensor to lateral inflow angles is very important. If the lateral inflow angle response is cosine shaped then the influence is zero. Otherwise, there will be a deviation that depends on the lateral inflow angle response.

The lateral inflow angle during operation is very different from the lateral angle of attack during stand still, where the angle is zero. This should be taken into account for the wind speed calibration method.

3.3.3 Sonic sensor lateral angular response

There are several wind tunnel tests available, for example [10] that show directional influence on sonic anemometers due to supporting structure and sonic sensor heads. The 35° tilt angle of the sonic sensor path does significantly reduce the basic influence of the sonic sensor heads on the flow in the sensor path. However, the arc tube supporting the sonic sensor heads influences the sonic sensor flow speed measurements.

The path wind speed as a function of the lateral inflow angle should ideally be cosine shaped. Deviations from this cosine shape, the lateral angular response, must be taken into account.

The lateral angular response should be determined and measured in a wind tunnel with the same setup as for wind tunnel calibration [8], see chapter 3.1.2. The mounting plate can be rotated around the supporting tube axis so that the center of the sonic sensor path is right above the axis. The flow directions may be set with preset inflow angles; alternatively with a very slow sweep:

- Lateral angles to sonic sensor (deg): 0, 2, 4, 6, 8, 10, 15, 20, 25, 30, 35, 40, 45, 50, 55, 60, 65, 70,

The response should be measured for tunnel wind speeds covering the range 4-16m/s, for example for 4, 8, 12 and 16m/s.

The rotation direction of wind turbines is almost always clockwise when the rotor is seen from the front. The inflow to the sonic sensor due to the rotation is thus coming from the left side when viewing the sonic sensor from the sensor foot. This corresponds to negative lateral inflow angles.

A lateral angular response was measured by Metek GmbH at 5 and 10m/s, see Figure 17. The measurements show an overspeeding topping at around 60° lateral inflow angle with a maximum of 2.5% deviation for negative angles and 5.5% for positive angles. The influence of wind speed is not seen to be significant.

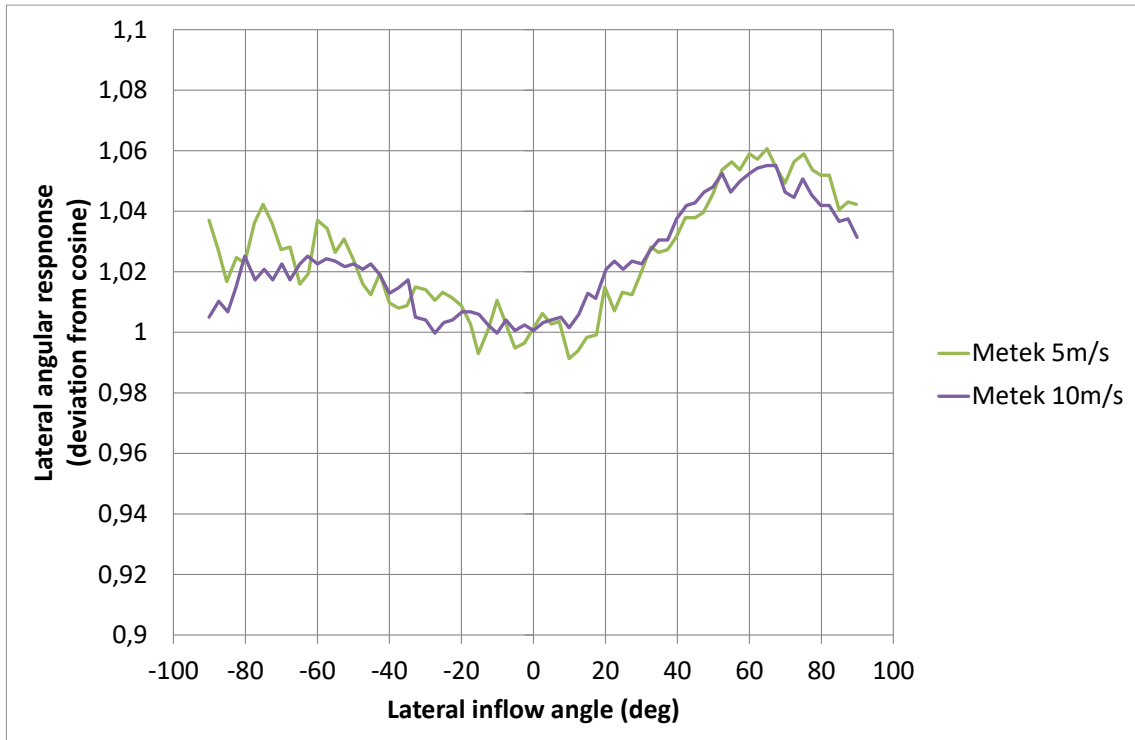


Figure 17 Lateral angular response measurement by Metek GmbH.

A measurement of the lateral angular response was also made in the accredited WindGuard wind tunnel. The measurements were performed with the mounting plate setup from [8], and for 4, 8, 12 and 16m/s wind speeds. Figure 18 shows the setup where the sonic sensor is yawed to have a negative lateral inflow angle. The measurements for each of the three sonic sensors are shown in Figure 19 to Figure 21. The results of sonic sensor 1 show very similar measurements as the Metek measurements but with a little more variations with wind speed. Sonic sensors 2 and 3 show more symmetric measurements, but with significantly different values for 4m/s. For sonic sensor 2 the values at 4m/s increases above 5% deviation and do not seem to have maxima around 60° inflow angles, while for sonic sensor 3 the values have maxima at 40° inflow angle and lies below all the other wind speeds. The reason for these variations is not known. There may be local geometry variations of the sonic sensors or the setup plate may have had a small variation in inflow angle while being rotated. Anyway, if the measurements on the three sonic sensors may be considered to express a statistical spreading of the characteristics the average of the three measurements can be used for fitting a deviation function. Figure 22 shows the measured average of the three sensors. The curves for the different wind speed are seen to fall very close and to show a symmetric pattern. Figure 23 shows the measured average of all sensors and all wind speeds together with a fitted curve. The maximum deviation is about 2.5% at about 50° lateral inflow angle. The fitted curve is expressed by:

$$\Delta c = 0.025 \cdot (\text{abs}(\sin(1.9\alpha)))^4 \quad (19)$$

Where α is the lateral inflow angle in radians



Figure 18 Setup of spinner anemometer on mounting plate according to [8] in WindGuard GmbH wind tunnel with a high lateral inflow angle

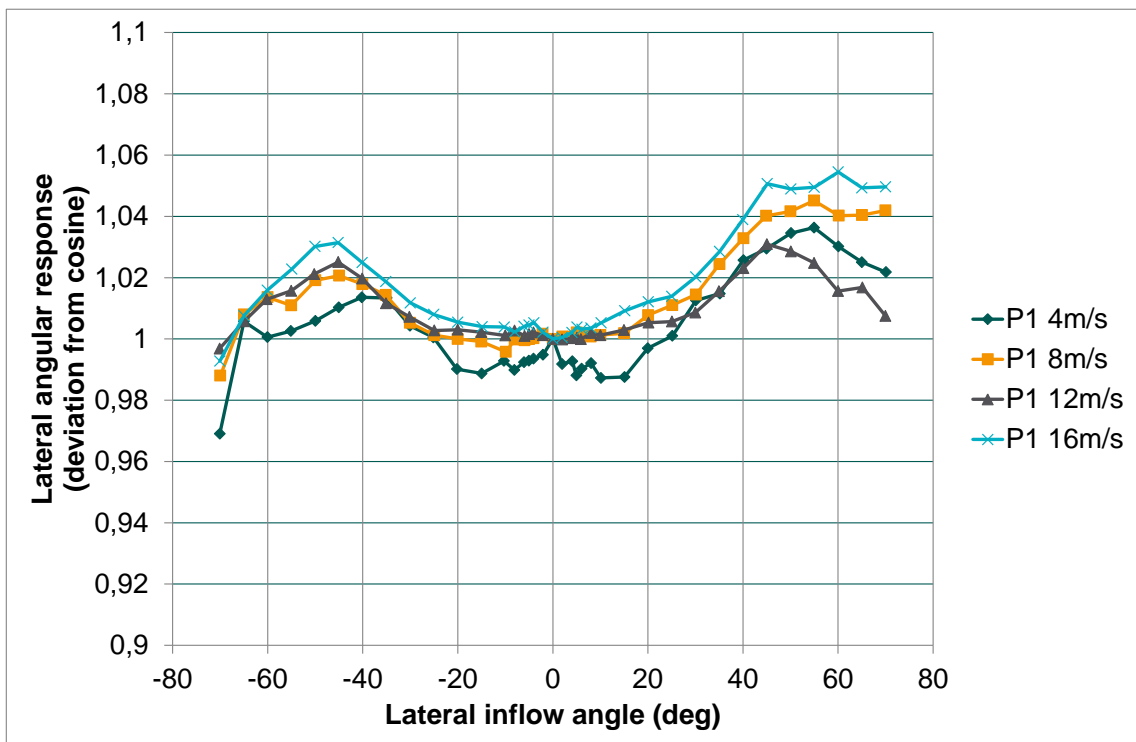


Figure 19 Lateral angular response of sonic sensor 1 measured in WindGuard GmbH wind tunnel

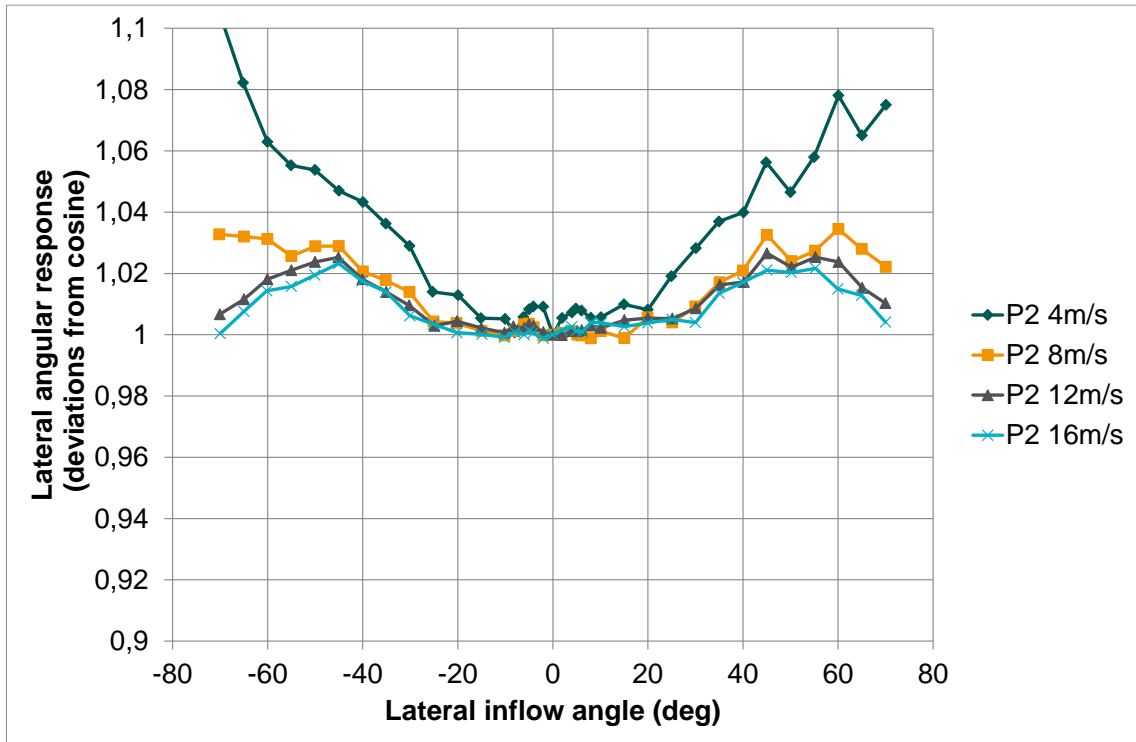


Figure 20 Lateral angular response of sonic sensor 2 measured in WindGuard GmbH wind tunnel

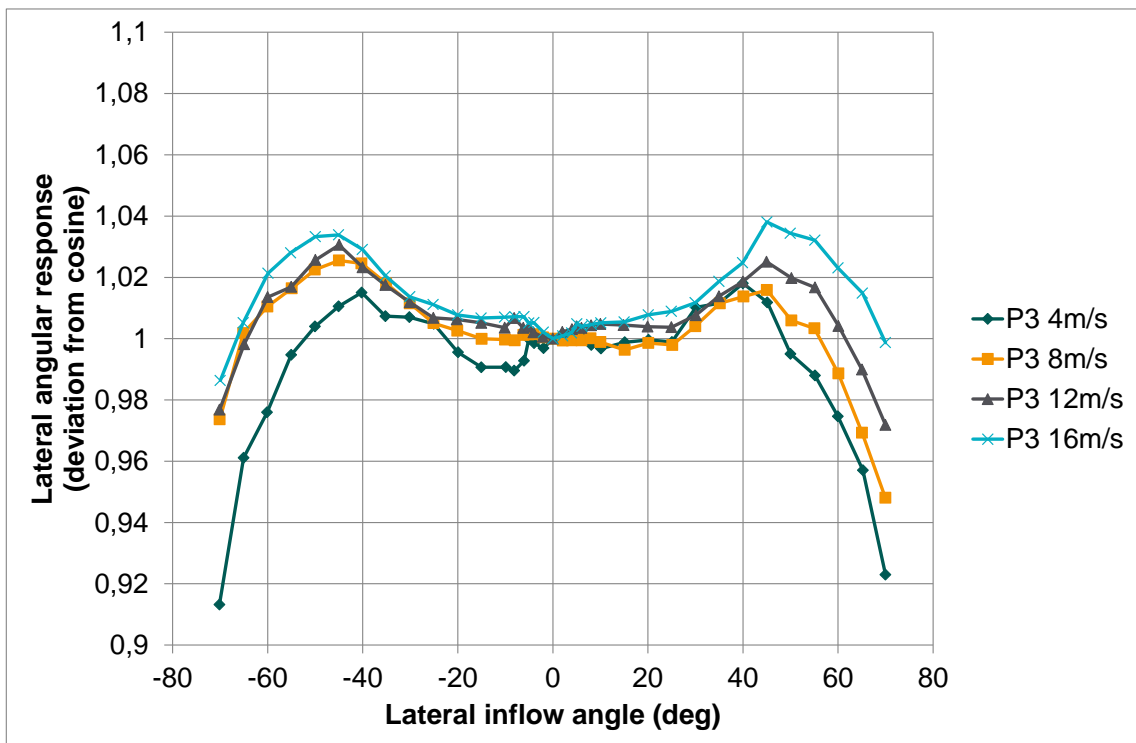


Figure 21 Lateral angular response of sonic sensor 3 measured in WindGuard GmbH wind tunnel

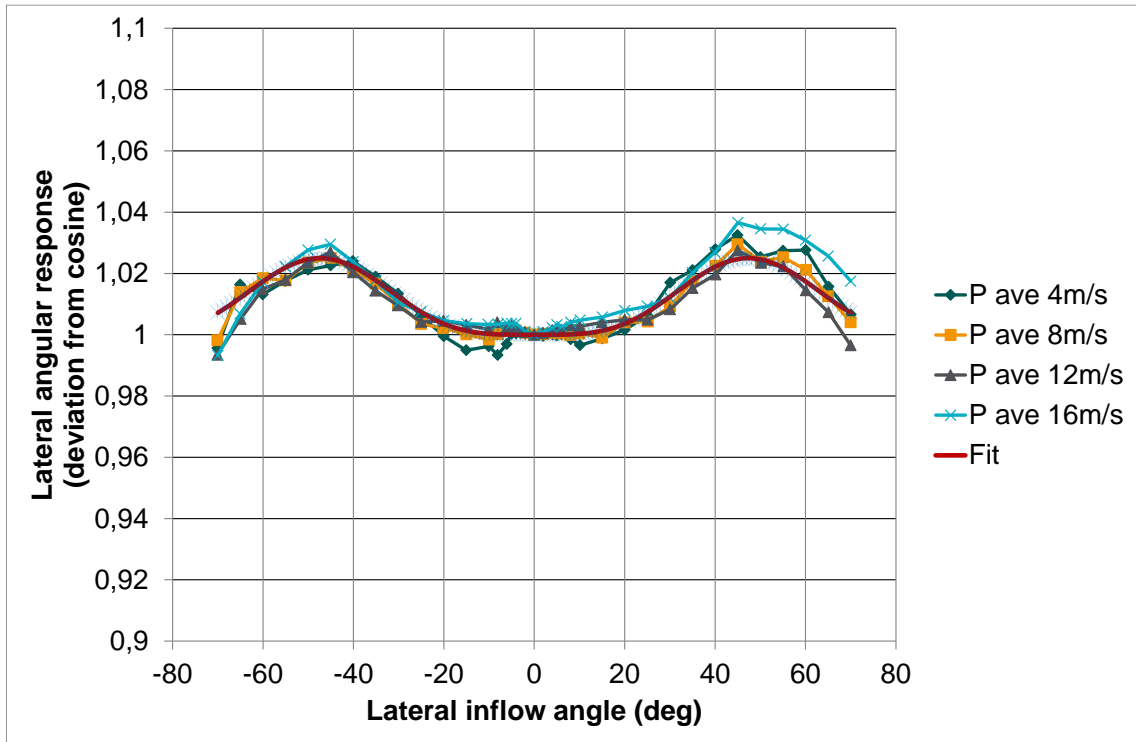


Figure 22 Average lateral angular response of all three sonic sensors at different wind speeds

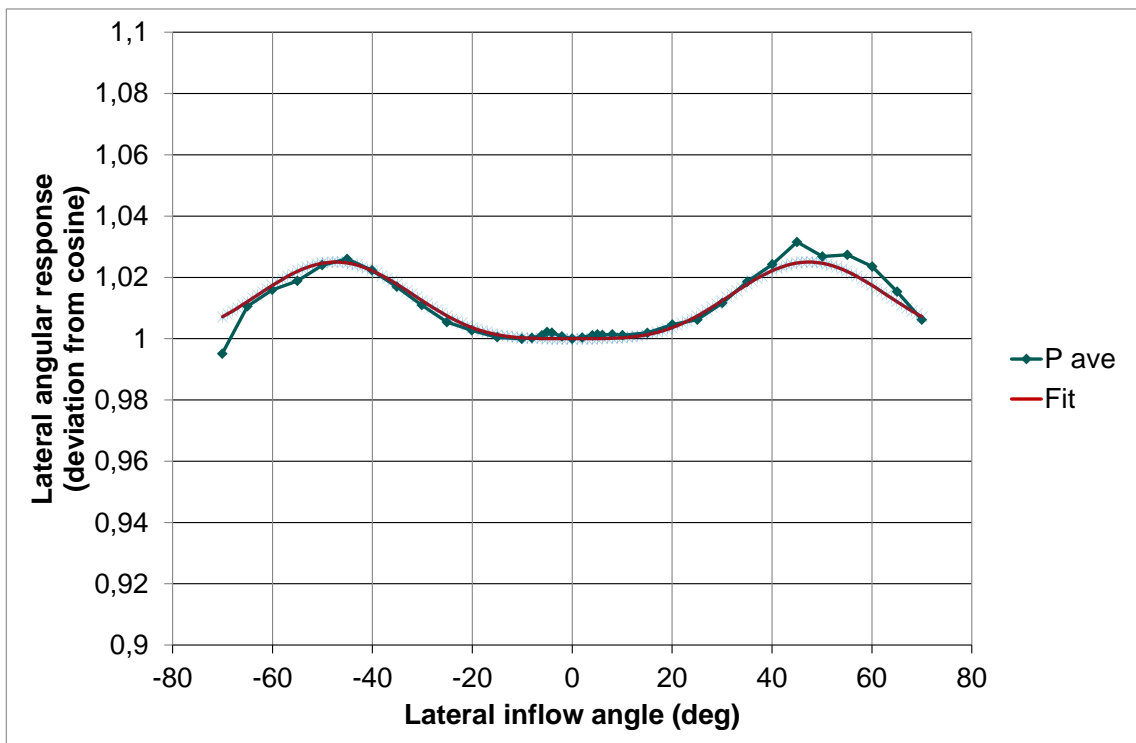


Figure 23 Average lateral angular response of all three sonic sensors and all four wind speeds. The fit applies to equation 19

3.3.4 Turbulence influence on uncertainty

A relevant question is if the sonic sensor is turbulence sensitive as the cup anemometer is. The cup anemometer is sensitive to turbulence because it is a dynamical mechanical device. The rotor is accelerated and decelerated with aerodynamic forces which over a 10min average time easily lead to systematic deviations. The turbulence influence on cup anemometers has been investigated in a wind tunnel with varying sinusoidal wind speed up to 3 Hz, and significant over-speeding has been registered. A similar investigation was been made on a 2D sonic anemometer, showing no influence on the sinusoidal wind speed variations in the wind tunnel [13]. This indicates that flow speed variations in the same direction on the sonic sensor do not seem to provide sensitivity to turbulence.

For directional sensitivity the influence on sonic sensors is different. The tilt responses of cup anemometers are normally not ideal cosine shaped and this has a significant impact on turbulence sensitivity. A sonic sensor has a similar response to flow angles as a cup anemometer has to tilt angles. This may especially be the case when the lateral angle varies as much as seen for the sonic sensors on a spinner anemometer.

The influence of turbulence on the spinner anemometer is therefore only significant through the lateral angular response of the sonic sensors. The atmospheric turbulence will give rise to variations of wind speeds in the sonic sensor paths and to variations in lateral inflow angles to the sonic sensors. These lateral inflow angle variations shall be added to the variations due to rotational speed, yaw misalignment and wind flow inclination angle to the rotor. The turbulence influence must thus be combined with other influences to find the overall response due to variations of lateral inflow angles during operation.

3.3.5 Determination of lateral inflow angle to sonic sensors

The lateral inflow angles to sonic sensors may be estimated with the sphere analogy. From the turbulent wind input on the rotor we will estimate the lateral inflow angles. The inflow wind speed to the spinner is assumed not to be rotated due to the rotor aerodynamics, and the lateral wind speed components are assumed to be constant over the spinner. With these assumptions it is a question about converting the inflow wind speeds to wind speed components in coordinate systems following each sonic sensor. The wind speed coordinate transformations are shown in the following figures. Definitions of inflow angle and tilt angles and transformation of wind speeds to a sloped flow is shown in Figure 24. Definitions of slope angle and tilt angle and conversion of inflow wind speed to sloped wind speed. The flow with a yaw misalignment is transformed to axial flow according to Figure 14, and the flow is then aligned vertically with the shaft axis in Figure 26. Finally, the lateral wind speed components are transformed to the local sonic sensor coordinate systems as shown in Figure 27. The coordinate shifts converts the inflow wind speeds to sonic sensors as follows.

From horizontal 10min artificial Mann-wind to sloped wind:

$$u_s = u_i \cos(\beta) - w_i \sin(\beta) \quad (20)$$

$$v_s = v_i \quad (21)$$

$$w_s = u_i \sin(\beta) + w_i \cos(\beta) \quad (22)$$

From sloped wind speed with yaw misalignment to axial directional flow:

$$u_g = u_s \cos(\gamma) - v_s \sin(\gamma) \quad (23)$$

$$v_g = u_s \sin(\gamma) + v_s \cos(\gamma) \quad (24)$$

$$w_g = w_s \quad (25)$$

From axial directional flow to axial aligned flow:

$$u_b = u_g \cos(\delta) - w_g \sin(\delta) \quad (26)$$

$$v_b = v_g \quad (27)$$

$$w_b = u_g \sin(\delta) + w_g \cos(\delta) \quad (28)$$

From axially aligned flow to lateral flow wind speeds at each sonic sensor:

$$w_{s1} = u_b \cos(\theta) - w_b \sin(\theta) \quad (29)$$

$$w_{s2} = u_b \cos(\theta + 2\pi/3) - w_b \sin(\theta + 2\pi/3) \quad (30)$$

$$w_{s3} = u_b \cos(\theta + 4\pi/3) - w_b \sin(\theta + 4\pi/3) \quad (31)$$

Now the lateral inflow angles may be determined by:

$$\alpha_{s1} = \text{atan}\left(\frac{\omega R + w_{s1}}{u_b}\right) \quad (32)$$

$$\alpha_{s2} = \text{atan}\left(\frac{\omega R + w_{s2}}{u_b}\right) \quad (33)$$

$$\alpha_{s3} = \text{atan}\left(\frac{\omega R + w_{s3}}{u_b}\right) \quad (34)$$

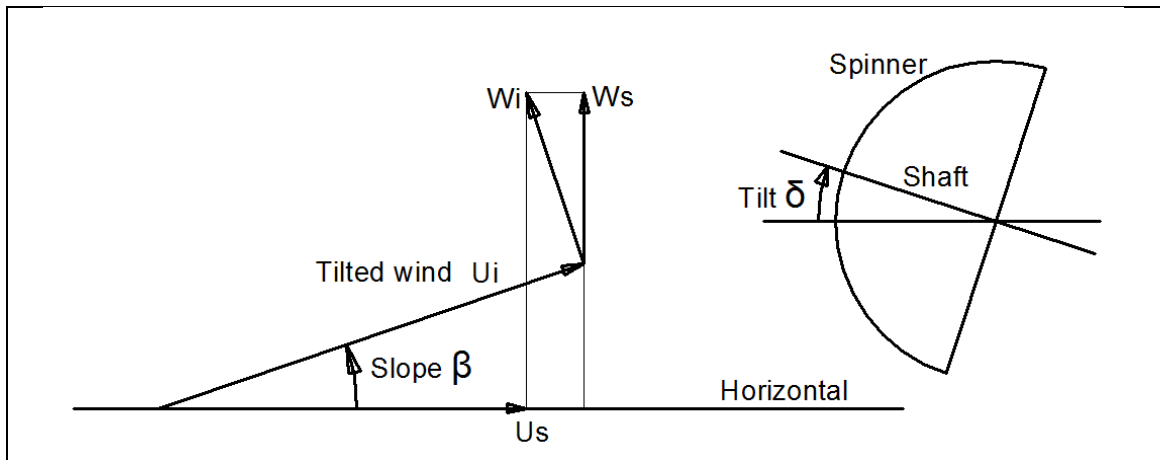


Figure 24 Definitions of slope angle and tilt angle and conversion of inflow wind speed to sloped wind speed, seen from the side

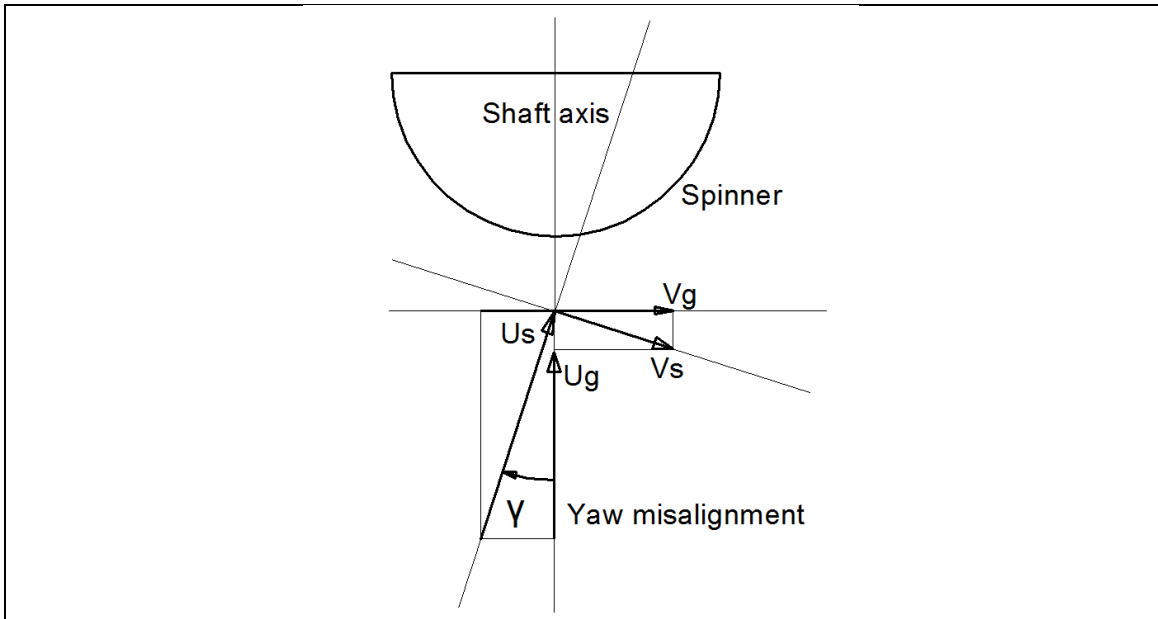


Figure 25 Definition of yaw misalignment direction and coordinate shift of wind components to shaft axis coordinate system, seen from above

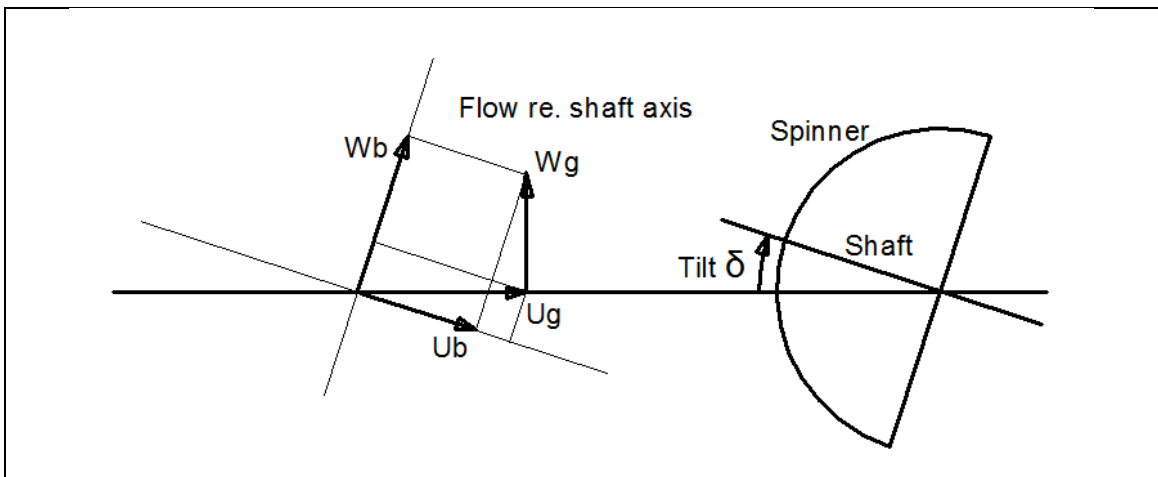


Figure 26 Coordinate shift to shaft axis coordinate system for finding lateral flow speed on sonic sensor due to wind input, seen from the side

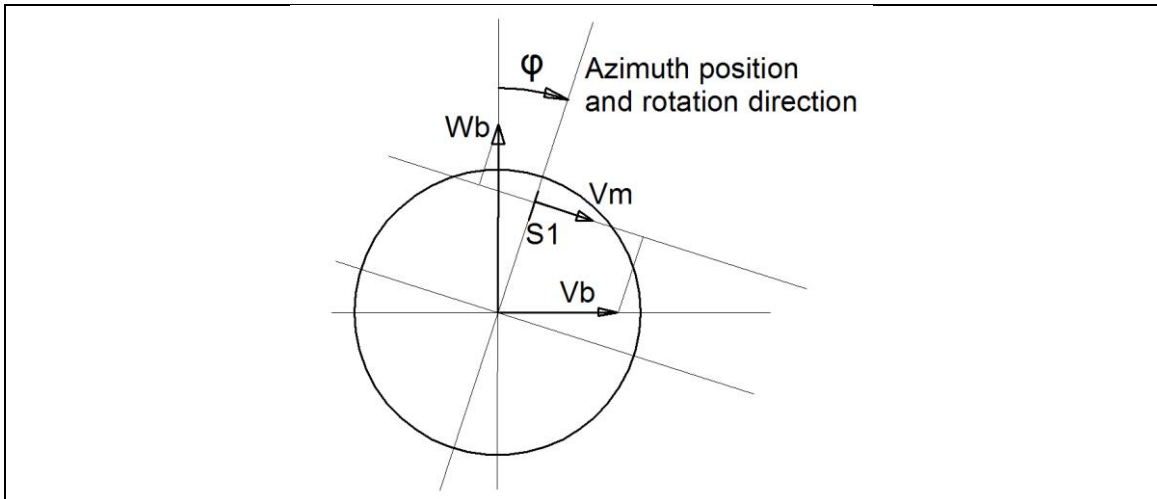


Figure 27 Conversion of winds in stationary shaft axis coordinate system to rotating shaft axis coordinate system and determination of lateral wind speed to sonic sensor 1, seen from the front. Lateral wind speed to sonic sensor 2 and 3 are determined in similar ways adding 120° and 240° to the azimuth position

3.3.6 Influence of vibrations on rotor azimuth position measurement

Rotor azimuth position is calculated from signals from the accelerometers mounted in the feet of the sonic sensors. The accelerometers are influenced by gravity, but also by accelerations of the spinner. Rotor rotation acceleration is cancelled out with the rotor azimuth position algorithm using three accelerometers. The nacelle vibrates along the shaft direction as well as sideways due to softness of the tower in tower bending. Vibrations in the vertical plane are limited due to stiffness in the vertical direction. Vibrations along the shaft direction are not influencing the accelerometers as the vibrations are perpendicular to the accelerometers. The most influential vibrations might therefore be lateral vibrations of the nacelle. However, local vibrations of the spinner surface also influence the accelerometers. As the accelerometers are mounted perpendicular to the spinner surface the up and down vibrations should not be important and merely the transversal vibrations should be important.

An example of a measured accelerometer signals is shown in Figure 28.

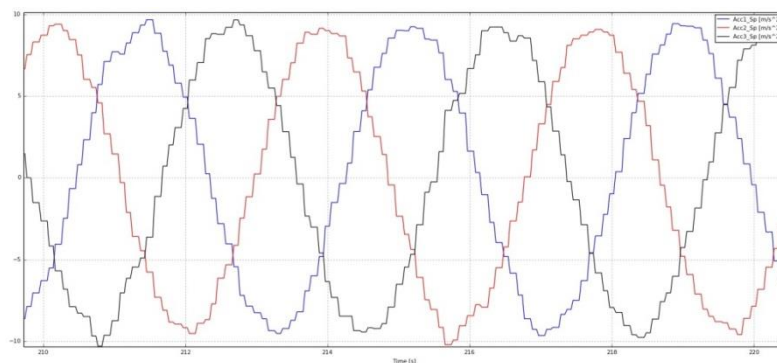


Figure 28 Measured accelerometer signals from three sonic sensors on a spinner anemometer (output frequency of sonic anemometer is 10Hz while sampling frequency is 35Hz)

The rotor azimuth position measurement may be simulated by adding a lateral sinusoidal vibration in the accelerometer equations:

$$P_1 = -G \sin \varphi + A_t + A_v \cos(\varphi) \sin(\omega_v t) \quad (35)$$

$$P_2 = -G \sin(\varphi + 2\pi/3) + A_t + A_v \cos(\varphi + 2\pi/3) \sin(\omega_v t) \quad (36)$$

$$P_3 = -G \sin(\varphi + 4\pi/3) + A_t + A_v \cos(\varphi + 4\pi/3) \sin(\omega_v t) \quad (37)$$

The influence of vibrations may be evaluated by using these equations in calculation of the spinner anemometer response. A simulation with a vibration frequency of 9Hz and an amplitude of 0.4m/s² is shown in Figure 29. The variations are seen to be significantly smaller than in Figure 28. However, the measurements in Figure 28 were made with 35Hz scanning on a 10Hz spinner anemometer output, which give the staircase type of signal which is not seen in Figure 29.

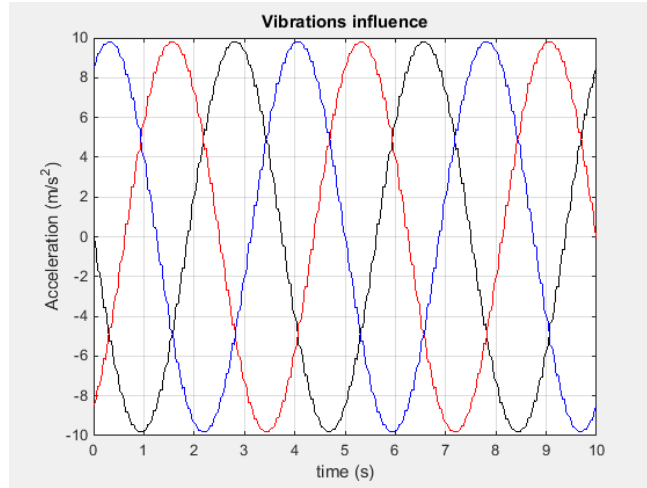


Figure 29 Simulated accelerometer signals from three sonic sensors with vibrations

3.3.7 Sonic sensor path temperature sensitivity uncertainty

The sonic sensors may be influenced by temperature. The sonic sensor path is elongated with increased temperature. The sensor arm is made of stainless steel which has a thermal expansion coefficient of $12 \cdot 10^{-6}/K$. For a temperature change of 20°C the expansion is 0.04mm, which for the sonic path length 160mm corresponds to a relative path length change of 0.024%.

The wind speed output is directly proportional to the path length as seen from the basis sonic sensor algorithm:

$$V = \frac{L}{2} \left(\frac{1}{t_1} - \frac{1}{t_2} \right) \quad (38)$$

However, temperature also changes the speed of sound as a function of the absolute temperature T :

$$c = 20.0470\sqrt{T} \quad (39)$$

This means that the time of flight is also changed. If we consider a change of the sonic sensor path length and a change of sonic speed we then get for the changed output wind speed V_{Δ} :

$$V_{\Delta} = \frac{L + \Delta L}{2} \left(\frac{1}{\frac{L + \Delta L}{c + \Delta c + V}} - \frac{1}{\frac{L + \Delta L}{c + \Delta c - V}} \right) = \frac{1}{2} (c + \Delta c + V - (c + \Delta c - V)) = V \quad (40)$$

Obviously, the output wind speed is the same as the actual wind speed, independent of temperature influence on path length and sonic speed. This means that uncertainties due to temperature influence may be neglected.

3.4 Other uncertainty components

3.4.1 Data acquisition system

The data acquisition system of spinner anemometer data is digital. No transmission losses are relevant for the measurements. The sonic sensor wind speed measurements are based on a 14bit analog to digital converter with a resolution of about 0.02m/s. The uncertainty on the horizontal 10min wind speed measurement is approximated as $u_{dNi} = 0.001/\sqrt{3} m/s$.

3.4.2 Use of default k constants

The uncertainty on the spinner anemometer measurements are influenced by the non-linear conversion algorithm. If the calibrations are inserted into the spinner anemometer box and the calibration path in Figure 31 is followed then no uncertainty need to be applied. If the default path in Figure 31 is used and the k_{1d} and k_{ad} values are used in the spinner anemometer box during measurements of 10min average values then an uncertainty must be added. Experience have shown that this uncertainty is very small.

3.4.3 Spinner geometry uncertainty

The geometry of the spinner is the basis for the air flow over the spinner and for the spinner anemometer to work as intended. Ideal rotational symmetric spinners with precisely positioned sonic sensors will provide the most accurate wind speed measurements when transferring nacelle transfer functions from one turbine to another. The spinner on the turbine where the NTF is measured will be the reference for other wind speed measurements on the same type of wind turbine. The precision of the geometry on the spinner is therefore important for the transfer of the NTF to another wind turbine. Deviations in spinner geometry should therefore be investigated in detail when an NTF is transferred to another turbine. The IEC61400-12-2 standard [7] is setting requirements for acceptable geometry variations in annex C. The mentioned geometry requirements within 100mm in deviations of the nacelle should be lowered significantly for geometry deviations of a spinner. The deviations in geometry from the reference spinner may be validated by photographic techniques where pictures of spinners with sonic sensors of the two turbines are compared by laying transparent photos over each other.

3.4.4 Rotor induction change

The measurement of the NTF is valid for the turbine under consideration. Criteria for the validity of an NTF are mentioned in [7]. If the wind turbine control is changed so that the induction in the center is changed then the NTF may not be valid any more. The same can be said if the blades are changed, for example by applying vortex generators on the inboard part of the blades. For each measurement campaign one should look out for induction changes that could reduce the validity of the NTF.

3.4.5 Limitations of conversion algorithm

The conversion algorithm is a theoretical assumption for the relations between measured sonic sensor wind speeds and the overall horizontal wind speed and inflow angles. The theoretical assumption seems to work quite well as documented by the wind tunnel measurements in [1]. However, the wind tunnel measurements showed a sonic sensor flow distortion effect, which

was evident in a dip in the sinusoidal wind speed curves. This flow distortion effect was in later designs eliminated by increasing the sonic sensor path angles to 35°. The conversion algorithm assumption may be valid for normal operational inflow angles while for larger inflow angles the aerodynamic flow over the spinner will deviate because of the spinner geometry and the flow will be separated when the sonic sensors come into the wake of the spinner. This may be important for the conditions during calibration of the k_α constant, but not for calibration of the k_1 constant. Only a small uncertainty should be considered for the measurement uncertainty of U_{hor} .

3.4.6 Seasonal variability

The standard [7] requires an uncertainty due to seasonal variability being added to the NTF uncertainty budget. The seasonal variability is an uncertainty component that is not part of the measurement uncertainty. It is an uncertainty component that is added when the measured NTF is extrapolated to be representative for a whole year. The uncertainty is proposed set to 2% in [7]. However, the 2% uncertainty may vary significantly from case to case. As the NTF is a relation between two measurements at the same hub height, the mast and the spinner anemometer, the influence due to atmospheric variations may be somewhat lower if the measurement is made in very flat terrain, Experience on seasonal variability of NTF's could be gained from successive NTF measurements during all seasons of the year with the spinner anemometer. When an NTF is transferred to power curve measurements at another season, the seasonal variability has to be taken into account.

In [7] the measurement of a power curve, NPC, is also required to add a seasonal variability. In this case the seasonal variability is considered for a generic power curve, while for a site specific power curve the uncertainty is questionable. For a measurement campaign lasting a few months the variability over a whole year is not known. Only in the case where a measurement campaign of a power curve of a few months needs to be made representative to a whole year or the whole life time of a wind turbine, this uncertainty on extrapolation of measured data should be added. Indeed, the uncertainty on seasonal variability in [7] is put on the power in the power curve since it represents the variability in power due to vertical shear and veer and is not due to the point wind speed measurement made by the spinner anemometer. This, of course, depends on how the power curve is defined with a hub height point wind speed measurement or an equivalent wind speed measurement taking care of vertical wind speed shear and veer.

The IEC standard [7] additionally mentions two more uncertainty components on the NPC, the variation to rotor inflow (2%) and the turbulence effect on averaging and binning (1%). These uncertainties are again mentioned for generic power curves, while for site specific power curves the uncertainties may be considered questionable.

3.4.7 Flow distortion due to terrain

The standard [7] requires an uncertainty due to influence of the terrain on the nacelle (upflow, turbulence, shear), to account for its effect on the correlation between nacelle wind speed and free wind speed measured during the NTF and the power curve. This uncertainty is connected with the sensitivity of the nacelle anemometer due to upflow, turbulence and shear. However, at the spinner, there has no been identified any flow distortion due to upflow, turbulence and shear. This term is therefore considered negligible for spinner anemometers.

3.5 Summary on uncertainty components

The uncertainty components are all summarized in Table 2, where the designation of each component follows IEC61400-12-2 [7] as much as possible. Table 2 also lists the parameter in the conversion algorithm on which the uncertainty component has an influence. Table 3 lists the sensitivity factors and assumed correlation coefficients.

The uncertainty from the wind tunnel calibrations ($u_{N1,V1,i}, u_{N1,V2,i}, u_{N1,V3,i}$) are assumed fully correlated if they are all calibrated in the same batch. All mounting uncertainties are considered uncorrelated because the mounting of sensors is a rather individual process. All other measurement uncertainties are considered uncorrelated as well in combination of the uncertainties.

Table 2 Uncertainty components related to spinner anemometer measurements according to IEC61400-12-2

Uncertainty component	Designation*	Influence on
1. Calibrations		
• Wind tunnel calibration [m/s]	$u_{N1,V1,i}, u_{N1,V2,i}, u_{N1,V3,i}$	V_1, V_2, V_3
• Angular calibration k_α [%]	u_{N41i}	k_α
• Wind speed calibration k_1 [%]	u_{N42i}	k_1
2. Operational characteristics	u_{N2i}	
• Inflow angle to rotor [°]	u_{N21i}	U_{hor}
• Turbulence [%]	u_{N22i}	U_{hor}
• Yaw misalignment [°]	u_{N23i}	U_{hor}
• Accelerometer vibrations [m/s ²]	u_{N24i}	P_1, P_2, P_3
• Shaft tilt angle increase [°]	u_{N25i}	δ
3. Sonic sensor mounting	u_{N3i}	
• Longitudinal position [m]	u_{N31i}	V_1, V_2, V_3
• Directional uncertainty [°]	u_{N32i}	V_1, V_2, V_3
• Sonic path angle [°]	u_{N33i}	V_1, V_2, V_3
• Lateral position [m]	u_{N34i}	$V_1, V_2, V_3, P_1, P_2, P_3,$
• Accelerometer alignment [°]	u_{N35i}	$P_1, P_2, P_3,$
4. Other uncertainty components		
• Data acquisition system [m/s]	u_{dNi}	U_{hor}
• Use of default k constants [%]	u_{N5i}	U_{hor}
• Spinner geometry (PC2) [%]	u_{N6i}	U_{hor}
• Rotor induction change [%]	u_{N7i}	U_{hor}
• Limitations on algorithm [%]	u_{N8i}	U_{hor}

* Index i relates to wind speed bin and numbers refer to IEC61400-12-2 uncertainty designations where possible

** PC2 relates to transfer of NTF to another wind turbine

Table 3 Sensitivity factors and correlation coefficients for uncertainty components related to spinner anemometer measurements according to IEC61400-12-2

Uncertainty component	Designation	Sensitivity factors on U_{hor}	Correlation coefficients
1. Calibrations			
• Wind tunnel calibration	$u_{N1,V1,i}, u_{N1,V2,i}, u_{N1,V3,i}$	$\left(\frac{\partial F}{\partial V_1}\right), \left(\frac{\partial F}{\partial V_2}\right), \left(\frac{\partial F}{\partial V_3}\right)$	1, 1, 1
• Angular calibration k_α	u_{N41i}	$\left(\frac{\partial F}{\partial k_\alpha}\right)$	0
• Wind speed calibration k_1	u_{N42i}	$\left(\frac{\partial F}{\partial k_1}\right)$	0
2. Operational characteristics	u_{N2i}	1	0
• Inflow angle to rotor			
• Turbulence			
• Yaw misalignment			
• Accelerometer vibrations			
• Shaft tilt angle increase			
3. Sonic sensor mounting	u_{N3i}		
• Longitudinal alignment	$u_{N31,V1,i}, u_{N31,V2,i}, u_{N31,V3,i}$	$\left(\frac{\partial F}{\partial V_1}\right), \left(\frac{\partial F}{\partial V_2}\right), \left(\frac{\partial F}{\partial V_3}\right)$	0
• Directional alignment	$u_{N32,V1,i}, u_{N32,V2,i}, u_{N32,V3,i}$	$\left(\frac{\partial F}{\partial V_1}\right), \left(\frac{\partial F}{\partial V_2}\right), \left(\frac{\partial F}{\partial V_3}\right)$	0
• Sonic path angle	$u_{N33,V1,i}, u_{N33,V2,i}, u_{N33,V3,i}$	$\left(\frac{\partial F}{\partial V_1}\right), \left(\frac{\partial F}{\partial V_2}\right), \left(\frac{\partial F}{\partial V_3}\right)$	0
• Lateral position alignment	$u_{N34,V1,i}, u_{N34,V2,i}, u_{N34,V3,i}$	$\left(\frac{\partial F}{\partial V_1}\right), \left(\frac{\partial F}{\partial V_2}\right), \left(\frac{\partial F}{\partial V_3}\right)$	0
	$u_{N34,P1,i}, u_{N34,P2,i}, u_{N34,P3,i}$	$\left(\frac{\partial F}{\partial P_1}\right), \left(\frac{\partial F}{\partial P_2}\right), \left(\frac{\partial F}{\partial P_3}\right)$	0
• Accelerometer alignment	$u_{N35,P1,i}, u_{N35,P1,i}, u_{N35,P1,i}$	$\left(\frac{\partial F}{\partial P_1}\right), \left(\frac{\partial F}{\partial P_2}\right), \left(\frac{\partial F}{\partial P_3}\right)$	0
4. Other uncertainty components			
• Data acquisition system	u_{dNi}	1	0
• Use of default k constants	u_{N5i}	1	0
• Spinner geometry	u_{N6i}	1	0
• Rotor induction change	u_{N7i}	1	0
• Limitations on algorithm	u_{N8i}	1	0

4. Modelling the measurand – combination of uncertainties

The combination of the uncertainties starts with the Guide to the Uncertainty in Measurements [11]. The measurand, or the output quantity of the spinner anemometer, is the horizontal wind speed U_{hor} . The input quantity measurements are the sonic sensor wind speeds and the accelerometer measurements. Any uncertainty component is related to these input quantities. The relationship of the spinner anemometer conversion algorithm relates the input quantities to the output quantity through the conversion algorithm. This is the basis for modeling of the measurand according to GUM.

4.1 Combination of uncertainties according to GUM

In order to calculate the uncertainty in U_{hor} , which is a function of the measured variables $V_1, V_2, V_3, k_1, k_\alpha, \delta, P_1, P_2,$ and P_3 , the uncertainty sources of the nine variables are modelled as additive variables ($x_1, \dots, x_j, \dots, x_N$) of zero average and a given standard deviation, where $N = \sum_{i=1}^9 n_j$ and n_j are the number of uncertainty components in the j^{th} measured variable ($V_1, V_2, V_3, k_1, k_\alpha, \delta, P_1, P_2,$ or P_3). Then we can express U_{hor} as a function of the nine variables as follows:

$$U_{hor} = F(V_1, V_2, V_3, k_1, k_\alpha, \delta, P_1, P_2, P_3) = f(x_1, \dots, x_j, \dots, x_N) \quad (41)$$

Using GUM [11] the combined uncertainty in the horizontal wind speed can in general be calculated by:

$$u^2(U_{hor}) = \sum_{i=1}^N \sum_{j=1}^N \left(\frac{\partial f}{\partial x_i} \right) \left(\frac{\partial f}{\partial x_j} \right) u(x_i) u(x_j) r(x_i, x_j) \quad (42)$$

where x_i and x_j are the standard uncertainties of the variables modelling the i^{th} and j^{th} uncertainty sources, and $r(x_i, x_j)$ is the correlation coefficient of those two variables. The factors $c_j = \left(\frac{\partial f}{\partial x_j} \right)$ are the sensitivity coefficients, and all the uncertainty sources associated to the same measured variable have the same sensitivity coefficient. For example, for all x_j associated with V_1 , $c_j = \left(\frac{\partial f}{\partial x_j} \right) = \left(\frac{\partial F}{\partial V_1} \right)$.

4.2 Modeling of the measurand according to GUM

The horizontal wind speed, U_{hor} , is obtained through the backwards conversion algorithm (see chapter 2.2.1) from the wind speed components in the fixed nacelle coordinate system:

$$U_{hor} = \sqrt{U_x^2 + U_y^2} \quad (43)$$

where U_x and U_y are derived from the wind speed components $U_{z,s}, U_{y,s}, U_{x,s}$ in the fixed shaft coordinate system:

$$U_x = U_{x,s} \cos \delta + U_{z,s} \sin \delta \quad (44)$$

$$U_y = U_{y,s} \quad (45)$$

$$U_z = U_{z,s} \cos \delta - U_{z,s} \sin \delta \quad (46)$$

These components can be expressed in terms of the vector wind speed U , the inflow angle relative to the shaft axis α and the flow stagnation azimuth position measured by the spinner anemometer θ , together with the rotor azimuth position φ and the shaft tilt angle δ .

$$U_x = U \cos \alpha \cos \delta - U \sin \alpha \cos(\varphi + \theta) \quad (47)$$

$$U_y = -U \sin \alpha \sin(\varphi + \theta) \quad (48)$$

Substituting U with the expression in equation 5 we obtain:

$$U_{hor} = \frac{V_{ave}}{k_1} \sqrt{(\cos \delta - \tan \alpha \cos(\varphi + \theta) \sin \delta)^2 + (\tan \alpha \sin(\varphi + \theta))^2} \quad (49)$$

The variables U_{hor} , α and θ contain a certainty degree of correlation between them, since they are obtained from the combination of V_1 , V_2 , V_3 , k_1 and k_α , as shown in equations 4, 6 and 29:

$$\theta = \arctan\left(\frac{V_2 - V_3}{\sqrt{3}(V_1 - V_{ave})}\right) + \pi \quad (50)$$

Since the uncertainties of V_1 , V_2 , V_3 , k_1 and k_α can be evaluated separately, U_{hor} can finally be expressed as follows:

$$U_{hor} = \frac{1}{k_1} \frac{1}{3} (V_1 + V_2 + V_3) \quad (51)$$

$$\sqrt{\left(\cos \delta - k_\alpha \frac{\sqrt{(2V_1 + V_2 + V_3)^2 + \frac{1}{3}(V_2 - V_3)^2}}{(V_1 + V_2 + V_3)} \cos\left(\varphi + \arctan\left(\frac{\sqrt{3}(V_2 - V_3)}{2V_1 + V_2 + V_3}\right) + \pi\right) \sin \delta \right)^2 + k_\alpha^2 \frac{(2V_1 + V_2 + V_3)^2 + \frac{1}{3}(V_2 - V_3)^2}{(V_1 + V_2 + V_3)^2} \sin^2\left(\varphi + \arctan\left(\frac{\sqrt{3}(V_2 - V_3)}{2V_1 + V_2 + V_3}\right) + \pi\right)}$$

The rotor azimuth position angle φ is obtained from the positions measured by the three accelerometers. Using formulas 10 to 12 it can be substituted by:

$$\varphi = \arctan\left(\frac{(2P_1 - P_2 - P_3)/3G}{(P_2 - P_3)/\sqrt{3}G}\right) \quad (52)$$

So, U_{hor} can be finally expressed as follows:

$$U_{hor} = \frac{1}{k_1} \frac{1}{3} (V_1 + V_2 + V_3) \quad (53)$$

$$\sqrt{\left(\cos \delta - k_{\alpha} \frac{\sqrt{(2V_1 + V_2 + V_3)^2 + \frac{1}{3}(V_2 - V_3)^2}}{(V_1 + V_2 + V_3)} \right)^2 + \cos^2 \left(\arctan \left(\frac{2P_1 - P_2 - P_3}{3G} \right) + \arctan \left(\frac{\sqrt{3}(V_2 - V_3)}{2V_1 + V_2 + V_3} \right) + \pi \right) \sin^2 \delta + k_{\alpha}^2 \frac{(2V_1 + V_2 + V_3)^2 + \frac{1}{3}(V_2 - V_3)^2}{(V_1 + V_2 + V_3)^2} + \sin^2 \left(\arctan \left(\frac{(2P_1 - P_2 - P_3)/3G}{(P_2 - P_3)/\sqrt{3}G} \right) + \arctan \left(\frac{\sqrt{3}(V_2 - V_3)}{2V_1 + V_2 + V_3} \right) + \pi \right)}$$

The different uncertainty sources on the output quantity U_{hor} are based on the input quantities, the variables $V_1, V_2, V_3, k_1, k_{\alpha}, \delta, P_1, P_2,$ and P_3 . All uncertainty components could be derived for these variables (or U_{hor} for operational uncertainties) and then be combined to the output quantity through sensitivity factors. This, however, will be extremely difficult by use of the ordinary GUM method. The variables are all varying significantly during operation of the wind turbine. It would be extremely difficult to determine sensitivities for each uncertainty component for all the relevant varying operational conditions.

Sources of uncertainty may affect several variables simultaneously, and thus affect uncertainty on U_{hor} in a rather complex way. The ordinary GUM approach is thus not a viable solution for the combination of uncertainties.

4.3 Overall simulation approach

Another approach for the uncertainty analysis of the spinner anemometer is proposed. This approach includes simulation of full 10min operation of the spinner anemometer in the wind and includes the full conditions during operation, and includes all necessary dependencies. For each uncertainty component the output of a full 10min operation can be derived for the horizontal wind speed. The influence of each uncertainty component can be derived without any of the other uncertainty components being applied. By simulation of the influence of all influential parameters directly to represent the uncertainty on the horizontal wind speed the sensitivity factors may all be set equal to one in combining the uncertainty components.

The lateral angular response is a built-in characteristic of the sonic sensor and has an influence as a systematic deviation of the measurements. The vibrations of the spinner and the tilting increase of the rotor shaft at higher wind speeds also have systematic influences on all measurements. The lateral angular response, vibration of the spinner and the tilt increase are therefore included in all simulations.

The environmental and operational conditions for the k_1 /NTF calibration and for wind speed measurement campaigns for power curves must be considered. The classification approach for cup anemometers in IEC61400-12-1, using class A, B and S environmental conditions, may here be used for the operational influence cases. For the k_1 /NTF reference calibration conditions the average operational conditions are used for reference deviations. For a

measurement campaign a class A or B may be used, or where the climate conditions are known, a class S may be used.

4.3.1 Operational conditions

The operational conditions of the spinner anemometer, derived from Table I.1 in [6], are shown in Table 4.

Table 4 Operational conditions for spinner anemometer uncertainty calculations

	Class A Terrain meets requirements in [6]	Class B Terrain does not meet requirements in [6]	Class S Special class with user defined ranges
	Range	Range	Range
Wind speed V[m/s]	4 to 16	4 to 16	4 to 16
Turbulence intensity	0,03 to 0,12 + 0,48/V	0,03 to 0,12 + 0,96/V	User defined
Turbulence structure $\sigma_U/\sigma_V/\sigma_W$	1/0,8/0,5*	1/0,8/0,5*	User defined or 1/0,8/0,5*
Average flow inclination angle (°)	-3 to 3	-15 to 15	User defined
Yaw misalignment (°)	-5 to 5	-10 to 10	User defined
Rotational speed (rpm)	As a function of wind speed	As a function of wind speed	As a function of wind speed
Tilt and tilt angle increase (°)	As a function of wind speed	As a function of wind speed	As a function of wind speed
Spinner vibrations	User defined	User defined	User defined
Lateral angular response	Wind tunnel measurement	Wind tunnel measurement	Wind tunnel measurement

4.3.2 Simulation model

A Matlab code was developed to simulate the influence of the uncertainty components. The application and propagation of uncertainties are described in Figure 31. The artificial wind input is generated by the Mann code [12], also used in cup anemometer classification [6]. The slope is added to the wind file and then a yaw misalignment is added. The reference wind conditions, U_{hor} , γ and β , are then derived from the wind file and the 10min average values are derived. The reference wind conditions are added individual deviations due to uncertainties on the calibrations k_1 and k_α , deviation on tilt angle and the individual azimuthal deviations on sonic sensors. These wind conditions are now the conditions that the spinner anemometer sensors “see”. The sonic sensor flow speeds are then derived with the inverse transformation. Uncertainties due to mounting and wind tunnel calibration are then added to the sonic sensor wind speeds and the accelerometer measurements to derive “measured V and P values”. The wind conditions are then derived for the default path and the calibrated path with the direct transformation with either the default k values or the calibrated k values. When the default k values are monitored, the 10min average value is calculated and then converted with the

inverse and direct transformations to the calibrated 10min average values. For the calibrated path the 10min average values are calculated directly. The differences to the reference wind conditions are then derived for the two different paths.

Note that for the default path, where the wind tunnel calibration values are not applied in the spinner anemometer box, the calibration values, normalized to the 35° sonic sensor path, have to be applied on the 10min sonic sensor wind speed values between the reverse and direct transformations. For the calibrated path the wind tunnel calibration, normalized to the 35° sonic sensor path, has to be applied in the spinner anemometer box.

4.3.3 Derivation of individual uncertainties

Uncertainties connected with uncertainty components in the measurements should only be applied once. We distinguish between the calibration campaign of k_1 /NTF and measurement campaigns, like wind measurements or power curve measurements. The average operational conditions under which the calibration of k_1 /NTF is made, are considered reference conditions for derivation of individual uncertainties. Deviations in U_{hor} by model calculations of the spinner anemometer characteristics for these reference calibration conditions are reference values for the calculation of the influence of individual uncertainty components. The operational conditions for measurement campaigns of wind or power curves are not in the same way referred to the reference calibration conditions as the reference condition is just one of the conditions considered.

Determination of the uncertainties is made according to Figure 30. The deviations in U_{hor} for each wind speed due to average calibration operation conditions are determined in 1). The calibration operational conditions may for example be: average turbulence 10%, inflow slope 0°, tilt 6° plus adding 1° for increasing wind speed and 3° yaw misalignment. Lateral angular response and spinner vibrations are included in all calculations.

The deviations due to calibration and mounting uncertainties are determined individually by applying them to the simulations. The deviations from the reference simulations are then extracted, and each component is in this way expressed as an uncertainty in U_{hor} .

SA uncertainty combination

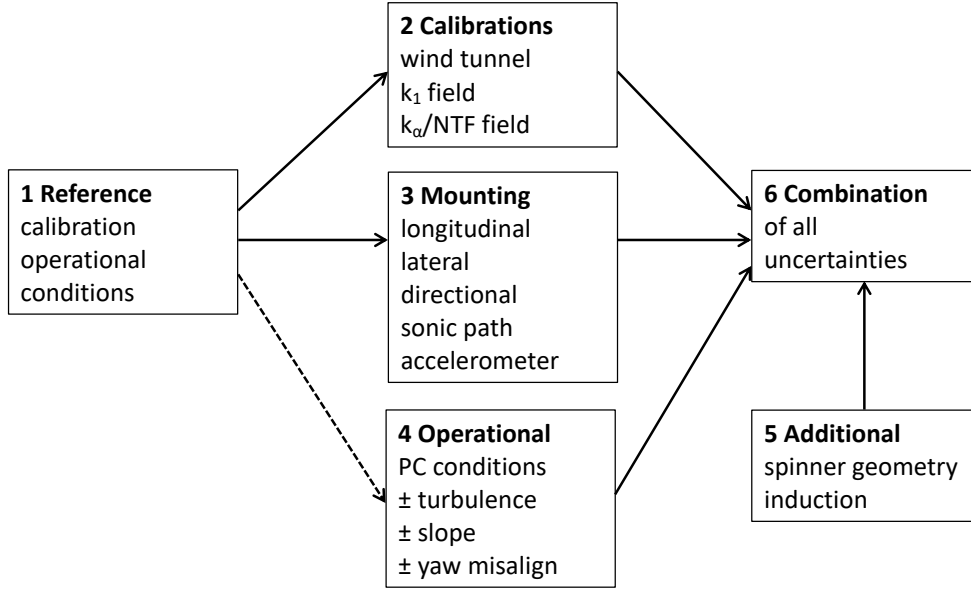


Figure 30 Combination of all uncertainty components. The reference operational condition 1 is part of the operational conditions in 4 and thus has a dashed line

4.3.4 Uncertainties due to operational characteristics

The operational conditions must be considered for the actual wind conditions for the campaign measurements. These may be the same conditions as for the calibration of k_1 /NTF.

The different combinations of the operating condition are simulated. Following the procedure in [6] on determination of classification index, the resulting envelope for the obtained deviations of all simulated cases for the input wind speed range has the following expression:

$$e_i = \pm \frac{k}{100} (5m/s + 0.5V_i) \quad (54)$$

where k is the class index number and V_i is the input wind speed. Assuming a rectangular frequency distribution of the errors due to different operational conditions, the resulting uncertainty due to operational characteristics can be expressed as:

$$u_{N2i} = \frac{1}{\sqrt{3}} \frac{k}{100} (5m/s + 0.5U_{hor,i}) \quad (55)$$

4.3.5 Combination of uncertainties

All uncertainty components are now expressed as uncertainties in U_{hor} . Combination of the uncertainty components may then be made with sensitivity factors equal to one and correlation coefficients equal to 1 or 0:

$$u^2(U_{hor}) = \sum_{i=1}^N \sum_{j=1}^N u(x_i)u(x_j)r(x_i, x_j) \quad (56)$$

The final combination of uncertainties is then:

$$u_{U_{hor}} = \sqrt{(u_{U_{11i}} + u_{U_{12i}} + u_{U_{12i}})^2 + u_{U_{41i}}^2 + u_{U_{42i}}^2 + u_{U_{2i}}^2 + 3u_{U_{31i}}^2 + 3u_{U_{32i}}^2 + 3u_{U_{33i}}^2 + 3u_{U_{34i}}^2 + 3u_{U_{35i}}^2 + u_{d_{Ni}}^2 + u_{U_{5i}}^2 + u_{U_{6i}}^2 + u_{U_{7i}}^2 + u_{U_{8i}}^2} \quad (57)$$

4.3.6 Operation procedure for simulation model

The simulation model of spinner anemometer wind speed uncertainty is now summarized according to the following procedure:

- 1) First, for the reference case during the calibration campaign of k_1 /NTF, the differences in U_{hor} according to Figure 31 for the average operating conditions (turbulence, inflow angle, yaw misalignment and shaft tilt angle plus its increase with wind speed) is calculated for each wind speed bin in the range 4-16m/s. Vibrations of spinner and lateral angular response are included in all calculations. These reference differences are extracted in the following difference calculations in order to isolate the influence of individual uncertainty components, except in case 4, where the overall influence due to climatic operating conditions is derived, and the reference case is included within this range.
- 2) Then differences in U_{hor} due to individual calibration uncertainties ($u_{N_{1,V1,i}}, u_{N_{1,V2,i}}, u_{N_{1,V3,i}}, u_{N_{41i}}, u_{N_{42i}}$) for the same reference average operating conditions are calculated. For each calibration uncertainty the difference in U_{hor} is subtracted the difference in U_{hor} from 1) to find the corresponding uncertainty based on U_{hor} ($u_{U_{11i}}, u_{U_{12i}}, u_{U_{13i}}, u_{U_{41i}}, u_{U_{42i}}$).
- 3) Then differences in U_{hor} due to individual mounting uncertainties ($u_{N_{31i}}, u_{N_{32i}}, u_{N_{33i}}, u_{N_{34i}}, u_{N_{35i}}$) for the same reference average operating conditions are calculated. For each mounting uncertainty the difference in U_{hor} is subtracted the difference in U_{hor} from 1) to find the corresponding uncertainty based on U_{hor} ($u_{U_{31i}}, u_{U_{32i}}, u_{U_{33i}}, u_{U_{34i}}, u_{U_{35i}}$).
- 4) Now, the differences in U_{hor} according to Figure 31 for the variation range of operating conditions (turbulence, inflow angle, yaw misalignment and shaft tilt angle plus its increase with wind speed) are calculated. The resulting envelope of deviations from equation 54 for each wind speed determines the uncertainty due to operational characteristics ($u_{U_{2i}}$) for the calibration campaign.
- 5) The uncertainties derived from step 2) to step 4) are now all combined with the other uncertainties according to equation 57.
- 6) For a measurement campaign where the operational conditions are different from the reference calibration campaign operational conditions step 4) is exchanged with the measurement campaign operation conditions and the uncertainties are combined again according to step 5) with equation 57.

SA uncertainty calculation

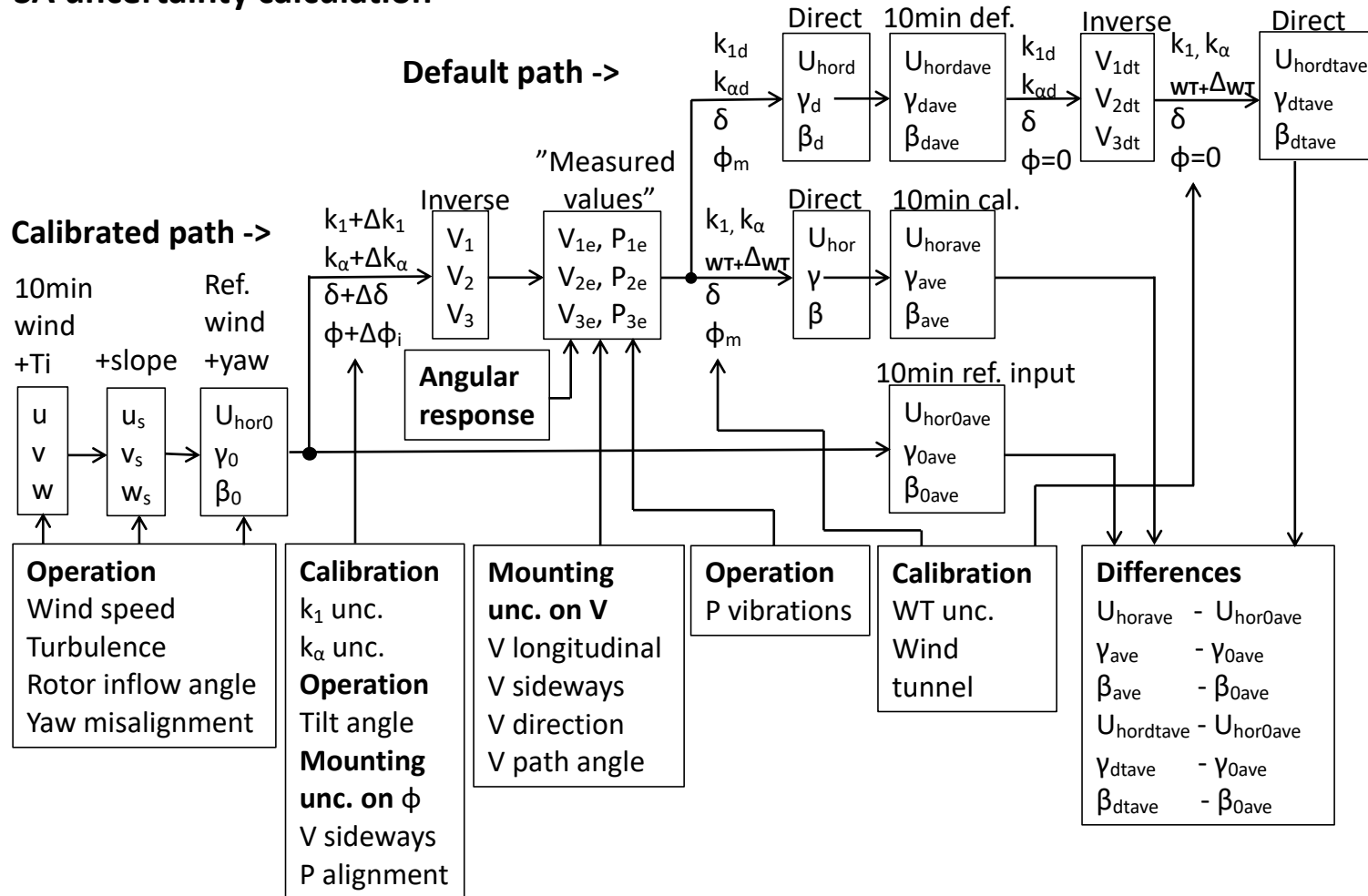


Figure 31 Flow chart of calculation code for propagation of uncertainties through the unlinear conversion algorithm

5. Nacelle transfer function

The nacelle transfer function, according to IEC6140-12-2 [7], relates the wind measurements on the nacelle to the free wind. When the measurement of the nacelle transfer function is made, the spinner anemometer constant k_1 is determined with the same dataset. The NTF with the correct constant k_1 is assumed to represent the induction in the centre of the rotor while the constant k_1 is the spinner anemometer constant that is used to determine the wind speed at the spinner.

The NTF is applied to convert wind speed measurements at the spinner to free wind speed measurements. The overall uncertainty of the NTF measurement is applied to the NTF and no uncertainty is applied to k_1 . We can consider k_1 as just a more correct value than k_{1d} while the NTF is actually transferring the traceable calibration to the spinner anemometer.

Result of measurement of a nacelle transfer function is shown in Figure 8. The uncertainties on measurement of the NTF are cup anemometer calibration, cup anemometer classification, mounting effects, flow distortion due to the terrain, data acquisition system, and spinner anemometer uncertainties. An example of uncertainties of the NTF measurement is shown in section 6.1 together with the combined uncertainties.

6. Free and absolute wind speed measurements with the spinner anemometer

Free and absolute wind speed measurements, made with the spinner anemometer, are achieved when applying the NTF according to IEC61400-12-2 [7] to the spinner anemometer measurements. The free wind speed measurement uncertainties include combination of the uncertainty of spinner anemometer measurements and the uncertainty of the NTF.

6.1 Uncertainty of the free wind speed measurements

The reference wind speed for a nacelle power curve (NPC) is the free wind speed, calculated from the application of the nacelle transfer function (NTF) to the spinner anemometer wind speed. According to IEC61400-12-2 [7], the uncertainty of this calculated free wind speed, $u_{V,i}$, is the combination of the uncertainty of the nacelle transfer function, $u_{V6,i}$, and the uncertainty of the spinner anemometer wind speed, $u_{Uhor,i}$.

$$u_{V,i} = \sqrt{u_{Uhor,i}^2 + u_{V6,i}^2} \quad (58)$$

The uncertainty of the free wind speed $u_{Uhor,i}$ was calculated in previous section.

The uncertainty of the nacelle transfer function, NTF, $u_{V6,i}$ is the combination of the following uncertainty components:

$$u_{V6,i} = \sqrt{u_{FS,i}^2 + u_{N,i}^2 + u_{M,i}^2 + s_{NTF,i}^2} \quad (59)$$

where

$u_{FS,i}$ is the uncertainty of the measured free wind speed by the mast cup anemometer, V_{FS}

$u_{N,i}$ is the uncertainty of the spinner anemometer wind speed, V_N

$u_{M,i}$ is the uncertainty due to seasonal variations (method);

$s_{NTF,i}$ is the statistical uncertainty of the nacelle transfer function wind speed ratio

The expressions in (58) and (59) rely on the assumption that all uncertainty components are uncorrelated, which seems to be a reasonable assumption in the most general case.

7. Example of measurement uncertainty of a spinner anemometer

An example of a wind speed measurement uncertainty calculation is made based on the Nørrekær Enge experiment, reported in [12]. That report already presents an uncertainty analysis with smaller detail. The present example will use the uncertainty method introduced in the previous chapters.

The wind turbine is no. 4 in the row of 13 wind turbines. It is a 2.3MW wind turbine with a 92m diameter rotor. A mast to hub height is mounted in the direction 210° in flat terrain [12]. Data for operational conditions during calibration of the spinner anemometer for wind speed measurements are given in Table 5.

For the reference operating conditions for the turbine during calibration, turbulence is set to the highest turbulences in class A for wind speeds 4-16 m/s. The inflow slope is set to 0° , and the yaw misalignment to 3° . The tilt angle is set to 6° with a linear increase by 1° from 4 to 16m/s. The rotational speed is set to a linear variation from 6rpm at 4m/s to 16rpm at 14m/s, and at higher wind speeds to 16rpm. The radius from the shaft axis to the centre of the sonic sensor path on the spinner is set to 0.65m, and the sonic sensor angle is set to 35° .

The lateral angular response of the sonic sensors is taken from wind tunnel tests, Figure 23. The fitted curve is used in the calculations.

The default spinner anemometer constants were set to $k_{1d} = 1.0$ and $k_{2d} = 0.7$. The calibrated constants are set equal to $k_1 = 0.61$ and $k_\alpha = 1.44$ with $k_2 = 0.878$.

Table 5 Wind turbine reference operational conditions during calibration of k_1 /NTF

Operational condition	Reference	Class A	Class B
Wind speed	4-16m/s	4-16m/s	4-16m/s
Turbulence	0.12+0.48/V	0.03 to 0.12+0.48/V	0.03 to 0.12+0.96/V
Rotational speed	6-16rpm for 4-14m/s	6-16rpm for 4-14m/s	6-16rpm for 4-14m/s
Flow inclination angle	0°	-3° to 3°	-15° to 15°
Yaw misalignment	3°	-5° to 5°	-10° to 10°
Tilt angle	6°	6°	6°
Tilt increase	1° for 4-16m/s	1° for 4-16m/s	1° for 4-16m/s
Lateral angular response (deviation from cosine: $+0.025 \cdot (\text{abs}(\sin(1.9\alpha)))^4$)	See Figure 23, Figure 17	See Figure 23, Figure 17	See Figure 23, Figure 17
Spinner vibrations, amplitude frequency	0.35m/s ² 6Hz	0.35m/s ² 6Hz	0.35m/s ² 6Hz
Sonic path center to shaft axis	0.65m	0.65m	0.65m
Sonic sensor path angle	35°	35°	35°

The calibration and mounting uncertainty components are listed in Table 6. The uncertainty on the wind speed constant k_1 , u_{N42i} is set equal to zero, as all uncertainty of the traceable calibration to free wind speed is put on the NTF, Figure 32.

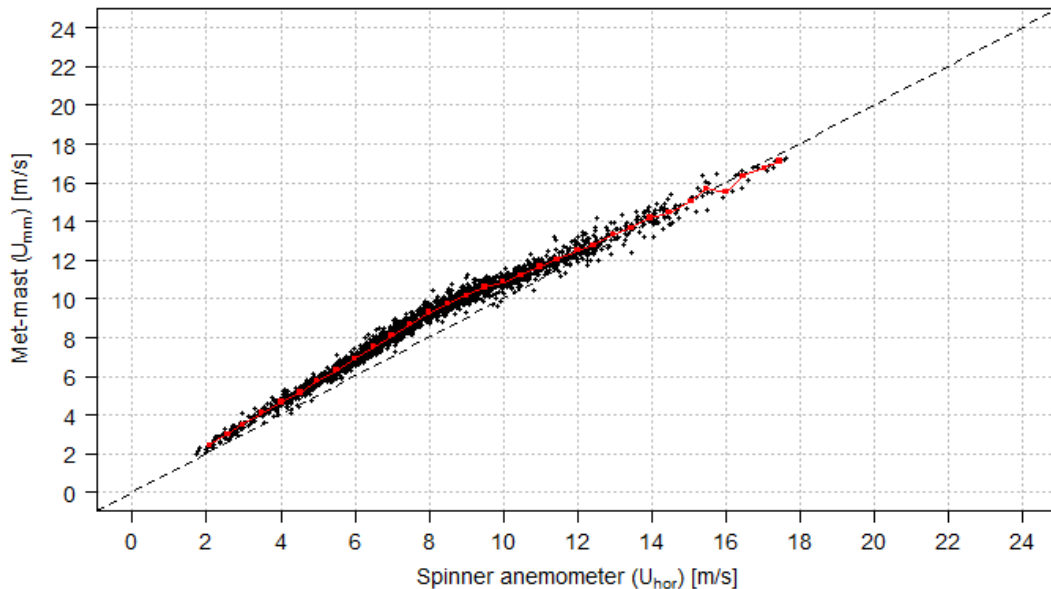


Figure 32 Nacelle transfer function [12]

The specific mounting uncertainties are described in actual geometrical terms, and then converted to an influence on the sonic sensor wind speeds or the accelerometer accelerations, which then again are converted to uncertainties on U_{hor} .

The uncertainty on the longitudinal alignment was obtained by photographic techniques where the sonic sensor positions were photographed with a long tele lens in a fixed position perpendicular to the shaft axis. The spinner curvature was aligned on all three photos and the sensor positions were merged into one photo. Figure 33 at left shows the sonic sensor positions on wind turbine no. 4 and at right the positions on wind turbine 5. Figure 34 shows both of the turbines sonic sensors combined. The span in longitudinal alignment is seen to be 5,6cm. We assume this range to cover the standard uncertainty range. We can thus set the longitudinal alignment standard uncertainty u_{N31i} to 2,8cm.

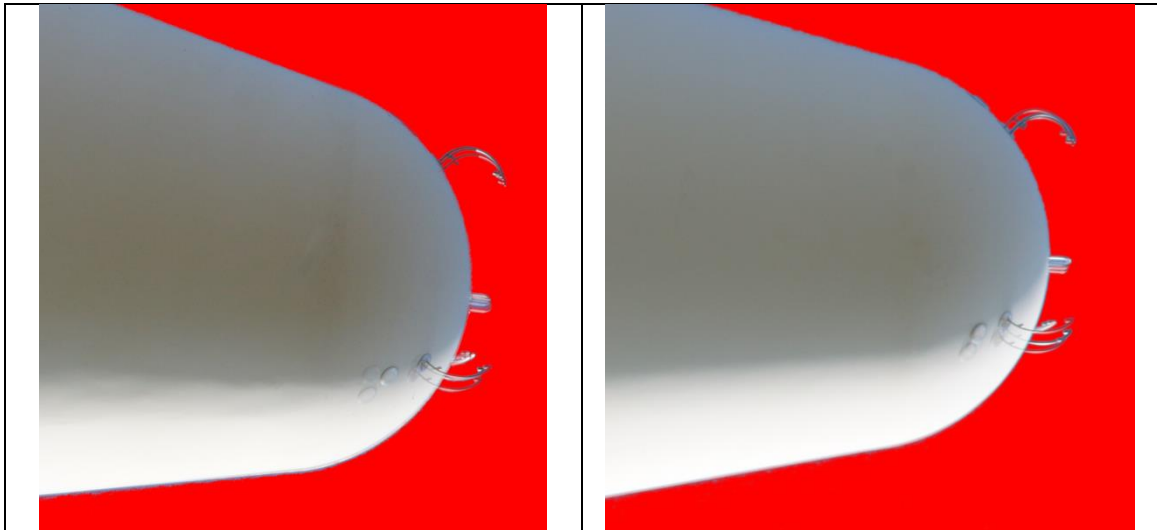


Figure 33 Merged photos of sonic sensor mountings. Left, wind turbine 4. Right, wind turbine 5. Photos by ROMO Wind. Merged photos by DTU.

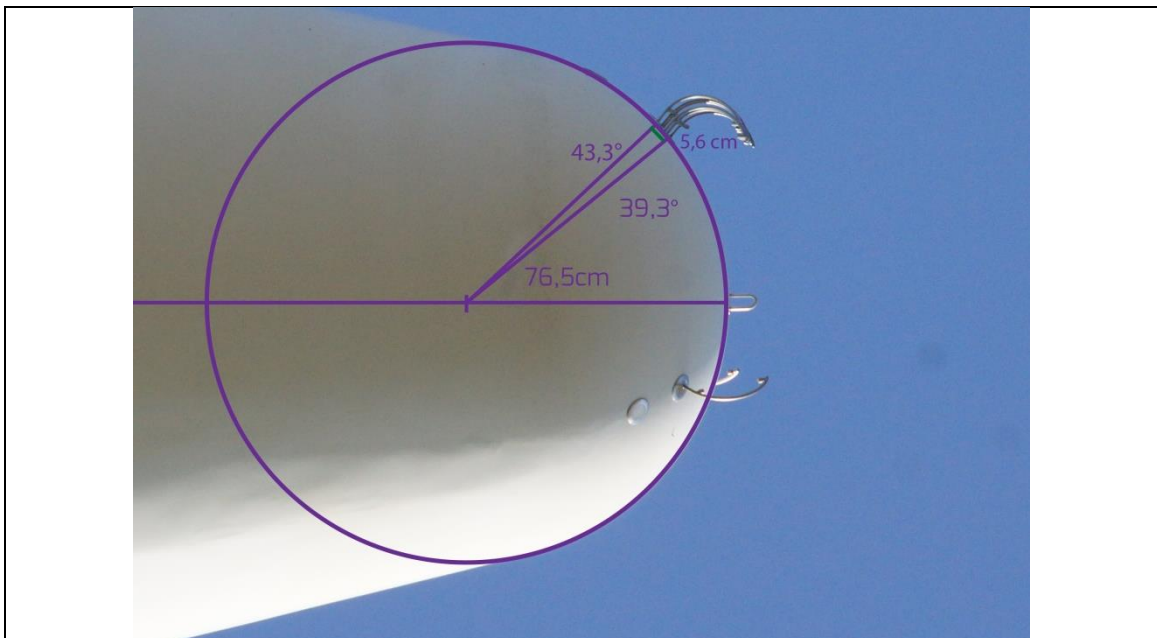


Figure 34 Merged photos of sonic sensors on turbine 4 and 5. Photos and merged photo by ROMO Wind.

The operational uncertainty is obtained following the procedure in chapter 4.3.4. Here, all possible combinations of the relevant operation condition limits (different yaw errors and wind

slopes etc.) are input to the simulation. The class index number can be then obtained from the envelope of the maximum wind speed deviations obtained from the simulations, for the wind speed range 4-16m/s.

The other uncertainty components in box 4, in Table 6, are insignificant in this example, since no rotor induction change, change of spinner geometry or significant seasonal variations have taken place. Only the uncertainty on the data acquisition is included and estimated as 0.0058m/s.

Table 6 Uncertainty components for spinner anemometer considered in this example

Uncertainty component	Component	Value (reference)	Influence on parameter	Uncertainty component on U_{hor}
1. Calibrations				
• Wind tunnel calibration	$u_{N1,V2,i}$	0.048m/s	V_1	u_{U11i}
	$u_{N1,V2,i}$	0.097m/s	V_2	u_{U12i}
	$u_{N1,V3,i}$	0.165m/s	V_3	u_{U13i}
• Angular calibration k_α	u_{N41i}	$0.1k_\alpha$	U_{hor}	u_{U41i}
• Wind speed calibration k_1	u_{N42i}	0	U_{hor}	u_{U42i}
2. Operational characteristics	u_{N2i}			u_{U2i}
• Inflow angle to rotor	u_{N21i}	-3° to 3°	U_{hor}	
• Turbulence	u_{N22i}	0.24 to 0.15	U_{hor}	
• Yaw misalignment	u_{N23i}	-5° to 5°	U_{hor}	
• Accelerometer vibrations	u_{N24i}	A:0.35m/s ² f: 6Hz	φ	
• Shaft tilt angle	u_{N25i}	6° to 7°	φ	
3. Sonic sensor mounting	u_{N3i}			
• Longitudinal position	u_{N31i}	28mm	V_1, V_2, V_3	u_{U31i}
• Directional uncertainty	u_{N32i}	2°	V_1, V_2, V_3	u_{U32i}
• Sonic path angle	u_{N33i}	1°	V_1, V_2, V_3	u_{U33i}
• Sonic azimuth position	u_{N34i}	10mm	$V_1, V_2, V_3,$ P_1, P_2, P_3	u_{U34i}
• Accelerometer alignment	u_{N35i}	5°	P_1, P_2, P_3	u_{U35i}
4. Other uncertainty components				
• Data acquisition system	u_{dNi}	0.0058m/s	U_{hor}	u_{Udi}
• Use of default k constants	u_{N5i}	0	U_{hor}	u_{U5i}
• Spinner geometry	u_{N6i}	0	U_{hor}	u_{U6i}
• Rotor induction change	u_{N7i}	0	U_{hor}	u_{U7i}
• Limitations on algorithm	u_{N8i}	0	U_{hor}	u_{U8i}

7.1 Spinner anemometer uncertainty

This section presents the results obtained following the simulation steps described in section 4.3.3 and 4.3.4. In this analysis, we have obtained the outputs of the simulations using the calibrated values of k_1 and k_α (“calibrated” path in the diagram in Figure 31) and the outputs of

the simulations using the default values of k_{1d} and k_{ad} (“default” path in the diagram in Figure 31).

7.1.1 Wind speed deviations in the reference scenario

The differences in U_{hor} for the reference operating conditions during the calibration campaign of k_1 /NTF as shown in Table 5 are calculated for each wind speed bin.

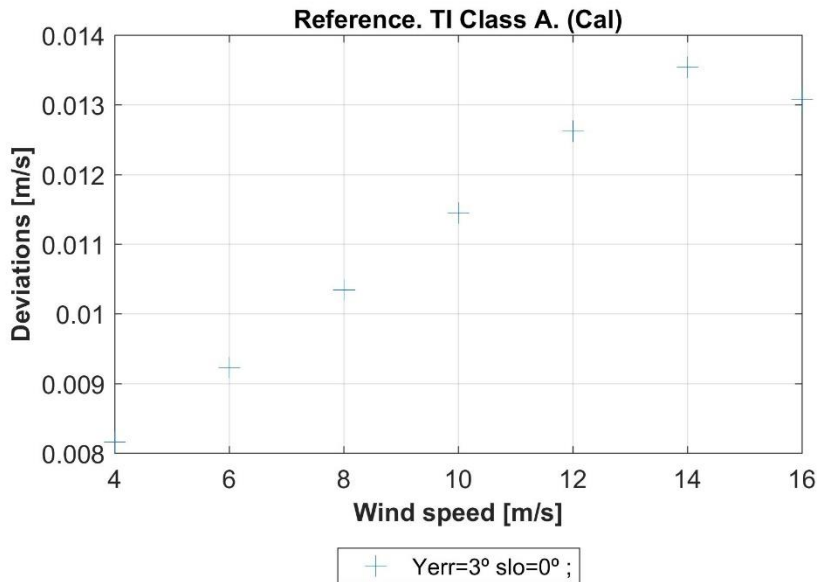


Figure 35 Deviation in U_{hor} for the reference operating conditions. “Calibrated” simulation path

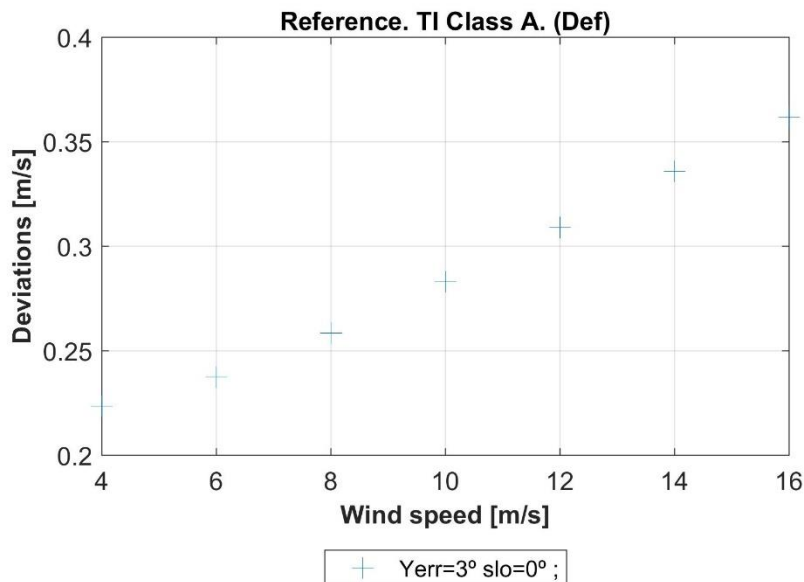


Figure 36 Deviation in U_{hor} for the reference operating conditions. “Default” simulation path.

7.1.2 Uncertainties due to calibrations

The differences in U_{hor} due to individual calibration uncertainties ($u_{N1,V1,i}$, $u_{N1,V2,i}$, $u_{N1,V3,i}$, $u_{N41,i}$, $u_{N42,i}$) are calculated in this section.

The uncertainties $u_{N1,V1,i}$, $u_{N1,V2,i}$, $u_{N1,V3,i}$ are the individual sonic sensor uncertainties from the wind tunnel calibrations. Calibration certificates of the three sonic sensors are given in Annex A. Following best practice, it is assumed that:

- The results of the sensor calibrations are applied on the measured spinner anemometer data, as described in section 3.1.2; either in the spinner anemometer box (calibrated path) or on the measured data afterwards (default path).
- The deviations between calibrated values and reference are small and there is a high degree of correlation between calibrated values and reference.

In this way, the uncertainties as well as any possible biases in the sensor path wind speeds are significantly reduced.

In tables 7 to 9, the reference wind speed along the sonic sensor path, V_n , is calculated according to formula 14. Its uncertainty, u_{V_n} , is derived according to equation 15 using the following values, using the normalized sensor path angle:

$$\begin{aligned}\varphi &= 35.0^\circ \\ u_\varphi &= 0.2/\sqrt{3} \\ u_t &= \sqrt{u_c^2 + u_{tr}^2}\end{aligned}$$

Where u_c is the wind tunnel uncertainty, stated in the certificate (converted to a coverage factor $k=1$) and u_{tr} is an uncertainty term that accounts for traceability between wind tunnels accredited by Measnet. According to [14], the differences between wind tunnels lies within $\pm 1\%$ of the reference wind speed; assuming a rectangular distribution, $u_{tr} = \frac{0.01}{\sqrt{3}} V_t$.

The values in tables 7 to 9 are taken from three example calibration certificates, enclosed in Annex A. $V_{n,cal}$ is the calibrated sonic sensor speed following equation 13. d_n is the difference between the calibrated sonic sensor speed and the reference tunnel speed on the path direction. The values of d_n , as well as the difference between measured sensor wind speed and reference, for the three sonic sensors are shown in Figure 37.

Table 7. Sensor path 1 calibration results. Obtained from the certificate in Annex A.

Path 1. $\varphi=35.0^\circ\pm 0.2^\circ$ ($u_\varphi = 0.2/\sqrt{3}$)					
Tunnel wind speed, V_t (m/s)	u_t (m/s)	Reference speed in sensor path direction, V_n (m/s)	$u_{V_n} = u_{N1,V1}$ (m/s)	Sonic speed, calibrated, $V_{n,cal}$ (m/s)	$d_n = V_{n,cal} - V_n$ (m/s)
4.127	0.026	3.381	0.022	3.392	0.011
5.115	0.032	4.190	0.027	4.190	0.000
6.042	0.038	4.949	0.032	4.950	0.001
7.020	0.044	5.750	0.037	5.750	0.000
7.954	0.050	6.516	0.042	6.509	-0.007
8.957	0.056	7.337	0.047	7.347	0.009
9.905	0.062	8.114	0.052	8.109	-0.005
10.877	0.068	8.910	0.057	8.910	0.000
11.820	0.074	9.682	0.062	9.663	-0.019
12.776	0.079	10.465	0.067	10.447	-0.018
13.743	0.086	11.258	0.072	11.255	-0.003
14.736	0.092	12.071	0.077	12.078	0.007
15.659	0.097	12.827	0.082	12.850	0.023

Table 8. Sensor path 2 calibration results. Obtained from the certificate in Annex A.

Path 2. $\varphi=35.0^\circ\pm 0.2^\circ$ ($u_\varphi = 0.2/\sqrt{3}$)					
Tunnel wind speed, V_t (m/s)	u_t (m/s)	Reference speed in sensor path direction, V_n (m/s)	$u_{V_n} = u_{N1,V2}$ (m/s)	Sonic speed, calibrated, $V_{n,cal}$ (m/s)	$d_n = V_{n,cal} - V_n$ (m/s)
4.161	0.026	3.408	0.022	3.425	0.017
5.107	0.032	4.183	0.027	4.186	0.002
6.042	0.038	4.949	0.032	4.952	0.003
7.014	0.044	5.746	0.037	5.745	-0.001
7.960	0.050	6.520	0.042	6.510	-0.010
8.935	0.056	7.319	0.047	7.308	-0.011
9.910	0.062	8.118	0.052	8.106	-0.012
10.863	0.068	8.898	0.057	8.900	0.002
11.859	0.074	9.714	0.062	9.706	-0.008
12.794	0.080	10.480	0.067	10.491	0.010
13.748	0.085	11.262	0.072	11.250	-0.012
14.719	0.092	12.057	0.077	12.051	-0.006
15.661	0.098	12.829	0.082	12.854	0.026

Table 9. Sensor path 3 calibration results. Obtained from the certificate in Annex A.

Path 3. $\varphi=35.0^\circ\pm 0.2^\circ$ ($u_\varphi = 0.2/\sqrt{3}$)					
Tunnel wind speed, V_t (m/s)	u_t (m/s)	Reference speed in sensor path direction, V_n (m/s)	$u_{V_n} = u_{N1,V3}$ (m/s)	Sonic speed, calibrated, $V_{n,cal}$ (m/s)	$d_n = V_{n,cal} - V_n$ (m/s)
4.119	0.026	3.374	0.022	3.369	-0.006
5.132	0.032	4.204	0.027	4.198	-0.005
6.061	0.038	4.965	0.032	4.966	0.001
6.996	0.044	5.731	0.037	5.737	0.006
7.949	0.049	6.511	0.042	6.523	0.011
8.936	0.056	7.320	0.047	7.316	-0.004
9.900	0.062	8.110	0.052	8.104	-0.006
10.845	0.067	8.884	0.057	8.892	0.009
11.815	0.074	9.678	0.062	9.668	-0.011
12.765	0.079	10.456	0.067	10.468	0.012
13.743	0.085	11.258	0.072	11.263	0.005
14.715	0.092	12.054	0.077	12.039	-0.015
15.660	0.098	12.828	0.082	12.830	0.002

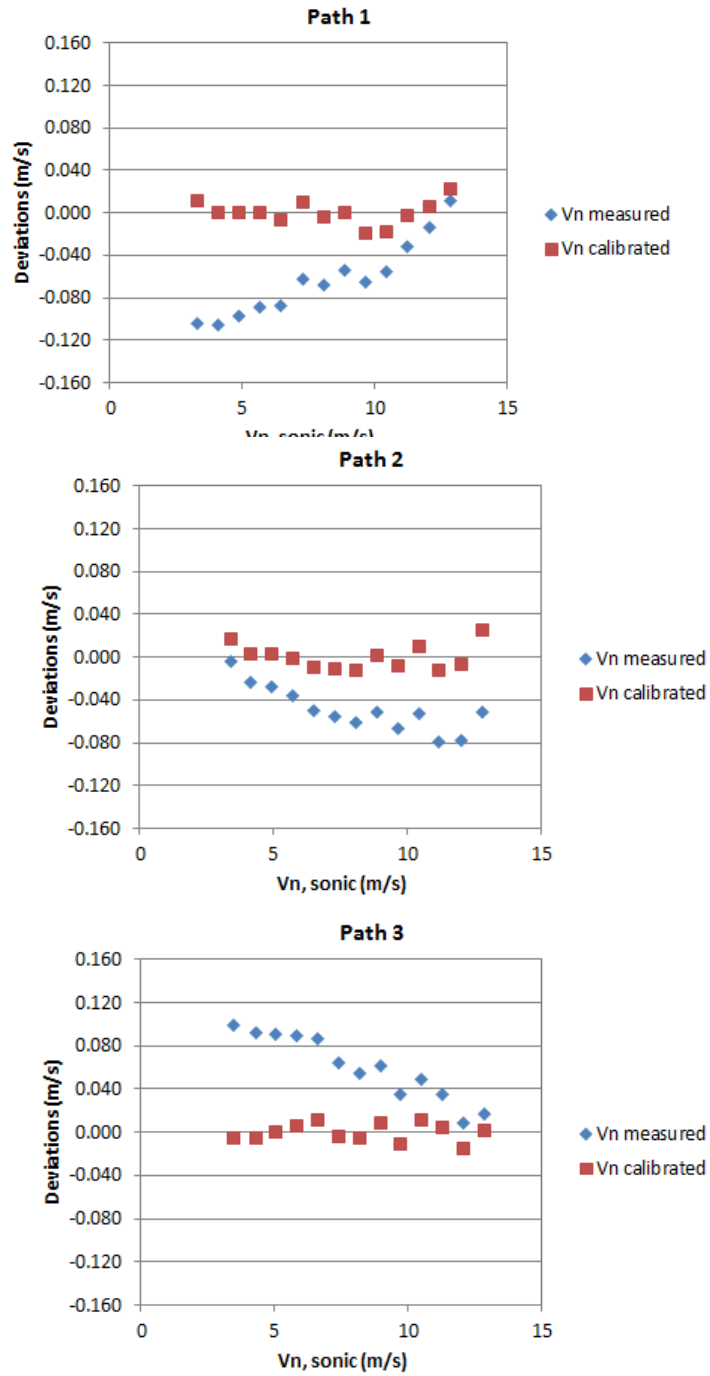


Figure 37 Wind speed deviations obtained in the calibrations: difference between calibrated sensor wind speeds, d_n (red squares) and difference between measured sensor wind speed and reference (blue diamonds). Results for the three sensors (path 1 –top-, path 2 –middle-, path 3 –bottom-).

In our simulations, we use as inputs the values of $u_{N1,V1,i}$, $u_{N1,V2,i}$, $u_{N1,V3,i}$ in Table 7 to Table 9. For simplicity, we model the uncertainty values by the following linear functions of the path wind speeds:

$$u_{N1,V1,i} = 0.0063V_{1,i} + 0.0003\text{m/s}$$

$$u_{N1,V2,i} = 0.0064V_{2,i} + 0.0003\text{m/s}$$

$$u_{N1,V3,i} = 0.0064V_{3,i} + 0.0003\text{m/s}$$

The resulting uncertainties on U_{hor} obtained for these input values are given in Figure 38 and Figure 39.

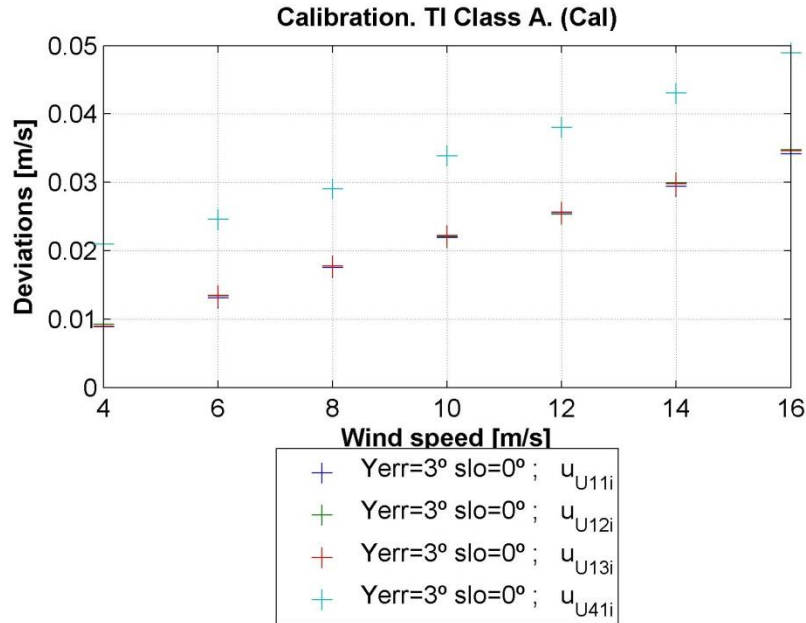


Figure 38 Uncertainties on U_{hor} by wind tunnel calibration uncertainties (u_{U11i} , u_{U12i} , u_{U13i}) and angular calibration (u_{U41i}), obtained for the “calibrated” simulation path. Wind speed calibration (u_{U42i}) is set to zero.

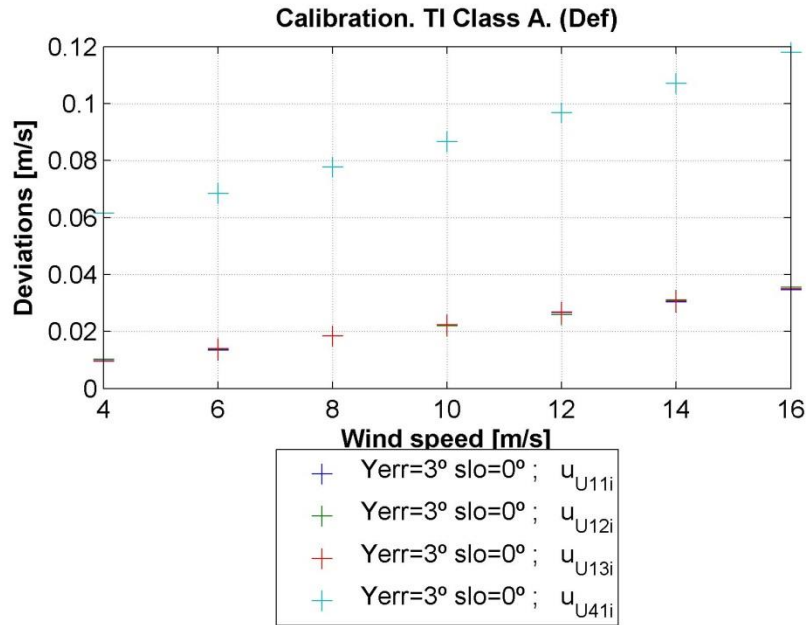


Figure 39 Uncertainties on U_{hor} by wind tunnel calibration uncertainties (u_{U11i} , u_{U12i} , u_{U13i}) and angular calibration (u_{U41i}), obtained for the “default” simulation path. Wind speed calibration (u_{U42i}) is set to zero.

Table 10 shows the difference obtained between the simulations of the “calibrated” and “default” path (see Figure 31) in sensor path calibration uncertainties and k_α calibration uncertainties. In order to facilitate the comparison, the sensor path calibration uncertainties are grouped in the following term: $u_{U1i} = u_{U11i} + u_{U12i} + u_{U13i}$.

Table 10 Difference between calibration uncertainty components, between the “calibrated” path and the “default” path, expressed as a percentage of the reference wind speed.

Reference wind speed, $U_{hor,i}$ (m/s)	Δu_{U1i}	Δu_{U41i}
4	-0.06%	-1.0%
6	-0.02%	-0.7%
8	-0.03%	-0.6%
10	0.00%	-0.5%
12	-0.02%	-0.5%
14	-0.02%	-0.5%
16	-0.01%	-0.4%

7.1.3 Uncertainties due to operational characteristics

The different combinations of the operating condition (different yaw errors and wind slopes) corresponding to class A (Table 4) are input to the simulations. The class index number is obtained from the envelope of the maximum wind speed deviations obtained from the simulations, for the wind speed range 4-16m/s.

For the calibrated path, class 0.2A was obtained as shown in Figure 40 and for the default path, class 3.2A was obtained as shown in Figure 41.

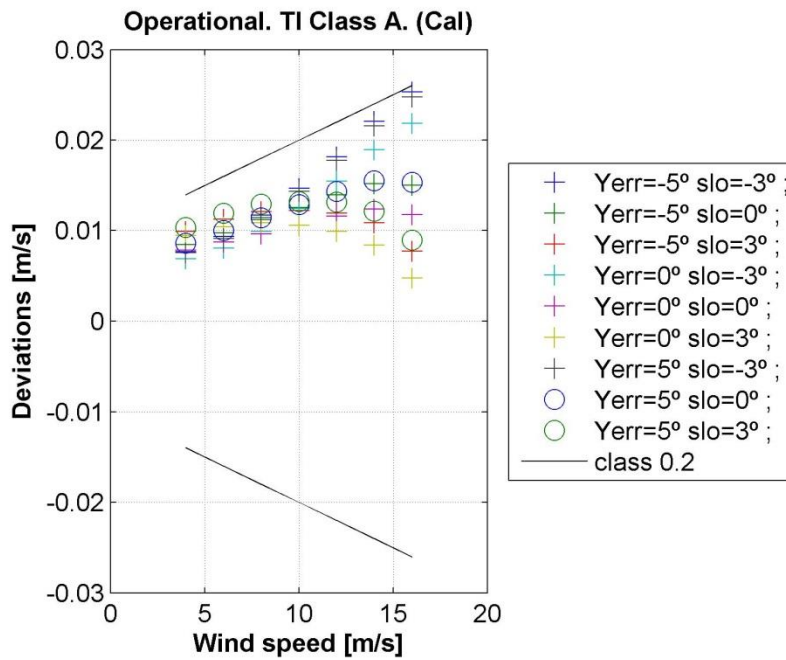


Figure 40 Deviations in U_{hor} obtained for class A operational conditions and yaw misalignment between -5° and 5° . “Calibrated” simulation path.

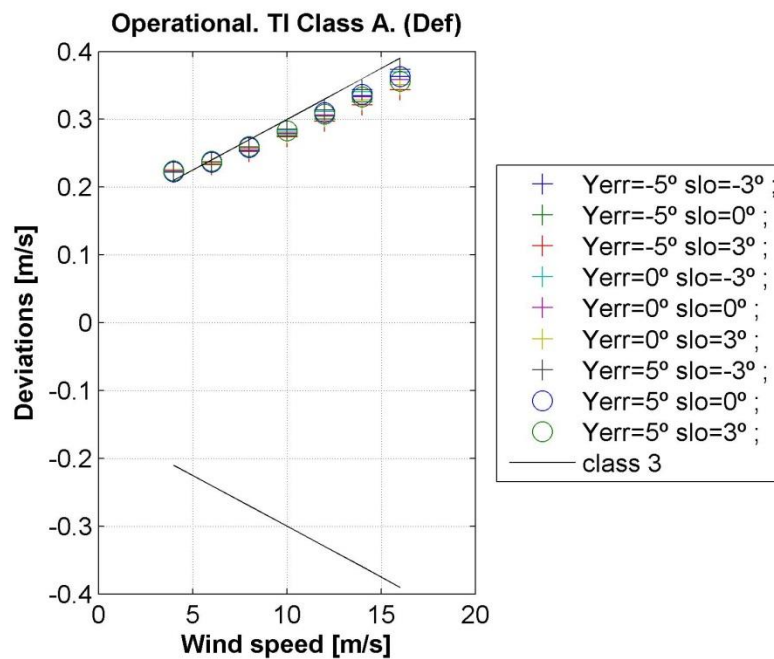


Figure 41 Deviations in U_{hor} obtained for class A operational conditions and yaw misalignment between -5° and 5° . “Default” simulation path.

7.1.4 Uncertainties due to mounting

The uncertainties in U_{hor} (u_{U31i} , u_{U32i} , u_{U33i} , u_{U34i} , u_{U35i}) due to individual mounting uncertainties are calculated individually for the reference average operating conditions. The deviations are shown in Figure 42 for the calibrated path and in Figure 43 for the default path.

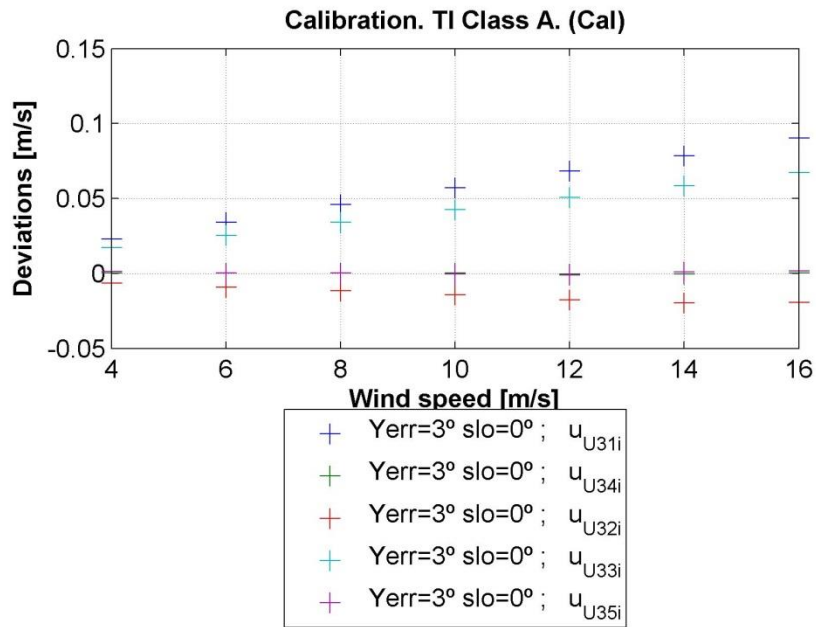


Figure 42 Uncertainties in U_{hor} due to mounting by longitudinal position (u_{U31i}), directional uncertainty (u_{U32i}), sonic path angle (u_{U33i}), sonic azimuth position (u_{U34i}), accelerometer alignment (u_{U35i}), obtained for the “calibrated” simulation path

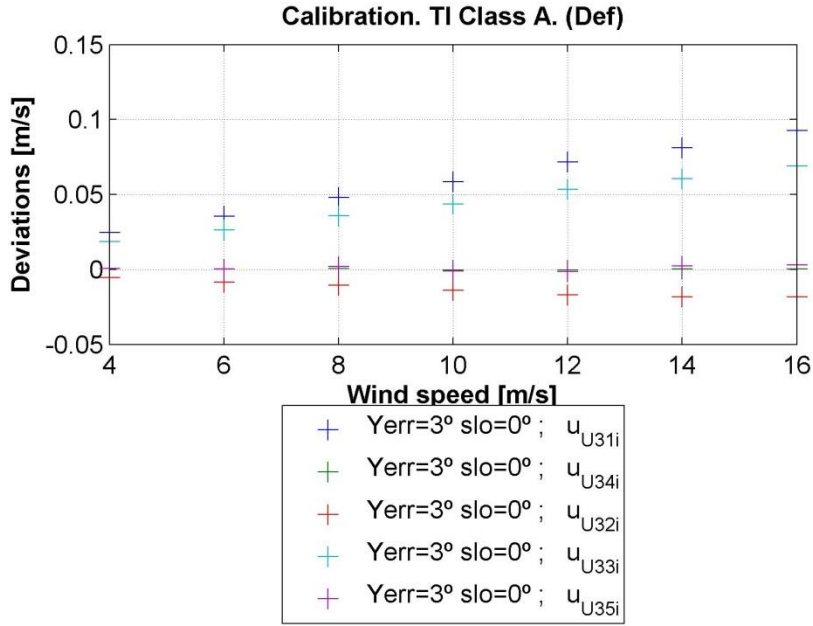


Figure 43 Uncertainties in U_{hor} due to mounting by longitudinal position (u_{U31i}), directional uncertainty (u_{U32i}), sonic path angle (u_{U33i}), sonic azimuth position (u_{U34i}), accelerometer alignment (u_{U35i}), obtained for the “default” simulation path

7.1.5 Total combined uncertainty on U_{hor}

The total uncertainty on the spinner anemometer wind speed measurement is obtained by combining the individual uncertainty components obtained from the simulations according to equation 57. Figure 44 shows the uncertainty components in U_{hor} from sections 7.1.2 to 7.1.4, as well as the resulting combined uncertainty. For clarity, the wind tunnel calibration uncertainties have been grouped into one term: $u_{U1i} = u_{U11i} + u_{U12i} + u_{U13i}$

The resulting uncertainty, $u_{U_{hor}}$, can be linearized and expressed as a function of U_{hor} , as follows:

$$u_{U_{hor}} = 0.0139U_{hor} + 0.0057m/s \quad (60)$$

The uncertainty components and combined uncertainty are given in Table 11.

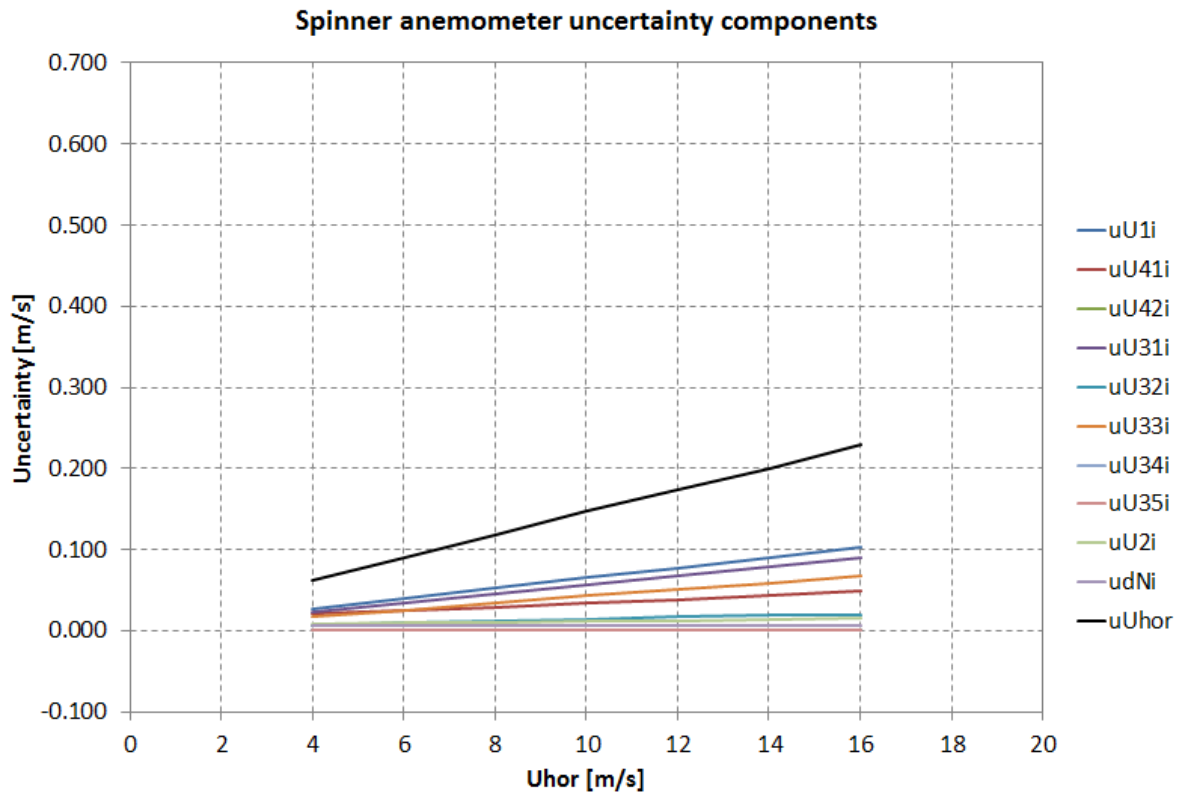


Figure 44 Resulting uncertainty in the spinner anemometer wind speed, $u_{U_{hor}}$, and individual uncertainty components of U_{hor} : calibration uncertainties ($u_{U_{1i}}$, $u_{U_{41i}}$, $u_{U_{42i}}$), mounting uncertainties ($u_{U_{31i}}$, $u_{U_{32i}}$, $u_{U_{33i}}$, $u_{U_{34i}}$, $u_{U_{35i}}$), operational uncertainty ($u_{U_{2i}}$) and data acquisition uncertainty (u_{dNi}).
 “Calibrated” simulation path.

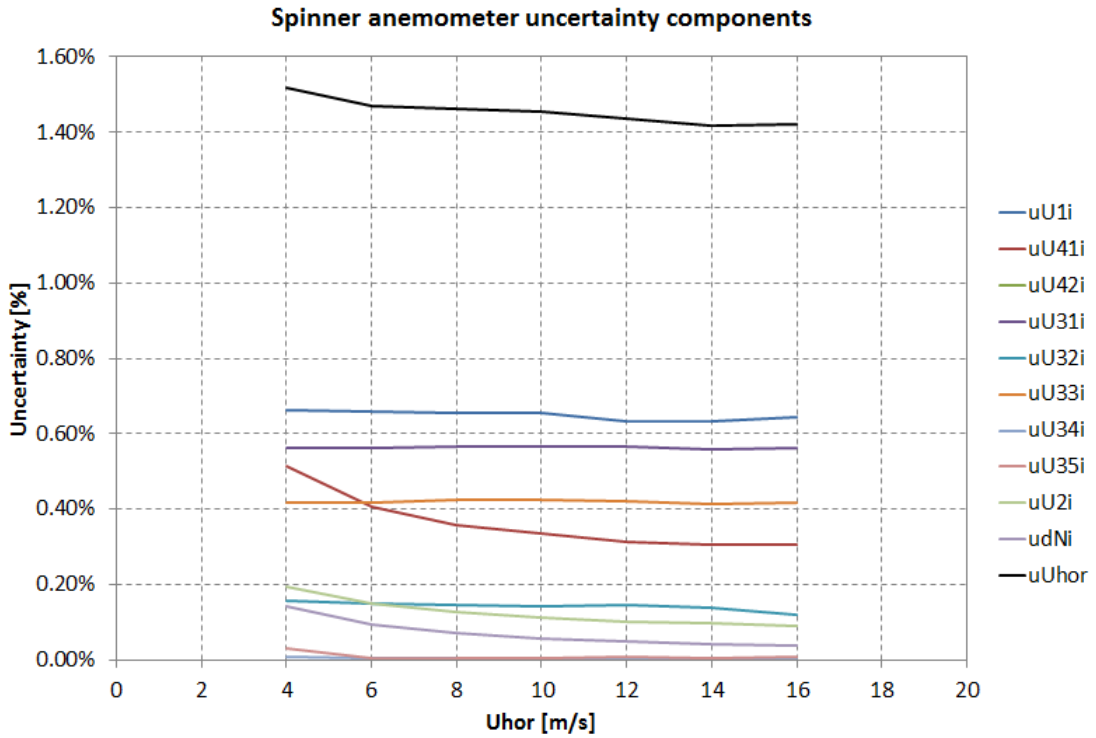


Figure 45 Resulting relative uncertainty in the spinner anemometer wind speed, $u_{U_{hor}}$, and individual uncertainty components of U_{hor} : calibration uncertainties ($u_{U_{1i}}, u_{U_{41i}}, u_{U_{42i}}$), mounting uncertainties ($u_{U_{31i}}, u_{U_{32i}}, u_{U_{33i}}, u_{U_{34i}}, u_{U_{35i}}$), operational uncertainty ($u_{U_{2i}}$) and data acquisition uncertainty (u_{dNi}).
 “Calibrated” simulation path.

Table 11 Individual uncertainty components of U_{hor} , and resulting uncertainty $u_{U_{hor}}$. “Calibrated” simulation path.

$U_{hor,i}$ (m/s)	$u_{U_{1i}}$ (m/s)	$u_{U_{41i}}$ (m/s)	$u_{U_{31i}}$ (m/s)	$u_{U_{32i}}$ (m/s)	$u_{U_{33i}}$ (m/s)	$u_{U_{34i}}$ (m/s)	$u_{U_{35i}}$ (m/s)	$u_{U_{2i}}$ (m/s)	$u_{U_{dNi}}$ (m/s)	$u_{U_{hor}}$ (m/s)	$u_{U_{hor}}$ (%)
4	0.027	0.021	0.023	0.006	0.017	0.00030	0.0012	0.008	0.006	0.062	1.5%
6	0.040	0.025	0.034	0.009	0.025	0.00024	0.0003	0.009	0.006	0.089	1.5%
8	0.053	0.029	0.046	0.012	0.034	0.00034	0.0003	0.010	0.006	0.118	1.5%
10	0.066	0.034	0.057	0.014	0.043	0.00036	0.0003	0.011	0.006	0.147	1.5%
12	0.077	0.038	0.068	0.018	0.051	0.00046	0.0011	0.012	0.006	0.174	1.4%
14	0.089	0.043	0.079	0.020	0.058	0.00027	0.0008	0.014	0.006	0.200	1.4%
16	0.104	0.049	0.090	0.019	0.067	0.00030	0.0015	0.015	0.006	0.229	1.4%

The difference in the total uncertainty results between the calibrated path and the default path are given in Table 12.

Table 12 Difference in uncertainty $u_{U_{hor}}$, between the “calibrated” path and the “default” path, expressed as a percentage of the reference wind speed.

Reference wind speed, $U_{hor,i}$ (m/s)	Calibrated path, $u_{U_{hor}}$ (m/s)	Default path, $u_{U_{hor}}$ (m/s)	$\Delta u_{U_{hor}}$
4	0.062	0.16	-2.5%
6	0.089	0.19	-1.7%
8	0.118	0.22	-1.3%
10	0.147	0.25	-1.0%
12	0.174	0.29	-1.0%
14	0.200	0.32	-0.9%
16	0.229	0.35	-0.8%

7.1.6 Total combined uncertainty on the free absolute wind speed measurement

The uncertainties on the k_1 /NTF calibration are shown in Figure 46 and the overall combined uncertainty on the free absolute wind speed measurement is shown in Figure 47.

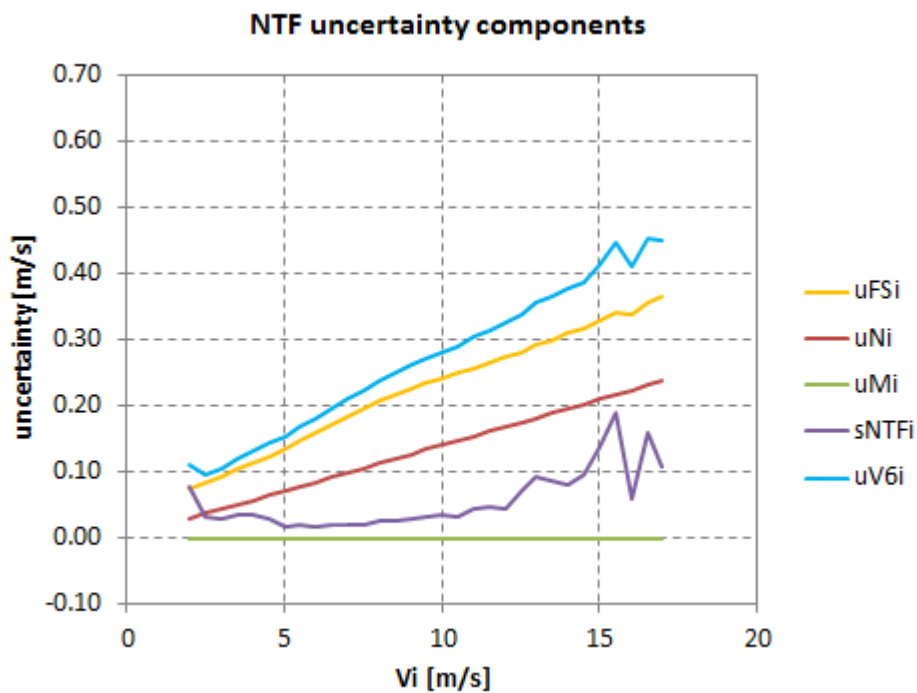


Figure 46 NTF uncertainty components, and resulting NTF uncertainty $u_{V6,i}$ (according to equation 59)

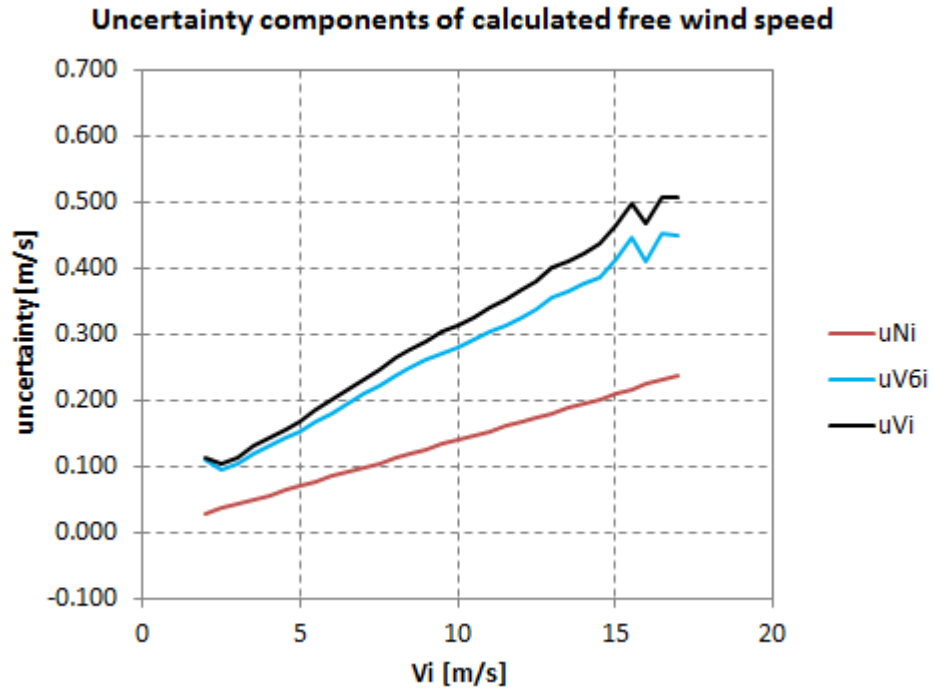


Figure 47 Uncertainty of calculated free wind speed, ($u_{V,i}$, black), together with spinner anemometer uncertainty ($u_{N,i}$, red) and NTF uncertainty ($u_{V6,i}$, blue) (according to equation 58)

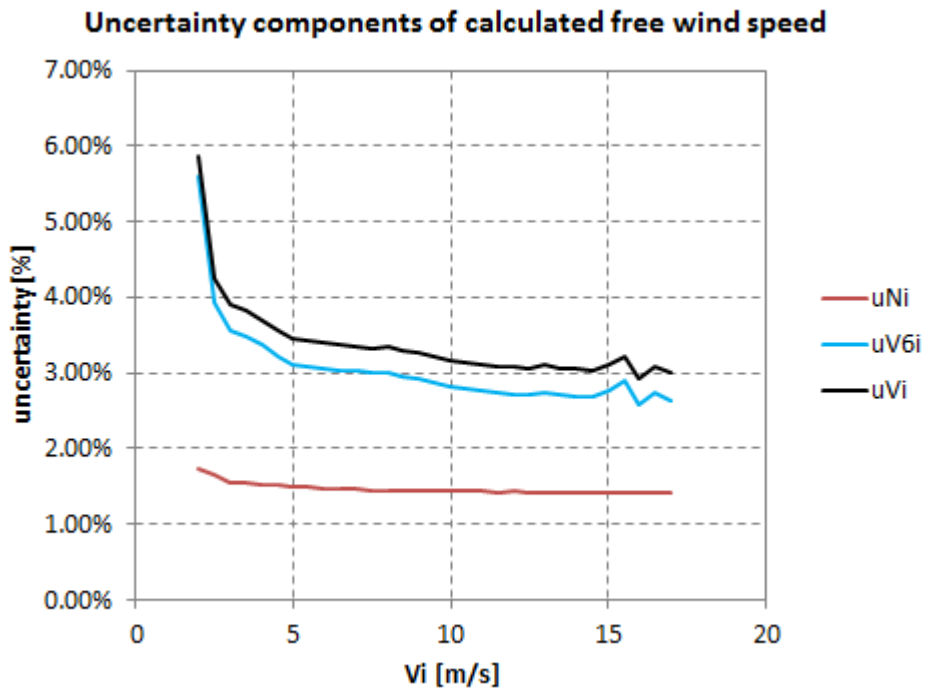


Figure 48 Relative Uncertainty of calculated free wind speed, ($u_{V,i}$, black), together with spinner anemometer uncertainty ($u_{N,i}$, red) and NTF uncertainty ($u_{V6,i}$, blue) (according to equation 58)

8. Examples of AEP uncertainty from spinner anemometer and mast power curves

In this section, the free wind speed uncertainty obtained in section 7.1.6 is applied to a nacelle power curve, where the free wind speed has been calculated from the application of the nacelle transfer function (NTF) to the spinner anemometer wind speed measurements. In this example, we use the power curve reported in [12] (bin averages of wind speed and power, and category A uncertainties in the power), as well as the category B uncertainties on electric power measurements, temperature and pressure (Table 13), also from [12]. The resulting nacelle power curve uncertainties are presented in Table 14, and they have been calculated following the requirements of IEC61400-12-2 [7], with the deviation of not including the seasonal uncertainty in the NTF (for plausibility, the NTF used was obtained simultaneously to the power curve). Uncertainty components not related to wind speed measurements, which are not part of IEC61400-12-1 [6], have not been included in this analysis, in order to make a consistent comparison between the two methods.

Table 13 Category B uncertainties on electric power, temperature and pressure measurements [12]

Uncertainty on electric power measurements	
$u_{P,i} = \sqrt{u_{P1,i}^2 + u_{P2,i}^2 + u_{P3,i}^2 + u_{dP,i}^2}$	
Current transformer (Class 0.2, 0.2% uncertainty at 20% load)	$u_{P1,i} = (0.002/\sqrt{3})P_i$ (kW)
Voltage Transformer (Class 1, 1,5% uncertainty at 20% load)	$u_{P2,i} = (0.015/\sqrt{3})P_i$ (kW)
Power transducer (class 0.5, range 5000kW)	$u_{P3,i} = (0.005(5000)/\sqrt{3})$ (kW)
Data acquisition system	~0
Uncertainties on temperature and pressure measurements	
Temperature sensor	$u_{T,i} = 0.51$ (°C)
Pressure sensor	$u_{B,i} = 30.0$ (Pa)

Table 14 Nacelle power curve. Bin values (V_i, P_i, Cp_i, N_i, s_i) obtained from [12]. Category B uncertainties calculated from Table 13 and section 7.1.6

Bin number	V_i (m/s)	P_i (kW)	N_i (-)	Cp_i (-)	$s_i, \text{Cat. A uncert}$ (kW)	Cat. B uncert (kW)	Combined uncert (kW)
6	2.61	-10.6	10	-0.142	1.8	14.6	14.7
7	3.05	0.7	30	0.006	1.7	14.7	14.8
8	3.46	19.1	31	0.111	2.5	15.5	15.7
9	4.00	58.6	24	0.219	4.1	17.6	18.1
10	4.51	104.2	38	0.273	4.5	19.7	20.2
11	4.99	181.8	68	0.351	3.7	29.9	30.1
12	5.54	287.4	90	0.407	3.4	37.1	37.2
13	6.02	381.1	91	0.42	4.2	40	40.2
14	6.52	512.7	103	0.445	5.1	55.9	56.1
15	7.00	649.4	131	0.455	4.7	64	64.2
16	7.49	798.4	141	0.457	5.2	72.3	72.5
17	7.99	979.4	165	0.462	5.8	90.9	91.1
18	8.49	1167.9	138	0.459	6.9	99.9	100.1
19	8.95	1364.8	115	0.457	7.6	118.8	119
20	9.51	1628.7	126	0.455	9.4	138.3	138.6
21	9.99	1876.2	143	0.452	9.2	158.4	158.7
22	10.50	2089.6	135	0.434	7.7	135.3	135.5
23	10.99	2231.9	124	0.404	5.6	100	100.2
24	11.48	2291.1	78	0.364	3.6	48.9	49.1
25	11.98	2303.7	71	0.322	2.4	26.7	26.8
26	12.53	2310.6	79	0.282	0.9	25.6	25.6
27	12.95	2308.4	35	0.256	3.6	25.2	25.5
28	13.51	2311.2	30	0.225	1.3	25.2	25.3
29	14.03	2312.2	23	0.201	0.4	25.2	25.2
30	14.44	2312.3	32	0.184	0.3	25.2	25.2
31	14.92	2313.5	6	0.168	0.5	25.2	25.2
32	15.55	2312.3	14	0.148	0.5	25.2	25.2
33	15.96	2311.0	4	0.137	0.3	25.2	25.2
34	16.49	2312.1	5	0.124	0.3	25.2	25.2
35	16.97	2313.0	5	0.114	0.6	25.2	25.2

As reported in [12], during the nacelle power curve campaign simultaneous measurements were available from a cup anemometer mounted a hub height on a met mast, as well as other meteorological sensors relevant for the measurement of a power curve similar to 61400-12-1 [6]. This power curve is displayed in Table 15.

Table 15 Met mast power curve, from [12]

Bin number	V_i (m/s)	P_i (kW)	N_i (-)	Cp_i (-)	s_i , Cat. A uncert (kW)	Cat. B uncert (kW)	Combined uncert (kW)
6	2.61	-7.6	11	-0.102	2.4	14.5	14.7
7	3.02	-1.2	27	-0.011	1.7	14.5	14.6
8	3.47	21.7	35	0.124	3	15.2	15.5
9	4.05	74	28	0.267	6.6	17.2	18.4
10	4.52	119.6	38	0.312	7	18.1	19.4
11	4.99	189	60	0.365	6.4	23	23.9
12	5.52	278.2	80	0.397	5.9	26.5	27.2
13	5.99	374.8	107	0.42	5.5	32.5	32.9
14	6.52	519.5	99	0.451	6.4	44	44.5
15	7	656.6	139	0.46	6.5	48.6	49
16	7.5	810.9	140	0.463	6.9	55.2	55.7
17	8.01	991.9	157	0.463	7.9	66.7	67.1
18	8.51	1179	149	0.46	10.6	74	74.8
19	9	1375.5	113	0.453	14.1	83.2	84.4
20	9.51	1646.6	124	0.461	14.6	114.8	115.8
21	10	1884.8	139	0.453	12.1	110.5	111.2
22	10.5	2078.5	130	0.431	10.8	93.3	93.9
23	11.01	2213	119	0.398	8.4	68.8	69.3
24	11.48	2285.4	84	0.363	5.1	46.3	46.6
25	12.01	2304.5	87	0.32	2.3	26.9	27
26	12.5	2306.7	59	0.284	2.1	25.2	25.2
27	13.03	2308.5	39	0.251	3.3	25.2	25.4
28	13.49	2310.4	27	0.226	1.5	25.2	25.2
29	14.01	2313.1	29	0.202	0.4	25.2	25.2
30	14.52	2312.1	30	0.182	0.4	25.2	25.2
31	14.92	2312.9	6	0.167	0.8	25.2	25.2
32	15.45	2311.9	12	0.151	0.7	25.2	25.2
33	15.99	2312.4	5	0.136	0.2	25.2	25.2
34	16.54	2311.8	6	0.123	0.2	25.2	25.2
35	16.95	2312.7	6	0.114	0.6	25.2	25.2

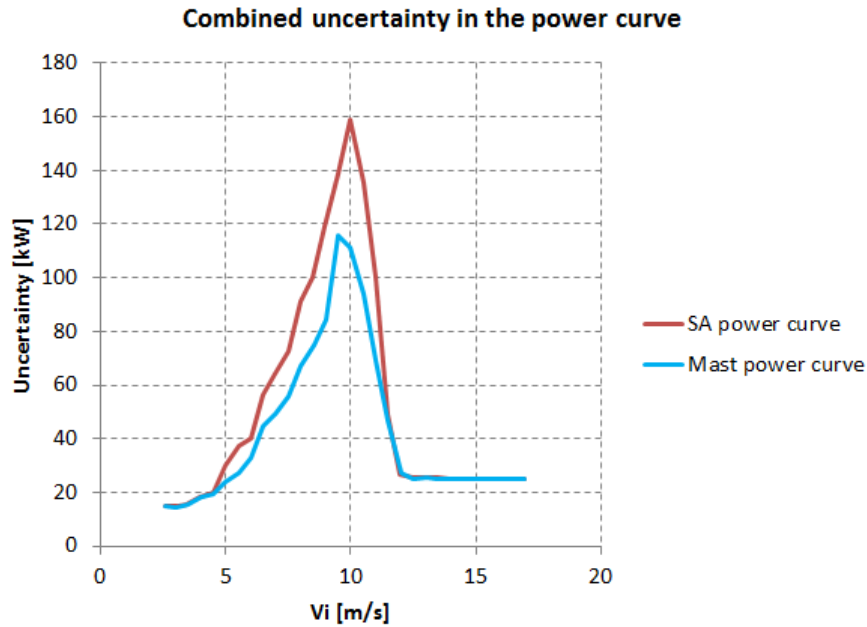


Figure 49 Combined uncertainty of the spinner anemometer power curve (red) and the met mast power curve (blue), in kW

The Annual Energy Production (AEP) and associated uncertainties calculated from the nacelle power curve (Table 14) and the met mast power curve (Table 15), are summarized in Table 16. The AEPs are calculated following the method described in the reference standards (assuming a Rayleigh distribution of the wind speed and an availability of the wind turbine assumed to be 100%, i.e. 8760 hours per year).

Table 16 Measured AEPs, calculated from the power curves obtained with the spinner anemometer and the met mast.

Estimated annual energy production at different mean wind speeds. The reference air density is 1.225kg/m ³ , cut-out wind speed is 25m/s.						
Hub height annual average wind speed (m/s)	Spinner anemometer			Met mast		
	AEP measured (MWh)	Standard uncertainty in AEP (MWh) (%)		AEP measured (MWh)	Standard uncertainty in AEP (MWh) (%)	
4	1715	242	14.1	1746	197	11.3
5	3432	354	10.3	3463	277	8
6	5384	434	8.1	5409	337	6.2
7	7185	475	6.6	7203	368	5.1
8	8570	484	5.6	8581	376	4.4
9	9456	472	5.0	9460	369	3.9
10	9886	449	4.5	9883	352	3.6
11	9959	420	4.2	9952	331	3.3

The differences between the AEP values given in Table 16 and in report [12] are mainly due to the fact that the reference wind speed in the power curves in Table 14 and Table 15 are the averages of the wind speed in the bin; whereas in the power curves in the reference report, the wind speed at bin centre is used.

9. Conclusions

An analysis of the uncertainty of spinner anemometer measurements has been made and influential uncertainty components have been identified. These comprise calibration uncertainties, mounting uncertainties, operational uncertainties and some additional uncertainties.

The calibration uncertainties comprise calibration of sonic sensors in wind tunnel, calibration for angular measurements k_α , and the combined calibration of the constant k_1 and the nacelle transfer function NTF.

The mounting uncertainties of the sonic sensors comprise longitudinal positioning, directional alignment, sonic path angle, sonic azimuth positioning and accelerometer alignment in the sonic sensor feet.

The operational characteristics that must be considered for general operation of the wind turbine and the spinner anemometer are: lateral angular response of sonic sensors, spinner vibrations, and shaft tilt angle increase. The climatic conditions that must be considered are: inflow angle to rotor, turbulence and yaw misalignment.

The ordinary GUM procedure for determination of the combined uncertainty was found not to be applicable due to very complex relationships of the influence parameters and high variability of sensor values during operation. An alternative simulation procedure was developed in which the spinner anemometer operation is simulated in detail. 10min averaged simulations are made in which artificial 3D winds are applied to the spinner. Operational influential components and uncertainty components are added and then the measurement process is simulated to the output horizontal wind speed of the spinner anemometer. The deviations to the applied artificial winds are determined for each category of influence component and the standard uncertainties are combined with the estimated correlation coefficients. The simulation procedure included a "calibrated" path where calibration constants are inserted into the spinner anemometer box, and a "default" path where only default constants are inserted, and 10min values are converted to calibrated values by an inverse and direct conversion of data where the correct calibration constants are applied.

The uncertainty calculation procedure was used for an example wind speed measurement based on a wind turbine at Nørrekær Enge wind farm. The example was built on the assumption of best practises. The uncertainty components were calculated for absolute wind speed measurements according to the standard IEC61400-12-2, with the following deviations:

- Not including the seasonal uncertainty in the NTF, because we consider an NTF for the measurement campaign, not extrapolated to a whole year. The inclusion of this uncertainty term, pre-defined as 2% of the wind speed, would eventually have resulted in an AEP uncertainty of 6.5% of the measured AEP, for an annual average wind speed of 8m/s.
- No uncertainty is considered to be added on the NTF due to terrain for measurement of the NPC, since the wind speed is measured on the spinner and not on the nacelle.

The differences between the horizontal wind speed uncertainty outputs of the “calibrated” and “default” paths simulations is 2.5% at 4m/s and less than or equal to 1% at 10m/s and higher wind speeds.

Assuming best practices (“calibrated” simulation results), the results of the example uncertainty calculations showed that the overall uncertainty on free spinner anemometer wind speed measurements is 4% at 4m/s, 3% at 8m/s, 3% at 12m/s and 3% at 16m/s of the horizontal wind speed.

The uncertainties in the AEP of a power curve obtained with a spinner anemometer, and a power curve obtained with a cup anemometer mounted at hub height on a met mast were calculated. For a hub height annual average wind speed of 8m/s, the AEP uncertainty in the spinner anemometer power curve was found as 5.6% of the measured AEP; while for the met mast it was 4.4% of the measured AEP.

References

1. Pedersen TF, Madsen HA, Møller R, Courtney, M, Sørensen NN, Enevoldsen P, Egedal P, "Spinner Anemometry – An Innovative Wind Measurement Concept", EWEC2007 Milan, paper and poster (poster award)
2. Pedersen TF, Sørensen NN, Vita L, Enevoldsen P, Optimization of Wind Turbine Operation by Use of Spinner Anemometer, Risø-R-1654(EN), August 2008
3. Pedersen TF, Demurtas G, Zahle F, "Calibration of a spinner anemometer for yaw misalignment measurements", Wind Energy 2014, we1798
4. Spinner Anemometer User Manual Version 9.27-3. Metek Meteorologische Messtechnik GmbH, Germany, 2012
5. ASTM D 6011 – 96 (reapproved 2003), Standard Test Method for Determining the Performance of a Sonic Anemometer/Thermometer, 2003
6. IEC 61400-12-1, Wind turbines – part 12-1: Power performance measurements of electricity producing wind turbines, 2005, International Electrotechnical Commission
7. IEC 61400-12-2, Wind turbines – part 12-2: Power performance measurements of electricity producing wind turbines based on nacelle anemometry, 2013-03, International Electrotechnical Commission
8. CBC 0C Decision/Clarification Sheet, Subject: Use of Spinner Anemometers, IEC61400-12-2: 2013, Annex H, 2012-02-02, CAC/CBC
9. Demurtas G, Pedersen TF, Zahle, Calibration of a spinner anemometer for wind speed measurements, Wind Energy
10. Evaluation of measurement data – Guide to the uncertainty in measurement (GUM), JCGM 100:2008
11. Mann J "Wind field simulation", Probabilistic Engineering Mechanics 13(4): 269-282, Oct 1998
12. Demurtas G, Power curve measurement with spinner anemometer according to IEC 61400-12-2, December 2015
13. Pedersen TF, Characterisation of a sonic anemometer, Risø-I-1857, 2003 (not published)
14. Measnet anemometer calibration procedure. Version 2. October 2009.

Acknowledgements

We would like to thank ROMO Wind A/S for their support and finance for this research study. Special thanks to Harald Hohlen for performing the lateral angular response measurements in the WindGuard GmbH wind tunnel, and special thanks to Henrik Pedersen and Nick Janssen, ROMO Wind, for providing data and consultation for the analysis.

Annex A – calibration certificates

Svend Ole Hansen ApS

SCT. JØRGENS ALLÉ 7 · DK-1615 KØBENHAVN V · DENMARK
 TEL: (+45) 33 25 38 38 · FAX: (+45) 33 25 38 39 · WWW.SOHANSEN.DK



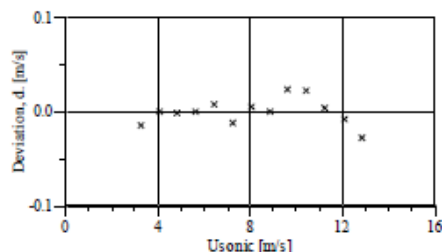
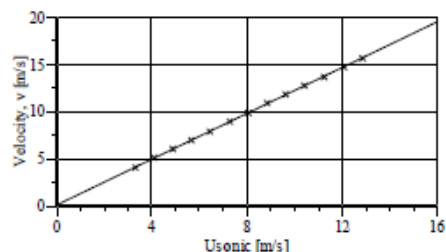
CERTIFICATE FOR CALIBRATION OF SONIC ANEMOMETER

Certificate number: 15.02.01029 Date of issue: February 13, 2015
 Type: Spinner Anemometer Path 1 Serial number: 0107114721_Path1
 Anemometer setting: OM=2
 Manufacturer: METEK GmbH, Fritz-Strassmann-Str.4, 25337 Elmshorn, Germany
 Client: ROMOWIND, Olof Palmes Allé 47, 8200 Aarhus N, Denmark

Anemometer received: February 4, 2015 Anemometer calibrated: February 11, 2015
 Calibrated by: cea Procedure: MEASNET, referring to IEC 61400-12-1
 Certificate prepared by: cea Approved by: Calibration engineer. aht
Anders Heltze-Thomsen

Calibration equation obtained: $v \text{ [m/s]} = 1.20746 \cdot U_{sonic} \text{ [m/s]} + 0.18431$
 Standard uncertainty, slope: 0.00113 Standard uncertainty, offset: 0.06327
 Covariance: $-0.0000149 \text{ (m/s)}^2/\text{m/s}$ Coefficient of correlation: $\rho = 0.999993$
 Absolute maximum deviation: -0.028 m/s at 15.659 m/s

Barometric pressure: 1025.3 hPa		Relative humidity: 23.0%							
Succession	Velocity pressure, q. [Pa]	Temperat. [°C]	Wind velocity, v. [m/s]	Sonic anemometer output Temperat. [°C]	Wind direct. [°]	Wind vel. [m/s]	Deviation, d. [m/s]	Uncertainty, u _c (k=2) [m/s]	
2	10.09	27.4	4.127	25.1	*	3.2770	-0.014	0.021	
4	15.50	27.4	5.115	25.1	*	4.0840	0.000	0.025	
6	21.62	27.4	6.042	25.1	*	4.8520	-0.001	0.029	
8	29.19	27.4	7.020	25.1	*	5.6610	0.000	0.033	
10	37.48	27.4	7.954	25.1	*	6.4280	0.008	0.037	
12	47.53	27.4	8.957	25.1	*	7.2750	-0.011	0.041	
13-last	58.12	27.4	9.905	25.1	*	8.0460	0.005	0.046	
11	70.09	27.4	10.877	25.1	*	8.8560	0.000	0.050	
9	82.76	27.4	11.820	25.2	*	9.6170	0.024	0.055	
7	96.68	27.4	12.776	25.2	*	10.4100	0.022	0.059	
5	111.87	27.4	13.743	25.2	*	11.2260	0.004	0.063	
3	128.64	27.4	14.736	25.3	*	12.0580	-0.008	0.068	
1-first	145.33	27.3	15.659	25.3	*	12.8390	-0.028	0.072	



EQUIPMENT USED

Serial number	Description
-	Boundary layer wind tunnel.
1256	Control cup anemometer.
-	Mounting tube, D = 25 mm
t1	PT100 temperature sensor, wind tunnel.
t2	PT100 temperature sensor, control room.
9904031	PPC500 Furness pressure manometer
X4650038	HMW71U Humidity transmitter
X4350042	PTB100AVaisala analogue barometer.
PS1	Pitot tube
HB2835279	Computer Board. 16 bit A/D data acquisition board.
-	PC dedicated to data acquisition.

Traceable calibrations of the equipment are carried out by external accredited institutions: Furness (PPC500) and Exova Metech.



Photo of the wind tunnel setup ($h \times b = 0.85 \times 1.75$ m). The shown anemometer is of the same type as the calibrated one.

UNCERTAINTIES

The documented uncertainty is the total combined uncertainty at 95% confidence level ($k=2$) in accordance with EA-4/02. The uncertainty at 10 m/s comply with the requirements in the MEASNET procedure that prescribes an absolute uncertainty less than 0.1 m/s at a mean wind velocity of 10 m/s, that is 1%. See Document 97.00.004 "MEASNET - Test report on the calibration campaign" for further details.

The calibration results are only valid for a wind direction parallel to the spinner anemometer.

Certificate number: 15.02.01029



CERTIFICATE FOR CALIBRATION OF SONIC ANEMOMETER

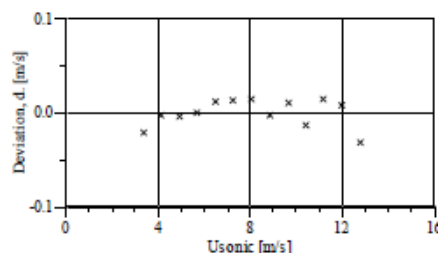
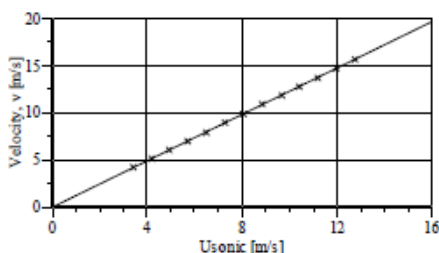
Certificate number: 15.02.00957 Date of issue: February 13, 2015
 Type: Spinner Anemometer Path 2 Serial number: 0107114721_Path2
 Anemometer setting: OM=2
 Manufacturer: METEK GmbH, Fritz-Strassmann-Str.4, 25337 Elmshorn, Germany
 Client: ROMOWIND, Olof Palmes Allé 47, 8200 Aarhus N, Denmark

Anemometer received: February 4, 2015 Anemometer calibrated: February 11, 2015
 Calibrated by: cea Procedure: MEASNET, referring to IEC 61400-12-1
 Certificate prepared by: cea Approved by: Calibration engineer. aht

Calibration equation obtained: $v \text{ [m/s]} = 1.22794 \cdot U_{\text{sonic}} \text{ [m/s]} + 0.00168$
 Standard uncertainty, slope: 0.00118 Standard uncertainty, offset: 7.38524
 Covariance: -0.0000168 (m/s)²/m/s Coefficient of correlation: $\rho = 0.999992$
 Absolute maximum deviation: -0.032 m/s at 15.661 m/s

Barometric pressure: 1025.0 hPa Relative humidity: 22.8%

Succession	Velocity pressure, q [Pa]	Temperat. wind tunnel [°C]	Wind velocity, v [m/s]	Sonic anemometer output			Deviation, d [m/s]	Uncertainty, u _c (k=2) [m/s]
				Temperat. [°C]	Wind direct [°]	Wind vel. [m/s]		
2	10.25	27.4	4.161	26.8	*	3.4040	-0.021	0.021
4	15.45	27.5	5.107	26.8	*	4.1600	-0.003	0.025
6	21.61	27.5	6.042	26.8	*	4.9220	-0.004	0.029
8	29.12	27.5	7.014	26.9	*	5.7100	0.000	0.033
10	37.51	27.5	7.960	26.9	*	6.4710	0.012	0.037
12	47.26	27.5	8.935	26.9	*	7.2640	0.013	0.041
13-last	58.13	27.5	9.910	26.9	*	8.0570	0.015	0.046
11	69.86	27.5	10.863	26.9	*	8.8470	-0.002	0.050
9	83.27	27.5	11.859	27.0	*	9.6480	0.011	0.055
7	96.90	27.5	12.794	27.0	*	10.4280	-0.013	0.059
5	111.92	27.5	13.748	27.1	*	11.1830	0.015	0.063
3	128.30	27.4	14.719	27.1	*	11.9790	0.008	0.068
1-first	145.33	27.3	15.661	27.0	*	12.7780	-0.032	0.072



EQUIPMENT USED

Serial number	Description
-	Boundary layer wind tunnel.
1256	Control cup anemometer.
-	Mounting tube, D = 25 mm
t1	PT100 temperature sensor, wind tunnel.
t2	PT100 temperature sensor, control room.
9904031	PPC500 Furness pressure manometer
X4650038	HMW71U Humidity transmitter
X4350042	PTB100AVaisala analogue barometer.
PS1	Pitot tube
HB2835279	Computer Board. 16 bit A/D data acquisition board.
-	PC dedicated to data acquisition.

Traceable calibrations of the equipment are carried out by external accredited institutions: Furness (PPC500) and Exova Metech.



Photo of the wind tunnel setup (hxb = 0.85x1.75 m). The shown anemometer is of the same type as the calibrated one.

UNCERTAINTIES

The documented uncertainty is the total combined uncertainty at 95% confidence level ($k=2$) in accordance with EA-4/02. The uncertainty at 10 m/s comply with the requirements in the MEASNET procedure that prescribes an absolute uncertainty less than 0.1 m/s at a mean wind velocity of 10 m/s, that is 1%. See Document 97.00.004 "MEASNET - Test report on the calibration campaign" for further details.

The calibration results are only valid for a wind direction parallel to the spinner anemometer.

Certificate number: 15.02.00957



CERTIFICATE FOR CALIBRATION OF SONIC ANEMOMETER

Certificate number: 15.02.00958 Date of issue: February 13, 2015
 Type: Spinner Anemometer Path 3 Serial number: 0107114721_Path3
 Anemometer setting: OM=2
 Manufacturer: METEK GmbH, Fritz-Strassmann-Str.4, 25337 Elmshorn, Germany
 Client: ROMOWIND, Olof Palmes Allé 47, 8200 Aarhus N, Denmark

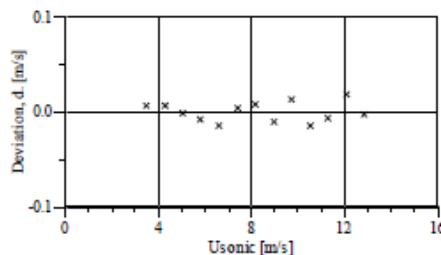
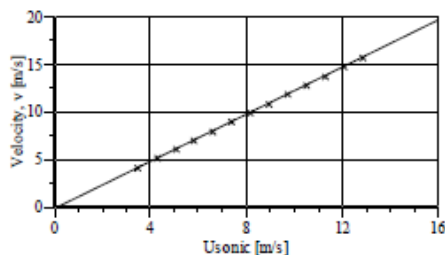
Anemometer received: February 4, 2015 Anemometer calibrated: February 11, 2015
 Calibrated by: cea Procedure: MEASNET, referring to IEC 61400-12-1
 Certificate prepared by: cea Approved by: Calibration engineer. aht

Calibration equation obtained: $v \text{ [m/s]} = 1.23249 \cdot U_{\text{sonic}} \text{ [m/s]} - 0.16930$
 Standard uncertainty, slope: 0.00083 Standard uncertainty, offset: -0.05252
 Covariance: -0.0000086 (m/s)²/m/s Coefficient of correlation: $\rho = 0.999996$
 Absolute maximum deviation: 0.018 m/s at 14.715 m/s

Anders Holtze Thomsen

Barometric pressure: 1024.8 hPa Relative humidity: 22.8%

Succession	Velocity	Temperat.	Wind	Sonic anemometer output			Deviation, Uncertainty,	
	pressure, q. [Pa]	wind tunnel [°C]	velocity, v. [m/s]	Temperat. [°C]	Wind direct. [°]	Wind vel. [m/s]	d. [m/s]	u _c (k=2) [m/s]
2	10.04	27.6	4.119	26.1	*	3.4740	0.007	0.021
4	15.58	27.6	5.132	26.1	*	4.2960	0.006	0.025
6	21.73	27.6	6.061	26.1	*	5.0560	-0.001	0.029
8	28.96	27.6	6.996	26.1	*	5.8200	-0.007	0.033
10	37.38	27.6	7.949	26.1	*	6.5980	-0.014	0.037
12	47.24	27.6	8.936	26.1	*	7.3840	0.004	0.041
13-last	58.00	27.6	9.900	26.1	*	8.1640	0.008	0.046
11	69.59	27.6	10.845	26.1	*	8.9450	-0.010	0.050
9	82.60	27.6	11.815	26.1	*	9.7130	0.014	0.055
7	96.40	27.6	12.765	26.2	*	10.5060	-0.014	0.059
5	111.73	27.6	13.743	26.2	*	11.2930	-0.007	0.063
3	128.11	27.6	14.715	26.2	*	12.0620	0.018	0.068
1-first	145.18	27.5	15.660	26.1	*	12.8450	-0.003	0.072



EQUIPMENT USED

Serial number	Description
-	Boundary layer wind tunnel.
1256	Control cup anemometer.
-	Mounting tube, D = 25 mm
t1	PT100 temperature sensor, wind tunnel.
t2	PT100 temperature sensor, control room.
9904031	PPC500 Furness pressure manometer
X4650038	HMW71U Humidity transmitter
X4350042	PTB100AVaisala analogue barometer.
PS1	Pitot tube
HB2835279	Computer Board. 16 bit A/D data acquisition board.
-	PC dedicated to data acquisition.

Traceable calibrations of the equipment are carried out by external accredited institutions: Furness (PPC500) and Exova Metech.



Photo of the wind tunnel setup (lxb = 0.85x1.75 m). The shown anemometer is of the same type as the calibrated one.

UNCERTAINTIES

The documented uncertainty is the total combined uncertainty at 95% confidence level ($k=2$) in accordance with EA-4/02. The uncertainty at 10 m/s comply with the requirements in the MEASNET procedure that prescribes an absolute uncertainty less than 0.1 m/s at a mean wind velocity of 10 m/s, that is 1%. See Document 97.00.004 "MEASNET - Test report on the calibration campaign" for further details.

The calibration results are only valid for a wind direction parallel to the spinner anemometer.

Certificate number: 15.02.00958

	<h2 style="text-align: center;">Kalpha Calibration Certificate</h2>	Doc. No.:	KA 002																																								
		Revision No.:	1																																								
		Revision Date:	2015.09.30																																								
		Prepared by:	NGJ																																								
		Approved by:	HSP																																								
		Page:	1 of 3																																								
Wind Turbine Type: SWT93 - 2.3MW																																											
Test Turbine Name: Nørrekær Enge 1,2,3,4,5,9,13 CALIBR. / TEST DATE: measurement campaigns in 09/2015 Client: Vattenfall Vindkraft A/S_Nordic		Record No. 0001 Prepared by: NGJ Date: 18/12/2015																																									
Calibration Method: <input checked="" type="checkbox"/> Yaw Test <input type="checkbox"/> Lidar Measurement Campaign		References [1] iSpin calibration procedures (ROMO Wind)																																									
Summary: Because the spinner of each turbine type is different, a Spinner Anemometer (SA) always needs to be calibrated before it can give any reliable output. Three calibrations have been made, first wind tunnel calibration [1] and by ROMO Wind: Kalpha and K1 calibration. After Kalpha calibration the spinner anemometer is capable to measure the yaw misalignment of a turbine and after K1 calibration it is, in addition to the yaw misalignment, also capable of measuring wind speed in front of the turbine. Kalpha is obtained from a yaw test, and K1 is obtained from a met-mast/Lidar campaign. To determine Kalpha a Risø yaw test was performed as described in [1]. A Risø yaw test is a measurement campaign where the wind turbine rotor is stopped, and the rotor is yawed in and out of the wind several times. ROMO Wind performs a Risø yaw test with the following parameters: <ul style="list-style-type: none"> • Yaw range: $\pm 60^\circ$ with respect to the mean wind direction • Mean wind speed: > 6 m/s • Yaw in/out repetitions: 6 • Rotor position: One blade pointing downwards or straight up, remaining two pointing up/down (vertically symmetric) • Measurement frequency: 10Hz The mean wind direction and wind speed on the day of the test are shown below. For a Risø yaw test to be as accurate as possible it is essential that the wind direction and wind speed stay constant over the duration of the test. Note that the uncorrected Spinner Anemometer (SA) wind speed is not calibrated to match the real wind speed. The difference between calibrated and uncalibrated SA wind speeds can be as high as a factor two. <table border="1" style="width: 100%; text-align: center;"> <thead> <tr> <th style="background-color: #006666; color: white;">Data statistics:</th> <th>NKE01</th> <th>NKE02</th> <th>NKE03</th> <th>NKE04</th> <th>NKE05</th> <th>NKE09</th> <th>NKE13</th> </tr> </thead> <tbody> <tr> <td>Mean wind direction [°]</td> <td>202,0</td> <td>185,96</td> <td>157,55</td> <td>108,21</td> <td>115,69</td> <td>184,0</td> <td>183,29</td> </tr> <tr> <td>Mean SA wind speed [m/s]</td> <td>3,83</td> <td>4,69</td> <td>4,71</td> <td>7,33</td> <td>4,74</td> <td>7,21</td> <td>6,80</td> </tr> </tbody> </table> The Kalpha calibrations were performed on the turbines on the following dates. Plots shown in this certificate are for turbine NKE02. <table border="1" style="width: 100%; text-align: center;"> <thead> <tr> <th style="background-color: #006666; color: white;">Turbine name</th> <th style="background-color: #006666; color: white;">Test date and time</th> </tr> </thead> <tbody> <tr><td>NKE01</td><td>2015-09-21 12:37</td></tr> <tr><td>NKE02</td><td>2015-09-22 06:38</td></tr> <tr><td>NKE03</td><td>2015-09-22 07:57</td></tr> <tr><td>NKE04</td><td>2015-09-14 11:06</td></tr> <tr><td>NKE05</td><td>2015-09-22 09:19</td></tr> <tr><td>NKE09</td><td>2015-09-24 12:29</td></tr> <tr><td>NKE13</td><td>2015-09-24 12:56</td></tr> </tbody> </table>				Data statistics:	NKE01	NKE02	NKE03	NKE04	NKE05	NKE09	NKE13	Mean wind direction [°]	202,0	185,96	157,55	108,21	115,69	184,0	183,29	Mean SA wind speed [m/s]	3,83	4,69	4,71	7,33	4,74	7,21	6,80	Turbine name	Test date and time	NKE01	2015-09-21 12:37	NKE02	2015-09-22 06:38	NKE03	2015-09-22 07:57	NKE04	2015-09-14 11:06	NKE05	2015-09-22 09:19	NKE09	2015-09-24 12:29	NKE13	2015-09-24 12:56
Data statistics:	NKE01	NKE02	NKE03	NKE04	NKE05	NKE09	NKE13																																				
Mean wind direction [°]	202,0	185,96	157,55	108,21	115,69	184,0	183,29																																				
Mean SA wind speed [m/s]	3,83	4,69	4,71	7,33	4,74	7,21	6,80																																				
Turbine name	Test date and time																																										
NKE01	2015-09-21 12:37																																										
NKE02	2015-09-22 06:38																																										
NKE03	2015-09-22 07:57																																										
NKE04	2015-09-14 11:06																																										
NKE05	2015-09-22 09:19																																										
NKE09	2015-09-24 12:29																																										
NKE13	2015-09-24 12:56																																										

	<h1>Kalpa Calibration Certificate</h1>	Doc. No.:	KA 002
		Revision No.:	1
		Revision Date:	2015.09.30
		Prepared by:	NGJ
		Approved by:	HSP
		Page:	2 of 3

Data limits:

In determining Kalpa there are two important factors: the reference yaw misalignment γ_{ref} , and the Spinner Anemometer (SA) yaw misalignment γ . γ_{ref} is computed from the turbine yaw position as follows:

$$\gamma_{ref} = \bar{\theta} - \theta$$

Where $\bar{\theta}$ is the mean wind direction and θ is the yaw position. The aim of Kalpa is to scale the SA output such that its measured yaw misalignment γ has a 1:1 relation with respect to γ_{ref} . i.e. the measured yaw misalignment corresponds to the actual yaw misalignment.

The Risø yaw test prescribes that the turbine is yawed in, and out of the wind by 60 degrees. At extreme yaw angles, the flow around the spinner becomes complex and is therefore not taken into account. The limits used for the data analysis are:

Obtained limits:	NKE01	NKE02	NKE03	NKE04	NKE05	NKE09	NKE13
gamma +/- [°]	90	90	90	90	90	90	90
gamma_ref +/- [°]	43	50	50	51	47	41	46

Results:

Plotting γ versus γ_{ref} gives a scatter plot which is essential for the determination of Kalpa. A value for Kalpa that yields a 1:1 relationship between γ and γ_{ref} is obtained, using an iterative procedure. The resulting plot can be seen in the figure below.

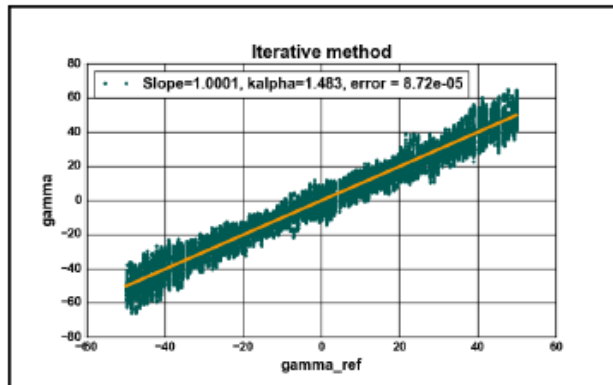


Figure 1: Corrected yaw misalignment γ versus turbine yaw angle γ_{ref} with least squares fit.

Conclusion:

The method shown above has been repeated for each of the test turbines. The average Kalpa was found to be equal to 1.45.

Results:	NKE01	NKE02	NKE03	NKE04	NKE05	NKE09	NKE13	Average
Kalpa	1,611	1,483	1,410	1,576	1,40	1,366	1,330	1,45

The uncertainty of Kalpa was described in [1] to be 10%. This means that a Kalpa with a value of 2 has an uncertainty of 0.2. The corrected, as well as the uncorrected time series for the yaw test can be seen in the figures below.

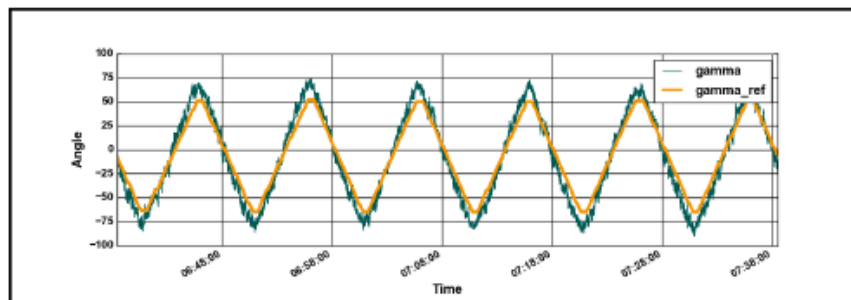


Figure 2: Uncorrected yaw misalignment γ versus turbine yaw angle γ_{ref}

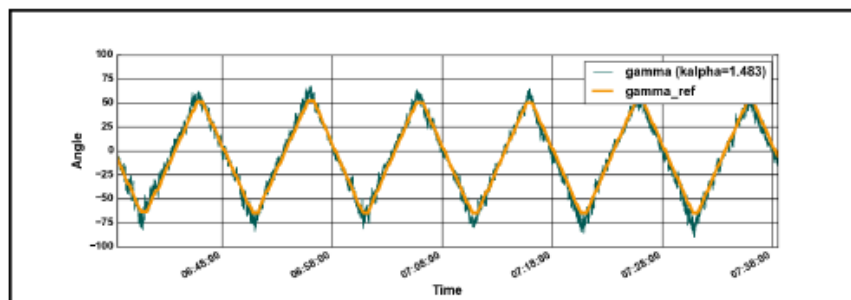


Figure 3: Kalpa corrected yaw misalignment γ versus turbine yaw angle γ_{ref}

Site-specific comments:

Note that the plots shown in this certificate serve to give an impression of the Kalpa calibration method. The final value for Kalpa is an average over 7 different turbines and was found to be 1.45.

The tests in this certificate are a verification of a previous yaw test performed by ROMO Wind, on the same turbine but with different setup. The Kalpa that followed from the previous test was 1.44 and is the value currently used by ROMO Wind.

DTU Vindenergi er et institut under Danmarks Tekniske Universitet med en unik integration af forskning, uddannelse, innovation og offentlige/private konsulentopgaver inden for vindenergi. Vores aktiviteter bidrager til nye muligheder og teknologier inden for udnyttelse af vindenergi, både globalt og nationalt. Forskningen har fokus på specifikke tekniske og videnskabelige områder, der er centrale for udvikling, innovation og brug af vindenergi, og som danner grundlaget for højt kvalificerede uddannelser på universitetet.

Vi har mere end 230 ansatte og heraf er ca. 60 ph.d. studerende. Forskningen tager udgangspunkt i 9 forskningsprogrammer, der er organiseret i tre hovedgrupper: vindenergisystemer, vindmølleteknologi og grundlag for vindenergi.

Technical University of Denmark
DTU Vindenergi
Frederiksborgvej 399
Bygning 125
4000 Roskilde
Telefon 45 25 25 25
info@vindenergi.dtu.dk
www.vindenergi.dtu.dk

